Universidad de Castilla-La Mancha
Escuela Internacional de Doctorado
Departamento de Ingeniería Eléctrica, Electrónica, Automática y Comunicaciones

Doctoral Thesis:
On the mechanical design, control approach and sensorization solution of planar cable driven parallel robots

Author:
Guillermo Rubio Gómez

Advisor:
Fernando José Castillo García

Toledo, octubre 2021

Foreword of the author

This thesis results from my work as research fellow at the University of Castilla-La Mancha, and was funded by the internal program for training of research staff. My very special thanks go to my supervisor Fernando José Castillo García for supporting my scientific and academic work for many years, for his role as team leader and his trust.

My gratitude also goes to the rest of my colleagues in the Mantis research group: David Rodriguez Rosa, Sergio Júarez Pérez, Francisco Moya Fernández, Andrea Martín Parra, Antonio Gonzalez Rodriguez and Daniel Duran Dovalle. For their immeasurable support in technical aspects, the valuable talks about cable robotics and mechatronics in general, the good working atmosphere and their friendship.

I would like to thank the members of the Robotics and Assistance Systems Group from the Fraunhofer Institute for Manufacturing Engineering and Automation, Marc Fabritius, Christoph Martin and Johannes Stoll for giving me the opportunity to do the research stay in Stuttgart, the support and the research collaboration.

I want to thank my friends from Cuenca, my university colleagues and friends from Toledo and Monterrey and my friends from Stuttgart, for all the support and good times spent during the years of this thesis.

Specially, I would like to thank my girlfriend Lis for all immense support throughout these years, and my family for its unconditional support, both in person and from the distance during the time spent abroad.

Abstract

Cable driven parallel robots are a special kind of parallel manipulators in which the end-effector is connected to a fixed frame by means of several cables instead of rigid links. The end-effector pose can be controlled by controlling the length of these cables.

This kind of robots offers several advantages compared to the conventional rigid ones. One of the main advantages is their scalability and thus the possibility of covering large workspaces, as long cables are easy to wind. Additionally, they present a high power to weight relation which results in high dynamic capabilities.

On the other hand, they present also several drawbacks as complex dynamics because cables are elastic elements that provide an unidirectional force transmission, they can pull but not push, therefore, positive cable tension must be guaranteed at all times. In practice, positiveness is not the only requirement for cable forces, they have to be kept between a minimum and a maximum limit for the feasible robot operation. In this sense, the feasible workspace of a Cable Driven Parallel Robot is defined as the set of platform poses where the robot end-effector can be balanced by means of forces within the feasible limits, under a certain externally applied wrench. Moreover, in the case of over-constrained cable driven parallel robots, i.e. with more cables than degrees of freedom, there are infinity possible cable force distributions that can balance the end-effector, this supposes an additional problem as one has to chose one among all the possible cable force distributions. This has been one of the major open problems in the field and extensive research has been carried out to propose methods to find feasible solutions to this mathematical problem. Additionally, the cable direction changes as the end-effector moves along the workspace yielding to a strong change in the load to be moved by each motor, which in turn results in an important reduction of the robot workspace and the necessity of complex control strategies to effectively reach the full workspace.

Due to these drawbacks, the range of real-world applications of cable driven parallel robots is still limited. This thesis focuses on the feasible application of cable driven parallel robots to both vertical and horizontal, large, planar workspaces. For these specific workspace characteristics, suspended cable robots, i.e. cable robots in which all cables act against the gravity direction are specially well suited, however, the conventional schemes require extremely high power for the motorization system if a large workspace has to be reached. To solve this problem, in first place, new mechanical designs are proposed to substantially increase the feasible workspace of such robots with reasonable tension limits. On the other hand, the proposed mechanical designs bring new challenges from the dynamical control point

of view.

In the case of vertical workspaces, the addition of a passive carriage which can freely slide along a guide attached to the top of the frame is proposed, which significantly increase the feasible workspace of the robot, for the same motorization system compared to the conventional one. On the other hand, this new design reduces the stiffness of the robot in the horizontal direction, which can cause undesired vibrations and low robustness from real operation environment perturbations as wind. To solve this problem, a specific control approach is proposed and tested in a robot prototype.

In the case of large, planar, horizontal workspaces, where occupancy of the space perpendicular to the working plane has to be reduced, the proposed solution consist of employing a close cable loop along with passive carriages in two opposite frame borders. This new design can significantly reduce the required power, even for very large workspaces. As drawback, undesired oscillations appear on the direction perpendicular to the carriages. To solve this problem, a specific control approach has been proposed as well. The performance of this control approach and the overall robot accuracy have been experimentally assessed in another robot prototype.

Finally, for any kind of CDPR, measuring tension is an critical matter, it is required for security reasons to avoid the possibility of cables break or actuators overload. Additionally some robots' control systems rely on these measurements as feedback. State of the art on systems to measure cable tension shows that they present important restrictions in terms of measuring range, precision and repeatability. In this sense, a novel device for measuring cable tension, specifically designed to be applied in CDPR, has been proposed and experimentally validated.

Contents

List of Tables

List of Figures

List of Symbols

A_i	—	Proximal anchor point of the i-th cable.
B_i	—	Distal anchor point of the i-th cable.
$\boldsymbol{a}_i$	—	Position vector of the proximal anchor point of the i-th cable.
$\boldsymbol{b}_i$	—	Position vector of the distal anchor point of the i-th cable.
$\mathbb{K}_0$	—	Inertial world coordinate system.
$\mathbb{K}_e$	—	Non-inertial end-effector coordinate system.
m	—	Number of cables.
n	—	Number of degrees-of-freedom.
$\boldsymbol{r}$	—	End-effector position.
$\boldsymbol{R}$	—	End-effector orientation.
$\boldsymbol{q}$	—	End-effector pose.
$\boldsymbol{f}_e$	—	Forces applied externally to the end-effector.
$\boldsymbol{\tau}_e$	—	Torques applied externally to the end-effector.
$\boldsymbol{w}_e$	—	Wrench applied externally to the end-effector.
$\boldsymbol{l}_i$	—	Vector of the i-th cable.
l_i	—	Variable length of the i-th cable.
l_i^0	—	Constant length of the i-th cable.
f_i	—	Force of the i-th cable.
$\boldsymbol{u}_i$	—	Unit vector of the i-th cable.
φ^{IK}	—	Inverse kinematics.
φ^{FK}	—	Forward kinematics.
φ^{ID}	—	Inverse dynamics.
φ^{FD}	—	Forward dynamics.
$\boldsymbol{A}^T$	—	Structure matrix.
$\boldsymbol{A}$	—	Transpose of the structure matrix.
$\boldsymbol{K}$	—	Stiffness matrix.
$\boldsymbol{K}_C$	—	Actuators stiffness matrix.
$\boldsymbol{K}_{OS}$	—	Overall stiffness matrix.
$\boldsymbol{K}_G$	—	Geometrical stiffness matrix.
k_i	—	Spring constant of the i-th cable.
k'	—	Material-dependent spring constant.
$\boldsymbol{V}$	—	Vector of voltage inputs to the actuators.

List of Acronyms

$CDPR$	—	Cable Driven Parallel Robot.
OC	—	Over-constrained.
DOF	—	Degrees of Freedom.
IK	—	Inverse Kinematics.
FK	—	Forward Kinematics.
OS	—	Operational Space.
JS	—	Joint Space.
$IRPM$	—	Incompletely Restrained Positioning Machines.
$CRPM$	—	Completely Restrained Positioning Machines.
$RRPM$	—	Redundantly Restrained Positioning Machines.
FD	—	Forward Dynamics.
ID	—	Inverse Dynamics.
DC	—	Direct Current.
SCR	—	Suspended cable robots.

Chapter 1

Introduction

In this chapter, cable driven parallel robots are introduced, along with their advantages and drawbacks. Following, the problem that is going to be addressed in this thesis is stated. Finally, the hypothesis and the objectives of the work are discussed, and the structure of the document is presented.

1.1 Motivation

Regarding their kinematics, robots can be defined as serial robots if their joints are coupled serially one after each other, being one example the robotic arms widely employed in industrial environments (see Figure 1.1 [1]). On the other hand, parallel robots have a set of actuators fixed on a frame and connected to the robot mobile tool or end-effector. Traditional parallel robots use rigid links to join the static frame to the end-effector, as the well-known delta robot (see Figure 1.2 [2]).

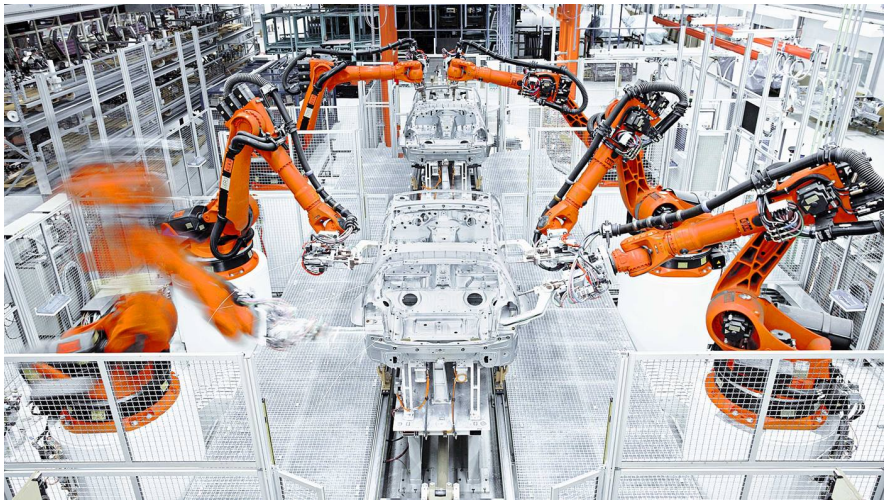

Figure 1.1: Example of serial robot

Cable driven parallel robots (CDPR) are a special type of parallel manipulators where rigid links are replaced by actuated cables [1]. This means that the end-effector is supported by a set of cables which length can be controlled, normally by means of a set motor-gearbox-winch that coil the cable in a drum as in [2–5]. Examples of CDPR using linear actuators to vary cable lengths can also be found in literature [6–8]. By varying the cables length it is possible to control the end-effector position (e.g. [9]) and/or orientation (e.g. [10]). The set of position and orientation of the end-effector will be called end-effector pose, hereafter. As an example, Figure 1.3 [3] shows an image of the IPAnema3 CDPR.

There are important advantages that these manipulators provide compared to the widely employed serial manipulators. CDPR present the most light-weight structure for a manipulator, from the point of view of the structural design [11]. Since the motors only have to move the payload and the cables, the energetic efficiency of a CDPR is considerably higher in the major part of their workspace. In this sense, they are able either to move a much higher mass or employ less energy than their serial robots counterparts where a motor has to move also every link and motor located from itself to the end-effector. For this reason, CDPR

[1] source: `www.kuka.com`
[2] source: `www.kuka.com`
[3] source: `www.ipa.fraunhofer.de`

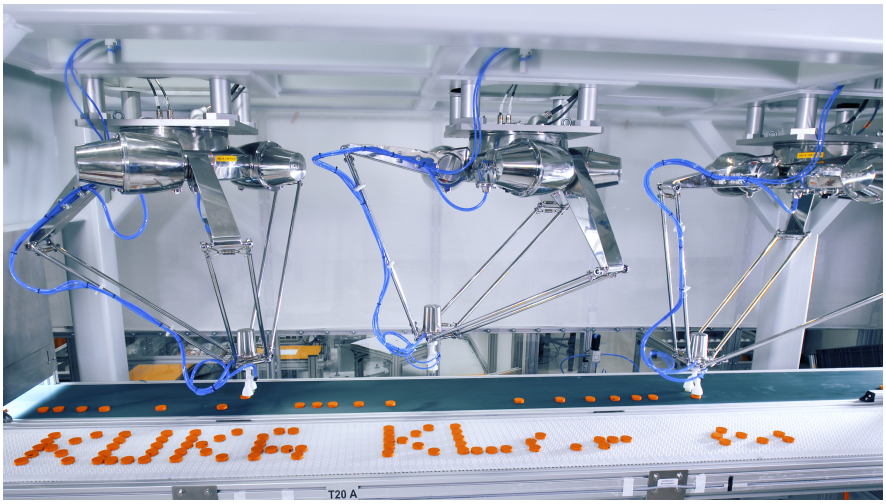

Figure 1.2: Example of parallel robots

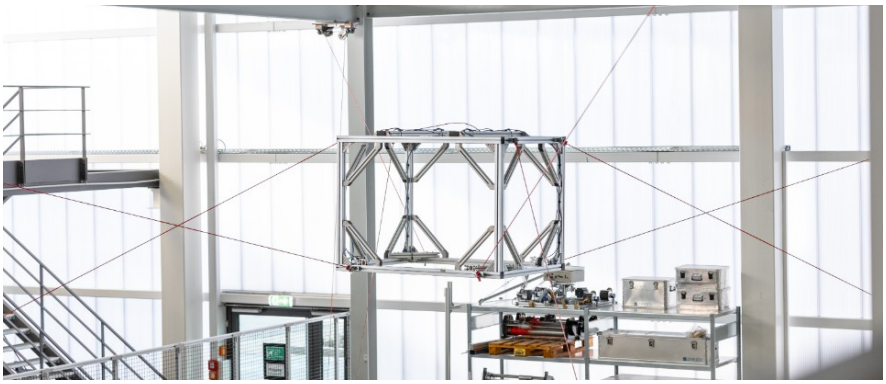

Figure 1.3: Example of a cable driven parallel robot

allow to achieve high dynamic capabilities, which make them interesting for operations like automatic inspection or pick-and-place. As the motors of CDPR can be smaller, for the same task, they are safer and more economical than the traditional serial ones [12]. Additionally, they are easily reconfigurable as the actuators can be attached to any fixed structure [13]. Finally, one of the main advantages of CDPR is their ability to cover large workspaces since very long cables are easy to wind [14].

Due to this, in the last two decades, the research effort in this field and the number of applications proposed for CDPR has grown up. Interesting applications have been proposed for CDPR including rehabilitation and assistance [15–22], production engineering [23], assembly of large scale components [24], construction [25, 26], logistics [27, 28], wind tunnels [29–31], sensorization [2, 32], cleaning of buildings with irregular shapes [33, 34] or aerospatial applications [35, 36].

On the other hand, the nature of cables adds several problems to those inherent to parallel

manipulators as the complexity of their forward kinematics or the presence of singularities [37]. Due to its nature, cables can only withstand traction efforts but not compression ones, therefore, cable tension must remain positive for each cable. Moreover, from the practical point of view, cable tensions must always stay over a certain limit as low tension causes cable sagging. Sagging is only modeled on complex kinematic models of CDPR as [38], where many cable parameters, which are difficult to measure or estimate are required. Using simple and more practical kinematic models with sagging cables will lead to a considerably lack of precision in the end-effector position and orientation. Sagging cables can also cause problems when coiling in the drums. Cable tensions also have an upper limit which in practice is mainly due to the maximum torque that can be generated by the actuator system. The break limit of the cable, which depends on the material and the quality of the cable anchors, also has to be considered when setting the upper limit tension. An extensive analysis on the nature of cable tension limitations in CDPR can be found in [39].

This practical or feasible limitations on cable tensions together with their high dependence on the end-effector pose strongly reduce the workspace of CDPR. Furthermore, CDPR dynamics are complex and strongly nonlinear [40]. As the end-effector moves, the direction of each cable varies strongly, this means that the tension of each cable also changes, changing the load that the actuators have to move. Due to this dynamic feature, the control effort required to achieve a high level of precision reaching a certain pose is normally high [41, 42].

For over-constrained (OC) CDPR (see Section 2.1 for a detailed explanation on OC CDPR) an additional problem arises, as for a certain end-effector pose, there are infinite possibilities for cable tension distributions of the robot that fulfill the end-effector equilibrium, i.e. the underlying mathematical problem is underdetermined.

There are several works that propose methods to obtain feasible cable force distribution for OC CDPR: in [1, 43] the problem is treated as a constrained optimization problem, in [44] the Dykstra algorihmt is employed, in [45–47] non-iterative approaches are proposed to obtain solutions to this problem, in [48, 49] authors proposed a geometrical, real-time capable method to obtain feasible force distributions for OC CDPR with two more cables than DOF. Dynamic cable force control is normally employed in OC CDPR [50, 51], along with end-effector pose control, to keep all cable forces within the feasible limits of the robot. In this sense, measuring cable tension becomes a key aspect in OC CDPR as it is normally required to achieve a proper control since the previously mentioned force control approaches rely on these measures. Additionally, any kind of CDPR in normal operation will require cable tension measurements for security reasons.

Although many applications have already been proposed for CDPR as mentioned before, they are mainly research works and prototypes proposals while still few CDPR are already in use for real applications. From the application point of view, this thesis is carried out in the frame of the European project DESDEMONA (DEtection of Steel Defects by Enhanced MONitoring and Automated procedure for self-inspection and maintenance) [1]. The project focuses on the development of integrated systems and procedures for the automatic inspection and preventive damage detection in steel and composite civil structures. In this context,

[1] source: `www.desdemonaproject.eu`

Figure 1.4: Vertical occupancy of Taborly bridge (Nantes)

CDPR can be employed for the automatic inspection of bridge desks or facades, by equipping the end-effector with the required inspection devices, e.g. conventional or infrared cameras, ultrasound sensors, etc. One particularity of these applications is that the robot must be able to cover large, flat surfaces that can be vertical (e.g. facades) or horizontal (e.g. bridge decks). Additionally, in the last case, it is common that the occupancy of the space perpendicular to the working plane must be strictly reduced, normally because a road or railway pass below the bridge to be inspected. Figure 1.4 illustrates the vertical occupancy of Taborly bridge, which is one of the cases of study of DESDEMONA project.

This thesis focuses on the problems that arise from the use of CDPR in two specific planar cases of study:

- Large and vertical workspaces.
- Large and horizontal workspaces.

In this thesis, two novel mechanical designs are proposed for the feasible application of CDPR to the previously mentioned tasks, notably improving the workspace size compared with the corresponding planar CDPR with conventional design. Their kinematic and dynamic models are presented, along with the proposed control approaches that guarantee the required accuracy and robustness for the robots operation. Additionally, prototypes have been developed for the validation of the mathematical models and control approaches proposed.

Additionally, the problem of measuring cable tension in CDPR is addressed. To this end, a new sensor for the accurate measurement of cable tension has been specifically designed for its application in any kind of CDPR. The mechanical principles of the measurement system, which improves its performance compared with the previously existing ones is exposed. The prototype has been build and experimentally validated.

1.2 Hypothesis

Considering the previous section, the following hypotheses are stated for this thesis:

- Planar CDPR can be successfully applied for specific tasks in planar workspaces if the mechanical design of the conventional robots is redesigned in such a way that the problems inherent to CDPR are strongly reduced. This redesign implies the need for new kinematic, static and dynamic models. By successfully developing these models, new control approaches can be designed that allow the accurate and robust operation of these new robots.
- An improved device for cable tension measurement can be obtained by employing a different measuring principle than the one employed in the conventional devices. This new device can be specifically designed to be easily employed in any kind of CDPR.

1.3 Objectives

The following objectives are proposed for this thesis:

- To design a new planar CDPR for its application in large and vertical surfaces, developing its kinematic, static and dynamic models and designing a control strategy that allows its accurate and robust operation.
- To design a new planar CDPR for its application in large and horizontal surfaces, minimizing the occupation of the space outside its workplane. To develop its kinematic, static and dynamic models and design a control strategy that allows its accurate and robust operation.
- To design a new device for cable force measurement, improving the accuracy and signal quality in comparison with the previously existing ones. This device must be easily applicable to any kind of CDPR.

1.4 Document structure

The rest of the document is structured as follows:

Chapter 2. Fundamentals, reviews the different classifications for cable-driven parallel robots and exposes its theoretical foundations.

Chapter 3. Problem statement and methodology, exposes the problems that are tackled in this thesis, along with the methodology employed to solve them.

Chapter 4. Results, includes the papers published as direct results of this thesis.

Chapter 5. Conclusions and future works, summarizes the conclusions reached during this work. Additionally the research work that would follow this thesis is outlined.

Chapter 2

Fundamentals

In this chapter the theoretical foundations of cable driven parallel robots are reviewed, with special interest on those aspects relevant for the specific problems being addressed in this thesis.

At first, the general concept and terminology is exposed. Subsequently, the kinematic models and static equilibrium of general CDPR are presented. The workspace analysis and the different definitions regarding workspace are introduced. The concept of stiffness, its implications and the involved parameters are outlined. The generics of dynamic modeling in cable driven parallel robots are exposed and the specific dynamic model considered for the robots under study in this work are introduced.

Finally, the basics of dynamic control applied to cable robots are outlined along with a state-of-the art review.

2.1 Concept and terminology

Figure 2.1 represents a clear scheme of a generic CDPR with its fundamental components. The frame is the fixed structure of the robot, cables are attached to it in the proximal anchor points, where the actuation system that control cable lengths is located. In most of CDPR cables exit the proximal anchor points through pulleys which orientation can vary depending on the end-effector position and orientation. Cables are attached to the end-effector in the distal anchor points.

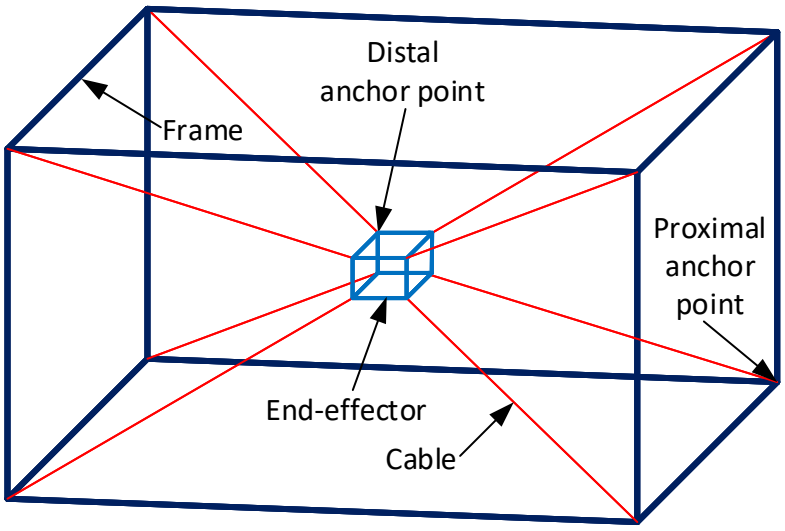

Figure 2.1: Concept and parts of a CDPR

Figure 2.2 shows the generic geometric model of a 3T3R (see Section 2.2) CDPR, where A_i and B_i are the proximal and distal anchor points of cable i, respectively, being m the number of cables. $\boldsymbol{a}_i \in \mathbb{R}^3$ is the position vector of A_i with respect to the world coordinate system κ_0 while $\boldsymbol{b}_i \in \mathbb{R}^3$ is the position vector of B_i with respect to the end-effector coordinate system κ_e. $\boldsymbol{r} \in \mathbb{R}^3$ is the Cartesian position of the end-effector and $\boldsymbol{R} \in SO_3$ is the rotation of the end-effector, both with respect to κ_0. Therefore, the pair $(\boldsymbol{r}, \boldsymbol{R}) = \boldsymbol{q}$ describes the transformation from κ_e to κ_0 and will be referred as end-effector *pose*. Finally, $\boldsymbol{f}_e \in \mathbb{R}^3$ and $\boldsymbol{\tau}_e \in \mathbb{R}^3$ are the external forces and torques applied to the end-effector, also referred hereafter as external wrench $\boldsymbol{w}_e$. Finally, $\boldsymbol{l}_i \in \mathbb{R}^3$ is the i-th cable vector in κ_0 and $\boldsymbol{u}_i = \frac{\boldsymbol{l}_i}{||\boldsymbol{l}_i||_2}$ its corresponding unit vector.

2.2 Classification and architecture

CDPR can be classified according to several different criteria as exposed in [52], for the scope of this work, two classifications are considered relevant:

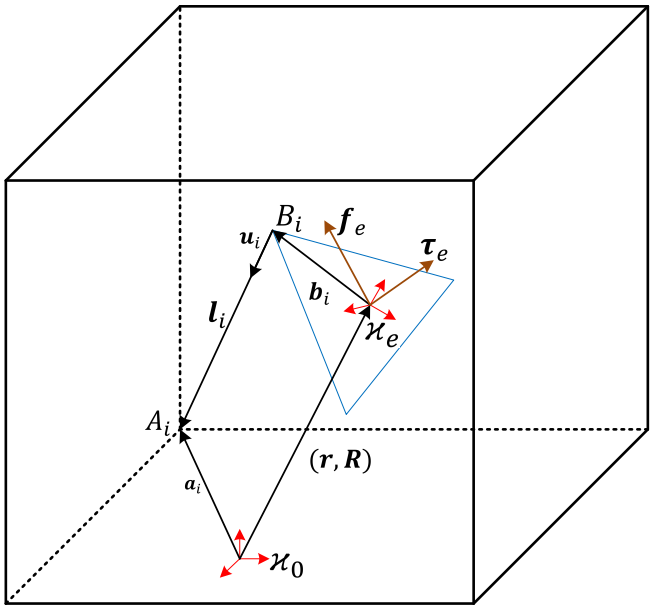

Figure 2.2: Geometry of a 3T3R CDPR

Kinematic classification. This classification, proposed by Ming and Higuchi [53], takes into account the number of cables of the robot (m) and the number of controllable degrees of freedom (DOF) of its end-effector (n). According to this, the following classification can be made:

- **Under-constrained** $m \leq n$, the robot can not withstand arbitrary wrenches $\boldsymbol{w}_e$ applied to the platform, additionally for a certain applied wrench, the stability of the robot depends on the end-effector pose and the number/direction of the DOF that can be controlled vary with the end-effector pose. If $m = n$ although the robot is kinematically fully constrained, they also belong to the under-constrained category in [53] as their static equilibrium relies on externally applied forces such as gravity. These first two categories are also referred to as Incompletely Restrained Positioning Machines (IRPM) (see Figure 2.3a).

- **Fully-constrained** $m = n + 1$, the forces that the robot can withstand depend on the maximum and minimum forces that can be generated by the robot. This kind of robots is considered as Completely Restrained Positioning Machines (CRPM) (see Figure 2.3b).

- **Over-constrained** $m > n + 1$, also called Redundantly Constrained Positioning Machines (RCPM). (see Figure 2.3c).

The last two kind of robots are not kinematically redundant as they only have one solution to the inverse kinematic problem, the redundancy refers to their actuation as there are more

kinematic constrains than DOF of the end-effector. As consequence, there are infinite possible force distributions that fulfill the static equilibrium of the robot.

Classification according to motion patterns. We consider motion patterns as the movements that can be generated by the superposition of the three purely translational and the three purely rotational displacements where these directions are consider as translation along and rotation about the axes of Euclidean coordinate system. In these sense the maximum number of DOF for a CDPR is 6. In the notation we will abbreviate translation as T and rotation as R, therefore, a CDPR with full movement in 3 dimensional translations and 3 rotations would be 3T3R.

If we consider only the spatial dimensions in which the robot workspace extends, one can consider three categories:

- **Linear robots** this kind of robots is trivial and have a one DOF purely translational motion.
- **Planar robots** move in a plane and thus have two translational DOF. They can also have a rotational DOF in the axis perpendicular to the moving plane (2T1R, see Figure 2.3b) or not (2T0R see Figure 2.3a).
- **Spatial robots** can move in the three-dimensional space i.e. they have 3 translational DOF (3T). The number of rotational DOF can also be restricted for this kind of robots yielding to 3T0R, 3T1R, 3T2R and 3T3R robots (see Figure 2.3c).

The robots under study on this thesis are specifically designed for applications on planar surfaces and where orientation control is not required, therefore they are considered as 2T0R CDPR in terms of motion pattern.

Suspended robots. Besides these classifications, when all cable forces act against the gravity for a certain pose then this pose is called *suspended*. When this happens in general, for each pose the robot can reach, the robot itself is called *suspended cable driven parallel* robot or simply *suspended cable robot* (see Figure 2.3a), this kind of robots rely on the gravity force acting as an extra cable to be balanced.

The different types of CDPR according to these classifications are depicted in Figure 2.3.

2.3 Kinematic models

The *inverse kinematic* (IK) model computes the cable lengths $\boldsymbol{l} = l_1, ..., l_m$ that correspond to a certain end-effector pose $\boldsymbol{q}$ for a given CDPR geometry A_i and B_i for $i = 1, ..., m$. In this sense the inverse kinematic model can be expressed as:

$$\boldsymbol{l} = \boldsymbol{\varphi}^{IK}(\boldsymbol{r}, \boldsymbol{R}) \tag{2.1}$$

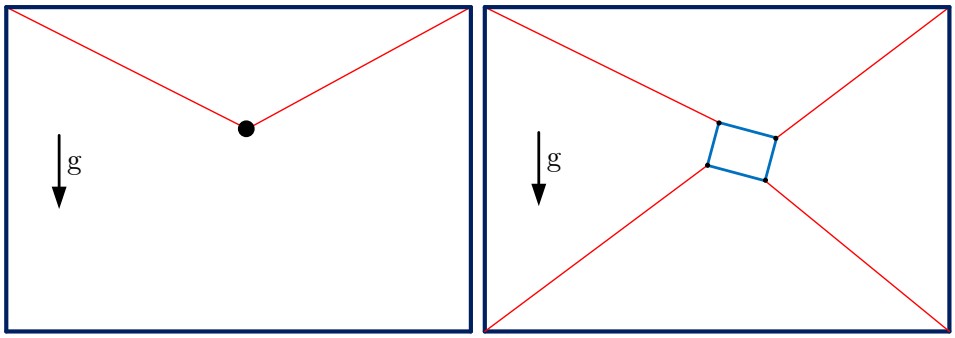

(a) Under-constrained planar robot with $m \leq n$ and 2T0R motion pattern

(b) Fully-constrained planar robot with $m = n + 1$ and 2T1R motion pattern

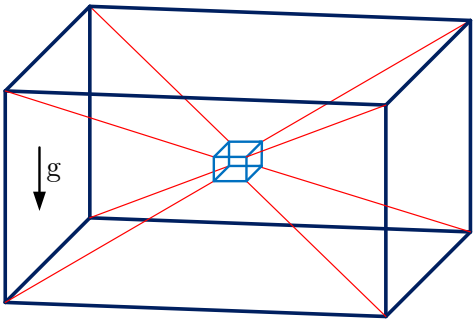

(c) Over-constrained spatial CDPR with $m \geq n + 1$ and 3T3R motion pattern

Figure 2.3: Classification of Cable Driven Parallel Robots

In general the inverse kinematics model is employed to obtain the required set-points for the actuators to generate the desired motion of the end-effector. The solution of this problem is unique and can be easily obtained for any generic CDPR. The IK model only takes into account the geometry of the robot, the existence of a solution in a certain pose does not guarantee the possibility of mechanical equilibrium in that pose [54].

Considering the notation exposed in Figure 2.2, the inverse kinematic model of a general CDPR can be obtained as presented in [55]. Applying a vector loop from the origin of κ_0 passing through the origin of κ_e, B_i and A_i and coming back to κ_0, the following can be expressed:

$$\boldsymbol{a}_i - \boldsymbol{r} - \boldsymbol{R}\boldsymbol{b}_i - \boldsymbol{l}_i = 0 \tag{2.2}$$

The cable vectors can be easily obtained as:

$$\boldsymbol{l}_i = \boldsymbol{a}_i - \boldsymbol{r} - \boldsymbol{R}\boldsymbol{b}_i \tag{2.3}$$

and cable lengths are simply their euclidean norm $l_i = ||\boldsymbol{l}_i||_2$.

This simple model does not consider the effect of any pulley located between the winch and the end-effector to guide the cable. For the scope of this work, this assumption is valid as no guiding pulleys are employed in [56] and, the ones employed in [57] have a constant orientation, therefore having no implications from a geometric point of view.

The *forward kinematic* (FK) model of a CDPR aims to determine the end-effector pose $(\boldsymbol{r}, \boldsymbol{R})$ from a given cable lengths $\boldsymbol{l}$:

$$(\boldsymbol{r}, \boldsymbol{R}) = \boldsymbol{\varphi}^{FK}(\boldsymbol{l}) \tag{2.4}$$

The end-effector pose is a required input in most closed-loop control systems for CDPR. However, measure the end-effector pose in CDPR is not always suitable due to high costs or to the lag introduced in the measurement. Therefore, the main application of FK models in CDPR is to estimate the end-effector pose in systems where it can not be directly measured but cable lengths can be obtained from the actuators encoders or resolvers. These measures are cost-effective and quick enough for being used in real-time systems. For a generic CDPR, the solution of the FK problem is significantly more difficult than the IK one [58]. Depending on the specific robot configuration and the value of $\boldsymbol{l}$ there might be one, multiple, none or even infinite solutions and, in general, no closed form for the model can be found. Instead, numerical approaches are employed to provide feasible solutions in real time to the control algorithm [54]. However, in the case of the CDPR under consideration in this thesis, due to its simplified geometry, a closed form of the FK model can be derived.

2.4 Statics

Determine whether the end-effector can be balanced by the cables in a certain pose, while, simultaneously, the force distribution fulfills certain conditions is required for determining the CDPR workspace (see Section 2.5). Following the analysis given in [55], and considering the most generic case of a 3T3R CDPR, the end-effector can be balanced if the following holds true:

$$\begin{cases} \sum_{i=1}^{m} \boldsymbol{f}_i + \boldsymbol{f}_e = 0 \\ \sum_{i=1}^{m} \boldsymbol{b}_i \times \boldsymbol{f}_i + \boldsymbol{\tau}_e = 0 \end{cases} \tag{2.5}$$

where $\boldsymbol{f}_i = f_i \cdot \boldsymbol{u}_i$ is the force vector of the i-th cable. Note that, according to the direction of $\boldsymbol{u}_i$ (see Figure 2.2), a positive cable force pulls the end-effector towards the robot frame and positive values for tension cause a decrement in cable length. These equations can be rewritten in matrix form to yield:

$$\boldsymbol{A}^T(\boldsymbol{r}, \boldsymbol{R})\boldsymbol{f} + \boldsymbol{w}_e = 0 \tag{2.6}$$

where:

$$\boldsymbol{A}^T(\boldsymbol{r},\boldsymbol{R}) = \begin{bmatrix} \boldsymbol{u}_1 & ... & \boldsymbol{u}_m \\ \boldsymbol{b}_1 \times \boldsymbol{u}_1 & ... & \boldsymbol{b}_m \times \boldsymbol{u}_m \end{bmatrix} \tag{2.7}$$

is a $n \times m$ matrix being n the number of DOF of the robot and m the number of cables, $\boldsymbol{f} = [f_1, ..., f_m]^T$ is the vector of cable forces and $\boldsymbol{w}_e = [\boldsymbol{f}_e, \boldsymbol{\tau}_e]^T$ is the matrix of external wrench applied to the end-effector. The matrix $\boldsymbol{A}^T$ is the transpose of the Jacobian matrix, frequently called as *structure matrix*, it depends on the end-effector pose and converts $\boldsymbol{f}$ from the joint space (JS) into the forces and torques applied by the cables to the end-effector in the operational space (OS).

The solutions that can be obtained from (2.6) depend on the CDPR type according to the previously exposed kinematic classification. For robots with $m < n$, the algebraic system is over-constrained and solutions to this equation can only be expected for certain end-effector poses if $\boldsymbol{A}^T$ has full-rank. For robots with $m = n$, $\boldsymbol{A}^T$ is quadratic and there exist exactly one solution for each pose. Finally, for robots of the kinds CRPM and RRPM with $m > n$ the equations system is under-constrained and there are infinite solutions to the problem. In this latter case, finding a solution becomes a key challenge as the unidirectional nature of cable forces ($\boldsymbol{f} > 0$) must also be taken into account. An extensive review on the different approaches employed to solve this problem in OC CDPR can be found in [47].

2.5 Workspace

From the formal point of view, and taking into account a generic CDPR, the workspace is the subset W of the Euclidean motion group SE_3, represented as the pair $(\boldsymbol{r}, \boldsymbol{R}) \in \mathbb{R}^3 \times SO_3$, that can be generated by moving the robot end-effector. Since this six-dimensional workspace is difficult to represent, there are several simplifications that, by considering application-driven restrictions, reduce or project it to a two or three dimensional space that can be easily visualized. A complete enumeration of the different commonly used subsets of W can be found in [59] (See Section 5.1.3).

For the scope of this work, as we study CDPR of the 2T0R kind, the constant orientation workspace W_{CO} is of interest. It is a slice of the general workspace for a fixed orientation of the end-effector:

$$\mathbb{W}_{CO}(\boldsymbol{R}_0) = \{\boldsymbol{r} \in \mathbb{R}^3 | (\boldsymbol{r}, \boldsymbol{R}), \boldsymbol{R} = \boldsymbol{R}_0\} \tag{2.8}$$

The dimension of this workspace is equal to the number of translational DOF of the robot. Determining the workspace of a robot consist of deciding whether each pose of the end-effector belong or not to its workspace. There are many criteria to determine it, in CDPR, the most basic one is checking if the end-effector can be statically balanced by cables with positive tension. Additional considerations can be the practical tension limits, maximum deflection angle of cables both in proximal and distal anchor points, the presence of kinematic singularities, the presence of obstacles, collision between cables or between cables and the end-effector, or the maximum cable length allowed by the actuation system. For the scope of this work we consider two criteria to determine the workspace:

- **Wrench-Closure Workspace** (WCW). For determining this workspace, only the positive restriction on cable forces is considered. Therefore, a pose belongs to the WCW if for every external wrench $\boldsymbol{w}_e$ the end-effector can be balanced with positive cable tensions and at least one solution exists to:

$$\boldsymbol{A}^T\boldsymbol{f} + \boldsymbol{w}_e = 0 \quad \text{s.t.} \quad \boldsymbol{f} > 0 \tag{2.9}$$

  This workspace definition does not consider practical limitations as upper or lower cable forces limits but only the most theoretical one, therefore its practical implications are limited.

- **Wrench-Feasible Workspace** (WFW). The practical upper and lower tension limits are considered for determining the WFW. In this sense, it is defined as the set of end-effector poses where, for any external wrench $\boldsymbol{w}_e \in Q$ there is at least one force distribution $\boldsymbol{f}$ that fulfills the following:

$$\boldsymbol{A}^T\boldsymbol{f} + \boldsymbol{w}_e = 0 \quad \text{with} \quad 0 < f_{min} < \boldsymbol{f} < f_{max} \tag{2.10}$$

  It is clear that the WFW depends both on the cable force limits (f_{min}, f_{max}) and on the set of external wrenches Q that must be withstanded by the end-effector. For the scope of this work, the WFW is computed considering that the robot only has to balance its own weight, i.e. $\boldsymbol{w}_e = [0, 0, -g \cdot m_e, 0, 0, 0]^T$ for the spatial case and $\boldsymbol{w}_e = [0, -g \cdot m_e, 0]^T$ for the planar case, where m_e is the end-effector mass.

  There are several points to take into account to set the upper limit f_{max}, however, the maximum force that can be generated by the motors often sets the effective upper limit. Special care must be taken to predict the force that can be generated by the drive brakes during and emergency situation. Other factors include the maximum force supported by the cables, even though CDPR are dimensioned so that breaking load of the cables is much higher than the maximum force that can be generated by the motors, the fixing of the cable to the driving mechanism can significant reduce the breaking load of the cable. In CDPR where the end-effector is reconfigurable to accomplish different tasks, it is also important to consider the different maximum forces that can be supported by the different end-effectors.

  Regarding the lower limit for cable forces f_{min}, the main aspect to consider is cable slackness. Sagging is an effect that will appear on every cable subject to the gravity effect, its magnitude depends on the cable length, density and tension. Tension reduces the cable sagging, therefore, if straight cables are consider by the robot models, ensuring a sagging low enough to be neglected is required. A detailed explanation on how to estimate f_{min} to neglect cable sagging can be found in [55], Section 3.4.5.2. Additionally, a minimum cable tension is required for the reliable operation of the robot: low tension can cause cables to slip in or even to leave the drums where they are being coiled and can also cause the cable to slip in the pulleys, which would lead to additional cable

wearing and will cause errors if the pulleys rotation is being measured and used as an input to the control system. An extensive study on the limitations of cable forces in CDPR can be found in [39].

2.6 Stiffness

The stiffness of a CDPR is defined as its ability to withstand arbitrarily applied forces and torques [55]. In a quantitative way, it is characterized as the infinitesimal displacements $\delta \boldsymbol{q}$ that the end-effector experiment when an infinitesimal wrench is applied to it $\delta \boldsymbol{w}_e$. If only linear effects are considered, the following relation can be obtained:

$$\delta \boldsymbol{w}_e = \boldsymbol{K}(\boldsymbol{q}) \delta \boldsymbol{q} \tag{2.11}$$

where $\boldsymbol{K}$ is the so-called *stiffness matrix* which depends on the pose $\boldsymbol{q}$ and relates the displacement $\delta \boldsymbol{q}$ to the applied wrench $\delta \boldsymbol{w}_e$ in the OS.

The robot stiffness results from the elastic deformation mainly of the cables. However, other components can have a significant elastic deformation that plays a role on the stiffness as the winches and actuators, the frame and the end-effector. If cables are modeled as linear springs [50], the relation between the length increment $\delta \boldsymbol{l}$ caused by a $\delta \boldsymbol{f}$ applied to them yields:

$$\delta \boldsymbol{f} = \begin{bmatrix} k_1 & & 0 \\ & \ddots & \\ 0 & & k_m \end{bmatrix} \delta \boldsymbol{l} = \boldsymbol{K}_c \delta \boldsymbol{l} \tag{2.12}$$

being $\boldsymbol{K}_c$ the actuator stiffness matrix and k_i the spring constant of the $i-th$ cable. If the cables are coiled in drums, k_i changes with cable length, therefore, $\boldsymbol{K}_c$ is pose dependent, and the expression of k_i yields:

$$k_i = \frac{k'}{l_i + l_i^0} \tag{2.13}$$

where k' is a material-dependent parameter, l_i is the variable cable length and l_i^0 is the constant cable length that results from the cable passing from A_i through different pulleys to the point where the cable is coiled in the drum. By using the structure matrix $\boldsymbol{A}^T$ and its transpose $\boldsymbol{A}$, (2.12) can be converted to OS to obtain the relation between $\delta \boldsymbol{w}_e$ and $\delta \boldsymbol{q}$:

$$\delta \boldsymbol{w}_e = \boldsymbol{A}^T \begin{bmatrix} k_1 & & 0 \\ & \ddots & \\ 0 & & k_m \end{bmatrix} \boldsymbol{A} \delta \boldsymbol{q} = \boldsymbol{K}_o \delta \boldsymbol{q} \tag{2.14}$$

This model of the stiffness does not consider the change in $\boldsymbol{A}^T$ caused by $\delta \boldsymbol{q}$. To consider this non-linear effect, the concept of *geometric stiffness* is introduced [50, 60], where the stiffness for a given pose yields:

$$\delta \boldsymbol{w}_e = -\boldsymbol{A}^T \delta \boldsymbol{f} - \frac{\partial \boldsymbol{A}^T}{\partial \boldsymbol{q}} \boldsymbol{f} \delta \boldsymbol{q} = \boldsymbol{K}_{os} \delta \boldsymbol{q} \tag{2.15}$$

being $\boldsymbol{K}_{os}$ is the overall stiffness matrix which reads, as shown by [50]:

$$\boldsymbol{K}_{os} = -\frac{\partial \boldsymbol{A}^T}{\partial \boldsymbol{q}} \boldsymbol{f} + \boldsymbol{A}^T \boldsymbol{K}_c \boldsymbol{A} = \boldsymbol{K}_G + \boldsymbol{K}_o \tag{2.16}$$

As can be observed, according to this model the stiffness of the robot also depends on the cable forces. This makes sense as the eigenfrequencies of the robot depends on the stiffness, on the other hand, the connection between cable tension and its eigenfrequency its well known from any string music instrument [55]. The overall stiffness matrix $\boldsymbol{K}_{os}$ has two different terms, the already explained $\boldsymbol{K}_o$ which represent the linear elongation of the cables, moreover, if non-linear models of cables are considered, this term will also be force-dependent. On the other hand $\boldsymbol{K}_G(\boldsymbol{f}, \boldsymbol{q})$ is the so-called *geometric stiffness matrix* and depends both on the end-effector pose $\boldsymbol{q}$ and on the cable forces $\boldsymbol{f}$. In [61] it is experimentally shown that for planar CDPR, the term that has more influence in the robot stiffness is $\boldsymbol{K}_G$.

As explained before, a high stiffness allows the CDPR to better withstand externally applied wrenches. The stiffness of a specific CDPR can be modified by using higher cable tensions. On the other hand, higher tensions can cause actuator overload and have also implications on the energy consumption of the robot. In this sense, a trade-off between stiffness and feasible cable tension values must be considered.

2.7 Dynamic models

The kinematic and static models of CDPR exposed so far always consider the robot in steady state. The dynamic models, on the other hand, provide insight on the time evolution of the forces, torques and accelerations of the different elements of the robot that cause its motion.

The robot *forward dynamics* (FD) relates the inputs of the actuation system to the torques it generates, to the cable forces and therefore with the acceleration of the end-effector. Considering the voltage input to the electric motors of the actuation system ($\boldsymbol{V}$) as the inputs, the FD read:

$$(\ddot{\boldsymbol{r}}(t), \ddot{\boldsymbol{R}}(t)) = \varphi^{FD}(\boldsymbol{V}(t)) \tag{2.17}$$

The FD consist of a system of ordinary differential equations, where those modeling the mechanical elements are naturally of second-order. This represents an initial value problem that is usually solved by means of numerical methods. By integrating the output of the FD, the linear/rotational speed $(\dot{\boldsymbol{r}}(t), \dot{\boldsymbol{R}}(t))$ and the pose $(\boldsymbol{r}(t), \boldsymbol{R}(t))$ of the end-effector versus time can be obtained. The FD of CDPR are of major utility as they allow to simulate the full behavior of the robot, when combined with kinematic and static models. This is specially useful for the design and optimization of the robot control system as well as for the structural and geometrical design of new robots when high dynamics are expected during its normal operation [62].

From its part, the *inverse dynamics* (ID) receives the motion of the end-effector and sought the forces and torques required to generate it:

$$(\boldsymbol{V}(t)) = \varphi^{ID}(\ddot{\boldsymbol{r}}(t), \ddot{\boldsymbol{R}}(t)) \tag{2.18}$$

The ID consist of a set of algebraic equations which in many cases can be computed in closed form and is useful in feed-forward control strategies [62].

Without taking into account any control strategy, the FD model of a generic CDPR that considers $\boldsymbol{V}$ as input and the end-effector acceleration, speed and pose, i.e. $(\boldsymbol{r}, \boldsymbol{R}), (\dot{\boldsymbol{r}}, \dot{\boldsymbol{R}}), (\ddot{\boldsymbol{r}}, \ddot{\boldsymbol{R}})$, as output is shown in Figure 2.4. The name *actuators* refers to the set motor-gearbox-drum used to coil the cables, $\boldsymbol{\tau}$ is the array of torques generated by each motor, $\boldsymbol{\theta}$ is the array of effective angles of each winch, $\boldsymbol{f}$ and $\boldsymbol{l}$ are the arrays of cable forces and lengths, respectively and $\boldsymbol{w}_e$ the externally applied wrench to the end-effector.

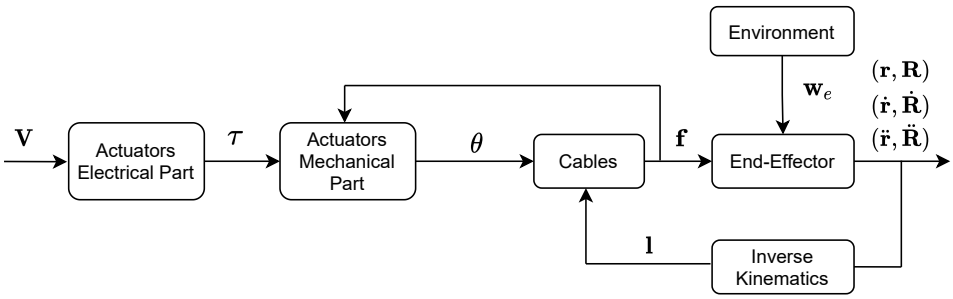

Figure 2.4: Structure of the forward dynamics of a generic CDPR

For the scope of this work, several assumption are made to expose the dynamic modeling of CDPR. Guiding pulleys employed in [56, 57] have an inertia low enough to disregard their dynamic effects. As this thesis studies the case of planar robots, only two translational and one rotational DOF will be considered for the end-effector, however, the specific robots under study do not have the rotational DOF, i.e. they are 2T0R CDPR from the motion pattern point of view. For the dynamic modeling inextensible and mass-less cables are considered according to [63]. Specifically, in [56] inextensible and mass-less cables are considered for dynamic modeling whereas in [57] cables are considered elastic only for stiffness analysis purposes.

Modeling of the actuators For modeling the actuators, the electrical behavior of direct current (DC) motors is considered as these kind of motors are employed in [56]. The relation between the input voltage ($\boldsymbol{V}^{m\times1}$) and the current ($\boldsymbol{I}^{m\times1}$) of the motor reads:

$$\boldsymbol{V} = \boldsymbol{R}\boldsymbol{I} + \boldsymbol{L}\dot{\boldsymbol{I}} \tag{2.19}$$

where $\boldsymbol{R}^{m\times m}$ and $\boldsymbol{L}^{m\times m}$ are diagonal matrix representing the resistance and inductance of the m motor windings, respectively. The relation between the windings current and the

torque generated by the motors $\boldsymbol{\tau}^{m\times 1}$ is given by the torque constant k_a, which, in general can be considered the same for every motor of the actuation system:

$$\boldsymbol{\tau} = k_a \boldsymbol{I} \tag{2.20}$$

From the mechanical point of view, the torque equilibrium equation in the drum can be expressed as:

$$\boldsymbol{\tau} = \boldsymbol{J}\ddot{\boldsymbol{\theta}} + \boldsymbol{\nu}\dot{\boldsymbol{\theta}} + \boldsymbol{\Gamma}(\dot{\boldsymbol{\theta}}, \boldsymbol{\tau}) + \boldsymbol{r}\boldsymbol{f} \tag{2.21}$$

where $\boldsymbol{J}^{m\times m}$ and $\boldsymbol{\nu}^{m\times m}$ represent the combined inertia and viscous friction of the motors axis, gearboxes and drums, respectively, $\boldsymbol{r}^{m\times m}$ is the effective radius of the drums, $\boldsymbol{f}^{m\times 1}$ is the array of cable forces, $\boldsymbol{\theta}^{m\times 1}$ is the array of motor angles and $\boldsymbol{\Gamma}(\dot{\boldsymbol{\theta}}, \boldsymbol{\tau})^{1\times m}$ is the array of Coulomb frictions, which can be modeled, for the $i-th$ motor as:

$$\Gamma_i(\dot{\theta}_i, \tau_i) = \begin{cases} \Gamma_i = \tau_s \cdot sign(\dot{\theta}_i) & if \quad |\tau_i| > \tau_s \ \ \& \ \ |\theta_i| > 0 \\ \Gamma_i = \tau_i \cdot sign(\dot{\theta}_i) & if \quad |\tau_i| \leq \tau_s \ \ \& \ \ |\dot{\theta}_i| > 0 \\ \Gamma_i = \tau_s \cdot sign(\tau_i) & if \quad |\tau_i| > \tau_s \ \ \& \ \ |\dot{\theta}_i| = 0 \\ \Gamma_i = \tau_i \cdot sign(\tau_i) & if \quad |\tau_i| \leq \tau_s \ \ \& \ \ |\dot{\theta}_i| = 0 \end{cases} \tag{2.22}$$

Note that two non-linear terms are present in (2.21), namely the torques applied by the cables, which depend on the end-effector pose and the overall cable force distribution in the robot, and the Coulomb friction. The non-linear behavior of cable forces has important implications on the design of control systems for CDPR (see Section 2.8). Assuming that the electro-mechanical differences between the actuators within the system are small enough to employ the same value for the parameters (R, L, J, ν) of each actuator, the following can be considered:

$$\begin{cases} \boldsymbol{R} = R \cdot \boldsymbol{I}_m \\ \boldsymbol{L} = L \cdot \boldsymbol{I}_m \\ \boldsymbol{J} = J \cdot \boldsymbol{I}_m \\ \boldsymbol{\nu} = \nu \cdot \boldsymbol{I}_m \\ \boldsymbol{r} = r \cdot \boldsymbol{I}_m \end{cases} \tag{2.23}$$

where R, L, J, ν, r are the nominal values of the motor winding resistance, motor winding inductance, drive set inertia viscous friction and effective radius, respectively, and $\boldsymbol{I}^m$ the $m \times m$ identity matrix.

Model of the end-effector The end-effector dynamic model relates the forces applied to the end-effector in the JS to its acceleration in the OS, with respect to the euclidean inertial reference system κ_0. As previously mentioned, for the dynamic modeling only two translational (translation along x and y axes) and one rotational (rotation about z axis ϕ_z) degrees-of-freedom will be considered. In this sense, the end-effector pose can be expressed as $\boldsymbol{q} = [x, y, \phi_z]^T$.

Considering inextensible cables and neglecting the dynamic effect of guiding pulleys, the forces that appear on (2.8) are the same that act on the end-effector, as explained in Section 2.4, they can be converted from the JS to the OS by means of the structure matrix $\boldsymbol{A}^T(\boldsymbol{q})$. The static equilibrium equation of the end-effector ((2.6), see Section 2.3) is only modified in the sense that the right term is no longer zero, but the translational and rotational acceleration of the end-effector appear:

$$\boldsymbol{A}^T\boldsymbol{f} + \boldsymbol{w}_e = \boldsymbol{M}\ddot{\boldsymbol{q}} \tag{2.24}$$

where the mass matrix $\boldsymbol{M}$ is:

$$\boldsymbol{M} = \begin{bmatrix} m_e & 0 & 0 \\ 0 & m_e & 0 \\ 0 & 0 & I_z \end{bmatrix} \tag{2.25}$$

being m_e and I_z the end-effector mass and inertia about the z-axis, respectively. Note that the friction between the end-effector and the air is disregarded as it can only have a noticeable influence in ultra-high speed application or for robots working in a fluid environment different from air (e.g. underwater robots) [62]. For the same reason, the effects of Coriolis acceleration are also neglected in the rotational dynamics.

2.8 Control strategies

2.8.1 Preliminaries

The control systems of CDPR can be broadly divided into two main categories: kinematic and dynamic control.

Kinematic control approaches only take into account the robot inverse kinematic model. The desired end-effector trajectory is therefore mapped from the operational space into the joint space by means of the inverse kinematic model, obtaining the desired angles for the robot actuator. Normally, state of the art servocontrollers are employed to set the desired motor angles. Note that servocontrollers use internal dynamic control for controlling the motor angles, however, from the CDPR control system design point of view, any dynamical considerations are disregarded when employing kinematic control. This approach is the most simple one and easy to implement, nevertheless, it strongly relies on the precision and completeness of the kinematic model and is not robust in front of any perturbation affecting the robot or unconsidered behavior of the robot in the kinematic model [64].

On the other hand, dynamic control approaches consider the dynamics of the robot, which normally can be divided in actuators or winches dynamics, cables dynamics and end-effector dynamics. As this is the approach employed in this thesis, fundamentals of dynamic control of CDPR will be addressed in more detail. As previously mentioned, the FD are specially useful to design effective control strategies for CDPR. From the control design point of view, several considerations are made. Firstly, the dynamics of the electrical part of the actuators can be neglected as long as the time constant of (2.19) is much lower than that of (2.21).

Ignoring the non-linear part of (2.21), and applying Laplace transform, the transfer functions of the electrical and mechanical part of the actuators read:

$$\begin{cases} \frac{I(s)}{V(s)} = \frac{1/R}{1+\frac{L}{R}s} \\ \frac{\theta(s)}{\tau(s)} = \frac{1/\nu}{s(1+\frac{J}{\nu}s)} \end{cases} \tag{2.26}$$

where the time constant of the electrical and mechanical parts are $T_e = \frac{L}{R}$ and $T_m = \frac{J}{\nu}$. It is well known from the nature of mechanical and electrical systems that $T_m >> T_e$. Consequently, the dynamics of the electrical part can be neglected in front of the dynamics of the mechanical part and (2.19) can be rewritten as an algebraic equation:

$$\boldsymbol{V} = \boldsymbol{R}\boldsymbol{I} \tag{2.27}$$

Additionally, by employing a servo-amplifier that establishes a closed loop to control the current in the motor winding, one can consider the torque generated by the motors as the input of the FD:

$$(\ddot{\boldsymbol{r}}(t), \ddot{\boldsymbol{R}}(t)) = \varphi^{FD}(\boldsymbol{\tau}(t)) \tag{2.28}$$

The structure of the torque control loop resulting when using a servo-amplifier to control the current in the motor winding is shown in Figure 2.5, where τ^* and I^* are the desired torque and current for the actuator, respectively.

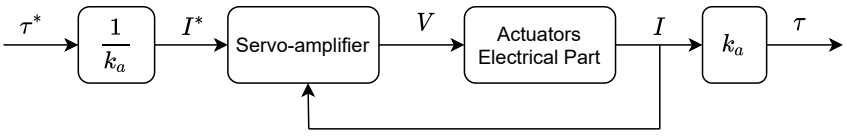

Figure 2.5: Structure of the torque control loop in the CDPR actuators

For control law design purposes, the performance of this control loop is considered to be good enough in terms of both transient and steady state to disregard its dynamics, therefore, the output of the controllers to be designed is the desired torque of the actuators. For the sake of simplicity, the torque control scheme will be omitted in the following schemes. Within dynamic control, two main categories can be considered: control in the operational space and control in the joint space [65].

2.8.2 Control in the operational space

This approach uses the end-effector pose desired trajectory $(\boldsymbol{r}^*, \boldsymbol{R}^*)$ as input, then the end-effector pose is either measured or estimated and used as feedback to the control loop, examples of this strategy can be found in [51, 66–68]. Figure 2.6 shows the general scheme of this control approach.

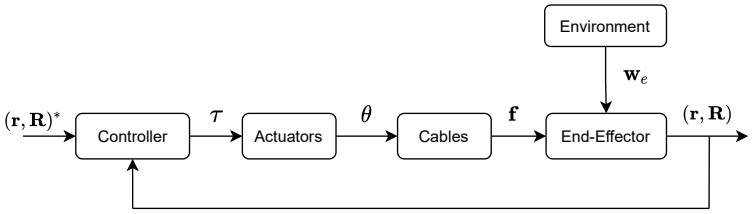

Figure 2.6: Scheme of the control of CDPR in the operational space

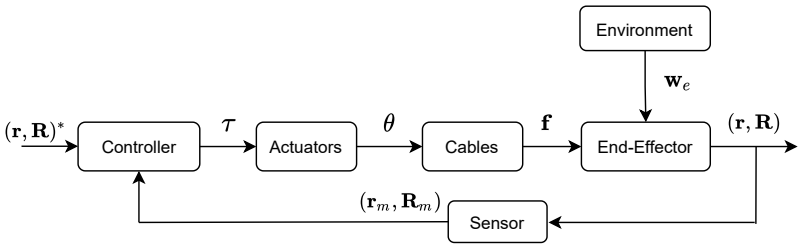

(a) Control in the OS with pose measurement

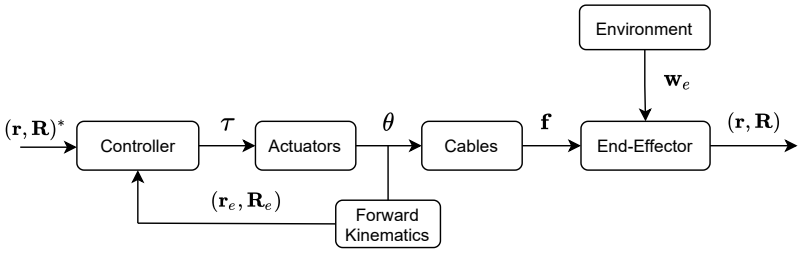

(b) Control in the OS with pose estimation

Figure 2.7: Different approaches for control in OS. $(\boldsymbol{r}_m, \boldsymbol{R}_m)$ is the measured pose from a sensing system and $(\boldsymbol{r}_e, \boldsymbol{R}_e)$ is the estimated pose from the encoders reading and the FK model.

This control approach relies on the knowledge of the end-effector pose, it can be directly measured (see Figure 2.7a) or estimated by means of the motor encoder readings and the FK model (see Figure 2.7b).

The most common approach to measure the end effector pose is by means of computer vision techniques as in [68–73], in this case the accuracy of the measurement is limited by the camera resolution. Moreover, as the measure is required as input to the control system, real-time image processing hardware and software are required, which can significantly increase the cost of the robot as in [74]. Laser techniques can also be employed for measuring the end-effector pose as in [14, 75], this technique provides high accuracy, however it requires a high cost in many practical cases. Examples of control approaches that rely on the end-effector pose estimation from motor encoders and the FK model can be found in [50, 51, 76, 77]. This latter approach presents the advantage that it only needs the readings from the robot actuator's

encoders, which are available in the vast majority of the scenarios. On the other hand, as previously mentioned FK models of parallel robots are normally computationally expensive and can yield to errors in the pose estimation that depends on the model accuracy and completeness. In [78], the end-effector pose is estimated through the observer linearization technique using the joints position and velocity.

In OS control, the controller inputs, i.e. the desired and measured/estimated end-effector pose, have size $1 \times n$, while the output is normally the torque reference for the actuators, with size $1 \times m$. In this sense, the controller has to deal with how the torque in the JS affects the wrench and therefore the pose in the OS. To compute the desired wrench to be applied by the cables to the end-effector, the pose error, i.e.:

$$E_q = (\boldsymbol{r}, \boldsymbol{R})^* - (\boldsymbol{r}, \boldsymbol{R}) \tag{2.29}$$

is employed as the input to different kind of controllers as P [77] or PID [51] controllers, adaptive robust controllers [79], H_∞ [71] or sliding mode controllers [80–82]. From the desired wrench, the corresponding cable forces distribution is obtained by means of the inverse, or pseudo-inverse in the case of OC CDPR, of $\boldsymbol{A}^T$ and its feasibility is guaranteed in the case of OC CDPR by means of additional algorithms normally based on the nullspace of $\boldsymbol{A}^T$. To apply the obtained cable force distribution in the robot, independent torque controllers are employed for each actuator in the JS.

2.8.3 Control in the joint space

In JS control, the desired cable lengths are computed from the desired end-effector trajectory and by means of the IK model, then the actuators angles are controlled to set the desired cable lengths using the measured angles from encoders as feedback, examples of this approach can be found in [2, 65, 67, 83–85]. In the case of OC CDPR, additional force control is usually implemented together with position control in the actuators to maintain a feasible force level in all cables as in [67, 85]. An overview of this control strategy topology can be seen in Figure 2.8.

The main advantages of this approach are that encoders are widely available in every commercial motor and provide an accurate and high speed measure of the motor angle. Additionally, the input to the controller is the array of desired motor angles with size $1 \times m$ and its output the array of motor torques of the same size, therefore an uncoupled controller can be used for each motor, allowing the employment of well-known control techniques.

On the other hand, this approach has several drawbacks. The correctness of the IK model plays a crucial role to achieve an accurate trajectory tracking in the OS by means of JS control. While there are complex kinematic models that take into account pulley geometry, cable elasticity and cable sagging due to its mass [38], the more complex the model, the more parameters it requires, being parameters regarding cable properties usually difficult to measure or estimate precisely [64]. Moreover, complex kinematic models require a considerable computational effort which is not always compatible with real-time control applications [86]. Cable length can not always be precisely related to motor angles, specially

in presence of non-neglectable flexible cables, or sagging cables due to cable mass or low tension [65].

Finally, due to the non-linear nature of CDPR dynamics, the load applied to each motor strongly varies with the end-effector pose, causing conventional linear control techniques to yield poor performance when applied to the control of CDPR in the JS [14].

To compensate the non-linear terms of the dynamics, a common approach is to use feed-forward linearization of the non-linear terms that appear on the actuators dynamic model as in [29, 65, 85, 87–90]. Different control approaches have been used to control CDPR in the JS as PD controllers [84, 85], impedance control [67] or fuzzy controllers [83]. In [65] a synchronization controller is employed to simultaneously eliminate tracking and synchronization error in the JS. In [91] a PD controller is employed in the JS to compute the desired torque for actuators, then converted to wrench in the OS and the dynamics of the end-effector compensated by means of inverse dynamics feed-forward. From this wrench, a feasible tension distribution is computed and the viscous and dry friction of the actuators compensated by another feed-forward term to obtain the final desired torque for the actuators. In [92], the use of a wave based control in the OS is proposed together with a conventional PD controller in the JS to avoid vibrations in the end-effector of deployable CDPR with high uncertainty in their model parameters.

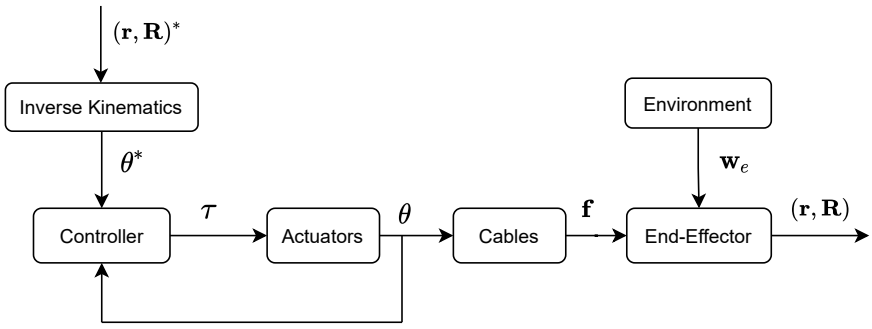

Figure 2.8: Scheme of the control of CDPR in the joint space

Chapter 3

Problem statement and methodology

In this chapter, in first place, an outlook on the currently open problems in the field of CDPR is provided, along with the classification of the contributions of this thesis within these currently open problems. The contribution of this thesis is organized in three specific works that address, respectively, the problem of using CDPR in large, vertical surfaces, the problem of using CDPR in large, horizontal surfaces and the problem of measuring cable tension in CDPR. Subsequently, the opportunities and challenges that arise regarding the application of CDPR to the previously kind of workspaces are outlined. Additionally, the importance and challenges regarding cable tension measurement in CDPR are explained. Finally, the different methodologies employed to address these problems are exposed.

3.1 Problem statement

3.1.1 Introduction and outlook

According to the proceedings of the 5th International Conference on Cable-Driven Parallel Robots [93] the most recent research on CDPR can be classified in the following fields:

- **Kinematics.** Research in this field focus on modeling complex effects like cable sagging and elasticity and improving the efficiency in solving such models by means of techniques as neural networks.
- **Statics and force distribution.** Works in this area study how to solve force distribution of over-constrained CDPR.
- **Control.** This subject is closely related to the previous one as over-constrained CDPR require a simultaneous control of the end-effector pose and cable forces. Research in this area includes new control approaches to tackle this issue.
- **Design.** New designs of CDPR are being investigated within this area. Special interest is found in reconfigurable or variable-structure CDPR for specific applications. Another line of work on this area is optimization of CDPR design to achieve greater workspace.
- **Calibration and performance improvement.** Works on this field investigate procedures for CDPR calibration and performance improvement in terms of accuracy and safety.
- **Applications.** This field includes new application proposals along with specific robot designs and prototypes evaluation.

Considering these research lines, the contributions of this thesis can be classified as shown in Figure 3.1. The application of CDPR for large, planar areas brings the need of designing two new mechanical concepts for planar CDPR to overcome the workspace limitations of the conventional ones, which constitutes the contribution to the *design* investigation line.

As the new designs incorporate significant differences in geometry, compared with the conventional planar CDPR, a reformulation of the well-known inverse kinematic model is required, therefore contributions to the *kinematics* line are also provided. The modified geometry causes a decrease in the stiffness of the robots which in turn generates undesired vibrations. These are compensated by means of specifically designed control approaches, constituting the contribution to the *control* line.

The importance of covering large, planar workspaces with the gravity oriented either in the same plane or perpendicular to the working plane comes from specific applications as the inspection of civil infrastructures, which represents the thesis contribution to the *applications* research line. A specific work has focused on the development of sensorization solutions for measuring cable tension in any kind of CDPR, which represents the contribution to the *calibration and performance improvement* research line.

Apart from the main contributions of this thesis, there are two additional contributions in the form of book chapters in the proceedings of the fourth and fifth International Conference on Cable-Driven Parallel Robots. In the first one [94], replacing conventional cables with chains and the using of counterweights are proposed for a planar, suspended CDPR to reduce the required power. This work represents a contribution to the *design* and *calibration and performance improvement* research lines.

In the second one [64], a methodology to keep cable forces within the desired limit in over-constrained CDPR is proposed. This approach employs the nullspace of the structure matrix to compute cable force corrections in real time. In this sense, it makes a contribution to the *statics and force distribution* and *control* research lines.

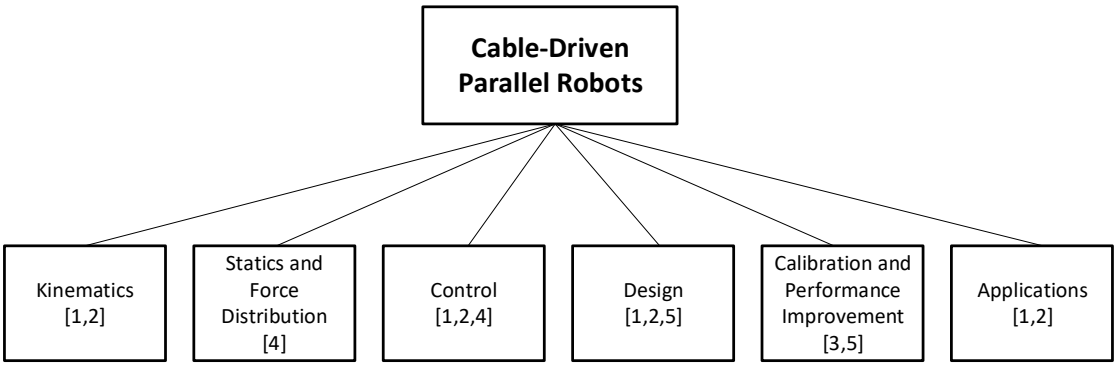

Main contributions:

[1] Rubio-Gomez, G., Juárez, S., Rodríguez-Rosa, D., Bravo, E., Ottaviano, E., Gonzalez-Rodriguez, A., & Castillo-Garcia, F. J. (2021). Addition of passive-carriage for increasing workspace of cable robots: automated inspection of surfaces of civil infrastructures. Smart Structures and Systems, 27(2), 387.

[2] Juárez-Pérez, S., González-Rodriguez, A., Rubio-Gómez, G., Rodríguez-Rosa, D., Ottaviano, E., & Castillo-Garcia, F. J. (2021). Closed loop cable robot for large horizontal workspaces. Smart Structures and Systems, 27(2), 397.

[3] Rubio-Gómez, G., Juárez-Pérez, S., Gonzalez-Rodríguez, A., Rodríguez-Rosa, D., Corral-Gómez, L., López-Díaz, A. I., & Castillo-García, F. J. (2021). New Sensor Device to Accurately Measure Cable Tension in Cable-Driven Parallel Robots. Sensors, 21(11), 3604.

Additional contributions:

[4] Fabritius M., Martin C., Gomez G.R., Kraus W., Pott A. (2021) A Practical Force Correction Method for Over-Constrained Cable-Driven Parallel Robots. In: Gouttefarde M., Bruckmann T., Pott A. (eds) Cable-Driven Parallel Robots. CableCon 2021. Mechanisms and Machine Science, vol 104. Springer, Cham.

[5] Rubio-Gómez G., Rodríguez-Rosa D., García-Vanegas J.A., Gonzalez-Rodríguez A., Castillo-García F.J., Ottaviano E. (2019) Chain Driven Robots: An Industrial Application Opportunity. A Planar Case Approach. In: Pott A., Bruckmann T. (eds) Cable-Driven Parallel Robots. CableCon 2019. Mechanisms and Machine Science, vol 74. Springer, Cham.

Figure 3.1: Contributions of this thesis to the different research lines of CDPR

In the following subsections the problems that are addressed in this thesis are discussed,

being classified from the application point of view. As the measurement of the cable tension is a common problem for any CDPR and, in general, it does not depend on the application, a specific subsection is devoted to this topic.

3.1.2 Inspection of large, vertical surfaces with CDPR

In the field of civil engineering, the inspection of large, vertical surfaces is a critical task to be performed for the maintenance of facades, bridges or dams [95]. While the traditional approach is to do this inspection manually, by a person who carries the needed equipment to the required place, this approach is slow, unsafe and subject to human errors (see Figure 3.2a [1] and 3.2b [2]). Due to this, different robotic solutions to this problems are being investigated in the recent years, including the use of crane-trucks [96, 97], unmanned vehicles [98] or unmanned aerial vehicles [99] in which the inspection tool (e.g. cameras, infrared, ultrasound sensors, etc) is placed in the robot or mechanism end-effector.

(a) Bridge inspection (b) Facade inspection

Figure 3.2: Manual inspection of large vertical surfaces

Additionally, other interesting applications that presents a large, planar and vertical workspace is the storage retrieval in high racks [28] (see Figure 3.3 [3]), or the maintenance of large vertical garden [100], being the only difference in these cases that the robot end-effector will carry the required tool instead of a sensor.

For these applications, CDPR of the suspended kind (see Section 2.2) results of special interest [100]. More specifically, a suspended cable robot (SCR) with 2 cables and 2 degrees-of-freedom (i.e. $2m2n$ SCR with planar translation and no rotation) is specially well suited, a scheme of a conventional SCR with this configuration is shown in Figure 3.4a. SCR present

[1] source: `www.palfinger.com/en/products/bridge-inspection-units`

[2] source: `www.proyectos.habitissimo.es/proyecto/inspeccion-de-fachadas-por-desprendimientos-1`

[3] source:`www.viastore.com/systems/en/warehouse-and-material-flow-solutions/automated-mini-load-storage-0`

Figure 3.3: Conventional approach for storage retrieval in high racks

several advantages as they require less actuators, which is the most expensive component of the robot. If the number of cables is the same as the number of controllable DOF, they belong to the constrained CDPR type, therefore, for a certain end-effector pose, there is only one solution for the cable force distribution. They can be deployed easier than the OC ones and they have less problems regarding cable interference.

On the other hand, having the same number of cables than controllable DOF means that, when cable lengths are fixed, the end-effector can not support arbitrarily applied wrenches, and its pose is determined by the externally applied wrench [101]. Additionally, not all degrees of freedom of the end-effector can be controlled. Note that, as long as the end-effector can be considered as a punctual mass, the rotation along the axis perpendicular to the working plane does not represent a problem, if the tool to be installed needs the end-effector to have certain dimensions, a purely translational motion while keeping a constant orientation can be achieved by arranging the cables by parallel pairs with the same length [102]. To avoid rotation around the horizontal and vertical axis and displacement in the axis perpendicular to the working plane, the cable structure can be replicated in that direction, without adding additional actuators, as proposed in [100].

Another important problem of this kind of robots is its limited workspace due to practical limitations as the maximum torque that can be exerted by motors and the minimum cable tension to avoid sagging and the subsequent lost of positioning accuracy. Figure 3.4b shows the shape of the workspace of a conventional $2m2n$ SCR. Due to the robot geometry, the workspace is limited in the upper part of the frame (zone A of Figure 3.4b) because cable angles with the vertical are close to 90°, therefore the required tension to balance the end-effector weight is also high. On the other hand, the workspace is also limited in the lateral (zone B of Figure 3.4b) since cables become slack due to low tensions.

To solve the workspace limitation, a new design for the $2m2n$ CSR that consist in the addition of a passive carriage to the upper part of the frame is proposed. This modification

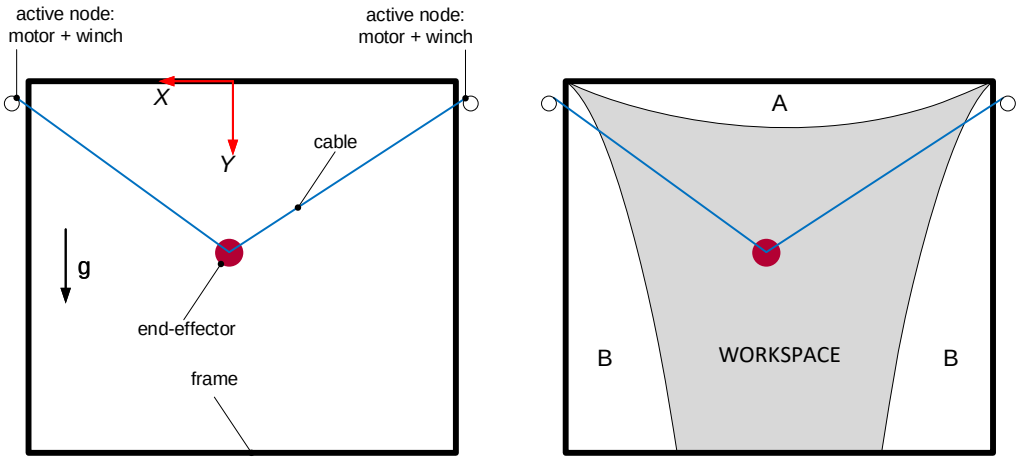

(a) Robot geometry and components (b) Workspace shape

Figure 3.4: Conventional $2m2n$ cable suspended robot

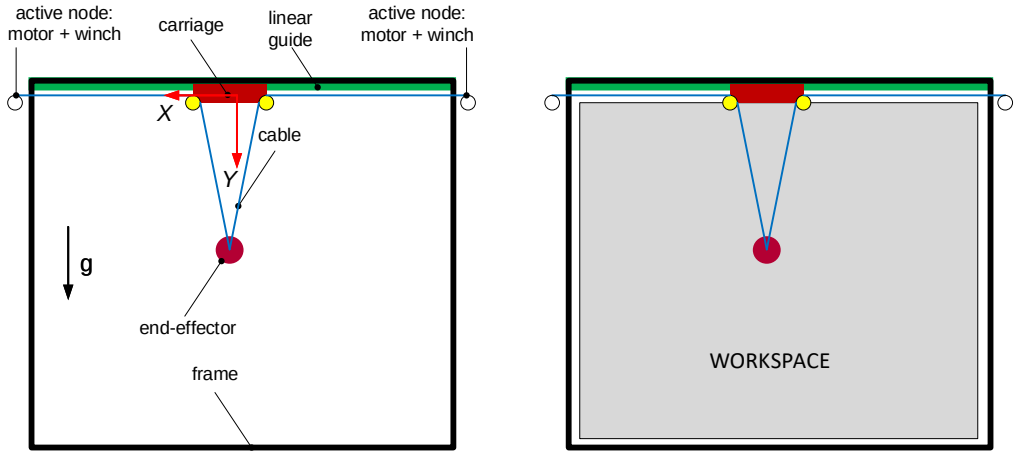

(a) Robot geometry and components (b) Workspace shape

Figure 3.5: Proposed $2m2n$ cable suspended robot

allows to extend the workspace of the robot to almost the whole size of the frame, as it allows to keep the angles formed by the cables and the vertical close enough to 0° to reduce the required cable tension. For this same reason, this new geometry of the robot yields to a reduction in the robot stiffness in the horizontal axis that causes undesired vibrations specially during the robot maneuvers. To solve this latter problem, a specific control strategy has been designed and tested as explained in the following section. Figure 3.5a shows a sketch of the proposed novel design and its components and Figure 3.5b shows the shape of the workspace that can be obtained with it. Note that this workspace is now rectangular and its only limited by the dimensions of the end-effector and the width of the carriages.

3.1.3 Inspection of large, horizontal surfaces with CDPR

The inspection of the bottom of large bridge decks is a task that has to be performed in a very large, planar, horizontal workspace, i.e. the gravity is perpendicular to the plane where the task has to be carried out. A common approach to perform this task is by using special crane-trucks that allow an operator to reach the bottom part of the bridge, as can be seen in Figure 3.6 [1]. Due to the characteristics of some bridges, the occupancy of the space below the bridge has to be strictly reduced, for example because a road, railway or river passes below the bridge. Another application that presents a large, flat workspace perpendicular to gravity is the automatic inspection or seeding in greenhouses.

Figure 3.6: Conventional approach for underbridge inspection

A SCR can be well suited for its application to automate the previously mentioned tasks,

[1] source: www.paxton-mitchell.com

by placing the required inspection device in the robot end-effector, avoiding the need of a human operator to reach the bottom of the bridge desk. In scenarios where the occupation of the space in the gravity direction has to be small, conventional SCR present serious problems as the required cable tension will be extremely high, due to the angles formed by the cables and the vertical direction, as can be seen in Figure 3.7, where mg is the external force applied to the end-effector, L represents the total width to be reached by the end-effector, S is the horizontal position of the end-effector, h the vertical occupancy of the robot, θ_1, θ_2, the angles formed by the cables and the horizontal, F_1, F_2 the cables tension and T_1, T_2 the torque to be generated by the actuators.

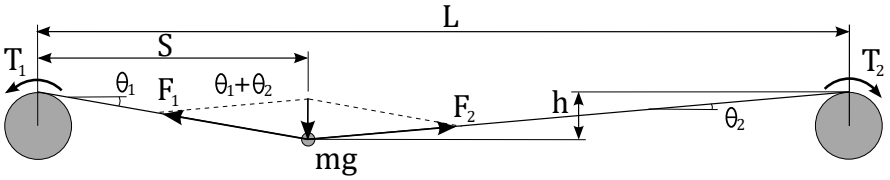

Figure 3.7: Conventional SCR applied to planar, horizontal workspaces

In this sense, a mechanical modification of the conventional SCR is proposed in this work focused on the application of the robot to large, planar, horizontal workspaces where the occupation of the space perpendicular to this plane has to be strictly reduced. The key aspect of this modification is the use of a closed cable loop, so that the cable does not end in a motorized winch but just passes through a pulley connected to a motor, the so-called drive pulley. The concept of the proposed new scheme for the SCR is shown in Figure 3.8. As can be observed, in a static situation, the tension of the entire cable loop remains equal, to move the end-effector, motors only have to exert torque to accelerate the system, allowing to pre-tense the system with a very high cable tension allowing the reduction of the occupation in the space perpendicular to the working plane.

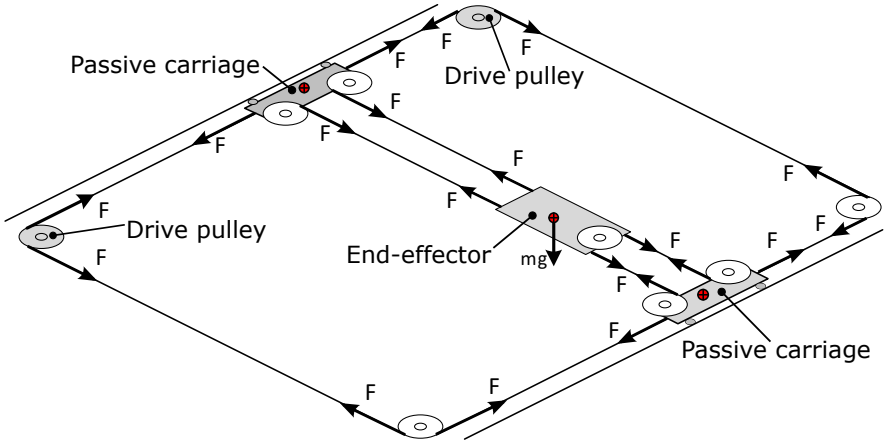

Figure 3.8: Proposed SCR applied to planar, horizontal workspaces

3.1.4 Cable tension measurement in CDPR

Measuring cable tension is a critical aspect in many types and applications of CDPR. As explained in Chapter 2, OC CDPR are those in which the number of cables is greater than the number of controllable degrees-of-freedom. While this fact has several advantages as the end-effector can withstand arbitrary external wrench, it also implies that there are infinite possible cable forces distributions that will balance the end-effector, both static- and dynamically. To deal with this problem, this kind of CDPR normally incorporate force control approaches that work in parallel with the end-effector position control system. For the force control system is a key aspect to have an accurate, real-time force measure to use as feedback to the control loop. In constrained CDPR, the relation between the force distribution and the end-effector pose is unique given the external wrench, therefore, by means of accurate cable forces measures the end-effector pose can be estimated. Additionally, any CDPR working in a real environment will require cable tension measures for security reasons.

There are commercial devices to measure force in cables that could be employed in CDPR, this devices are shown in Figure 3.9. However, their range, resolution or latency make them unsuitable for an extensive application in CDPR.

(a) ABQ Industrial (b) Captronic (c) Weite Technologies Co.

Figure 3.9: Commercial devices for measuring cable tension.

Due to this, most of the CDPR prototypes employ customized cable force sensors, some of them are reviewed in the work of Kraus et al. [103] and will also be reviewed in detail in the following chapter (see Section 4.4).

In this work a device specially designed for measuring tension in CDPR is proposed, it is based on a three pulley mechanism that allows the cable to run freely through it and can be placed near the robot frame. Cables cause a deformation proportional to their tension and this deformation is measured by means of strain gauges. The concept of the proposed device can be observed in Figure 3.10.

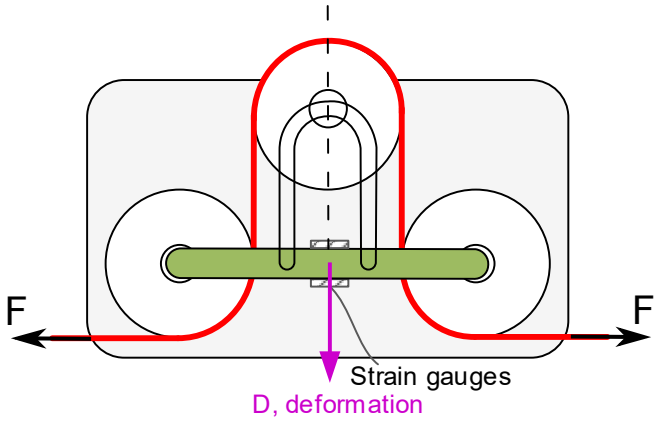

Figure 3.10: Proposed device for measuring cable tension in CDPR

3.2 Methodology

The mechanical designs of the robots explained in Sections 4.2 and 4.3 and the device for measuring cable tension explained in Section 4.4 has been developed by using the 3D computer assisted design software Solidworks^{TM}.

Regarding the CDPR proposed in Section 4.2, the simulation of the dynamic model and the designed control system has been performed by using the mathematical software Matlab® and the simulation software Simulink® from Mathworks.

To build the robot prototype, the frame has been made of Bosch technical profile, the winches use Maxon RE40 DC motors coupled to a worm gearbox with a ratio of 1:62 and the drums where cable is rolled have been 3D-printed in PLA plastic. The passive carriage has been 3D printed and its position is measured by means of a close-loop cable connected to a encoder MR type L from maxon motors with 512 pulses per revolution. The end-effector consist of two precision weights of 1kg each, marked with a red dot in the center to measure the end-effector pose by means of computer vision techniques, with the aim of assessing the positioning accuracy. Dimensions the different components are detailed in Section 4.2. Fishing lines with a resistance of 80 kg have been employed, being attached to the end-effector in its middle point.

The control of the motors has been realized by means of two ESCON 70/10 servo-amplifiers from Maxon Motors, configured in current control mode. The position control loop is performed by means of a MyRio 1900 FPGA-based controller from National Instruments, where PID controllers and the robot inverse kinematic model are implemented, achieving a real time control loop with 1ms cycle time. This controller also provides the graphical user interface for the operation of the robot and the data acquisition of the signals. The encoders of the RE40 DC motors provide the MyRio controller the required feedback for the position control loop. The measurement of the end-effector pose has been performed by means of a camera with 30 frames per second and a resolution 1920×1024 pixels from Logitech. The image processing for pose measurement and the processing of the acquired data have been

performed with the Image Processing Toolbox of Matlab®.

Regarding the CDPR proposed in Section 4.3, the frame, end-effector and the passive carriages have been made of steel. The passive-carriages run on steel guides attached to the frame. Pulleys are made of nylon and steel cable is employed. Dimensions of the components are detailed in Section 4.3.

The calculation of the natural frequency of the robot along its workspace has been performed in Matlab® while the experimental validation of the model has been carried out by using a camera with 60 frames per second and a resolution of 1080×720, image processing and data analysis for natural frequency model validation have been performed using Matlab®.

For the motorization of the built prototype, Nema 34 stepper motors with nominal speed of 3000rpm and torque of 12Nm have been used. They are controlled by means of position servocontrollers 86HSE12N, from Vikye. The reference for the servocontrollers, obtained after converting the desired end-effector trajectory to motor angles by the inverse kinematics and then compensated by dynamic inversion has been computed in Matlab®, and sent to an Arduino® Mega controller which in turn sends these values to the servocontrollers. To asses the pose positioning performance the same vision system as described to measure the natural frequency has been used.

In relation with the force measurement sensor exposed in Section 4.4, the prototype to validate the sensor proposal has been built in aluminum, its dimension are designed to guarantee that the bending moment generated by the cable tensions in the measuring bar is higher than the axial moment. Dimensions are detailed in Section 4.4.

The employed strain gauges have a gauge factor of $K_s = 2$ and the signal generated is measured by means of a National Instruments USB-6341 data acquisition board. To validate the device, it has been loaded with weights, measured with a GRAM DSX-30 precision weighting scale. All the data processing and analysis have been performed in Matlab ®.

Chapter 4

Results

This chapter presents the direct results of this thesis, which are three papers published in scientific journals indexed in the Journal Citation Reports (JCR).

The first of the papers is devoted to the mechanical design, kinematics, control and validation of a CDPR for large, planar, vertical surfaces.

The second one, presents the design, kinematics, control and experimental validation of a CDPR for large, horizontal planar working spaces.

Finally, the third paper details the mechanical design, instrumentation and validation of a device for measuring cable tension specifically designed for its application in CDPR.

4.1 Overview of the main contributions

Table 4.1 lists the papers published as direct result of this thesis, along with the author order in the paper and performance indicators of the journals where they are published.

Table 4.1: Papers published as direct results of this thesis

Title	**Author order**	**Journal**	**2020 Impact Factor**	**Journal Rank (JCI)**	**Category**
Addition of Passive Carriage for Increasing Workspace of Cable Robots: Automated Inspection of Surfaces of Civil Infrastructures [56]	First	Smart Structures and Systems	3.342	40/135 (Q1)	Engineering, Mechanical
Closed Loop Cable Robot for Large Horizontal Workspaces [57]	Third	Smart Structures and Systems	3.342	40/135 (Q1)	Engineering, Mechanical
New Sensor Device to Accurately Measure Cable Tension in Cable-Driven Parallel Robots [104]	First	Sensors	3.576	14/72 (Q1)	Instruments & instrumentation

4.2 Contribution 1

Smart Structures and Systems, *Vol. 27, No. 2 (2021) 387-396*
DOI: https://doi.org/10.12989/sss.2021.27.2.387

Addition of passive-carriage for increasing workspace of cable robots: automated inspection of surfaces of civil infrastructures

Guillermo Rubio-Gómez [1], Sergio Juárez [1], David Rodríguez-Rosa [1], Enrique Bravo [1], Erika Ottaviano [2], Antonio Gonzalez-Rodriguez [1] and Fernando J. Castillo-Garcia*[1]

[1] *School of Industrial and Aerospace Engineering, Av. Carlos III, 45071 Toledo, Spain*
[2] *DICeM, University of Cassino and Southern Lazio, Via G. Di Biasio 43, 03043 Cassino, Italy*

(*Received July 16, 2020, Revised September 28, 2020, Accepted October 10, 2020*)

Abstract. Cable-driven robots are parallel manipulators in which rigid links are replaced by actuated cables. The end-effector is then supported by a set of cables commanded by motors that are usually placed in a fixed frame. By varying the cables length, it is possible to change the end-effector position and/or orientation. Among the advantages presented by cable robots are they light-weight structure, high energy efficiency and their ability to cover large workspaces since cables are easy to wind. When high-speed operation is not required, a safer solution is to design cable-driven suspended robots, where all vertical components of cables tension are against gravity direction. Cable-driven suspended robots present limited workspace due to the elevated torque requirements for the higher part of the workspace. In this paper, the addition of a passive carriage in the top of the frame is proposed, allowing to achieve a much greater feasible workspace than the conventional one, i.e., with the same size as the desired inspection area while maintaining the same motor requirements. In the opposite, this new scheme presents non-desired vibration during the end-effector maneuvers. These vibrations can be removed by means of a more complex control strategy. Kinematics and dynamics models are developed in this paper. An analysis of sensor system is carried out and a control scheme is proposed for controlling the end-effector pose. Simulation and experimental results show that the feasible workspace can be notoriously increased while end-effector pose is controlled. This new architecture of cable-driven robot can be easily applied for automated inspection and monitoring of very large vertical surfaces of civil infrastructures, such as facades or dams.

Keywords: parallel robot; cable-driven robot; dynamics model; vibration control; automated inspection

1. Introduction

Inspection and maintenance of steel and composite large vertical structures are critical issues for sustainability of existing and new infrastructures (Huang *et al*. 2016). Classical approaches rely on large human activities eventually performed in unsafe conditions (Lee *et al*. 2010). Overcome the problem using robots, UAV or on site contactless global automated measurements for self-inspection and maintenance can be pursued at the present state-of-art of the current mechatronics (Jung *et al*. 2019, Kim *et al*. 2014).

Cable-Driven Parallel Manipulators (CDPMs) are a class of parallel robots in which, instead of using rigid bodies only, the fixed frame and platform are connected by several cables, which can be exerted or retracted by an actuation systems. Cables are wounded around drums that are fixed on the frame and suitable actuation and transmission system composed by rotary motors and pulleys allow controlling the length and direction of the cables to operate a tool, called end-effector. Main characteristics are a very large workspace, lightweight structure and relatively low-cost systems. In particular, the reduction of the moving masses may lead to good dynamic properties; in addition, changing the configuration for the actuation and pulleys the CDPM can be reconfigured, being also modular. These are important features for applications requiring a manipulator being brought to work on site.

CDPM were introduced a few decades ago, but they have become much more interesting from theoretical and applied research than their classical counterparts composed by rigid links only. More specifically, if classical parallel manipulators are still used and mainly confined as motion simulators, CDPM ranges from industry, entertainment, rehabilitation and recently civil engineering, just to cite some.

One of the first application of cable systems is RoboCrane (Bostelman *et al*. 1996). It uses the basic idea of the Stewart platform parallel manipulator but adding cables. The NIST RoboCrane has the capacity to lift and precisely manipulate heavy loads over large volumes with fine control in all six degrees of freedom. In addition, NIST developed an advanced RoboCrane controller. The graphic off-line control capability of this controller made programming of numerous controllers easy and fast (Bostelman *et al*. 1996).

Kawamura presented in Kawamura *et al*. (1995) an ultrahigh speed robot design, FALCON-7 that is a cable-driven parallel system. The introduction of elasticity in the

*Corresponding author, Professor,
E-mail: fernando.castillo@uclm.es

ISSN: 1738-1584 (Print), 1738-1991 (Online)

cables modelled as nonlinear spring improved the system transient response, but it also complicated the study of stability. Their experimental results showed stable manipulator performance. Further development of the model was proposed in Kawamura *et al*. (2000) to reduce vibration.

A large CDPM was developed to be applied as advanced virtual reality simulator (CableRobot Simulator 2020), in which the motion of the cabin is controlled by eight unsupported steel cables attached to winches. A CDPM was proposed in Yangwen *et al*. (2010) as suspension system for airplane model testing in low-speed wind tunnel, also proposing a method for measuring the aerodynamic parameters of the airplane model.

Very large CDPM developed for load transportation in industrial environment are manipulators belonging to the IPAnema family of CDPM, described in Pott *et al*. (2013); CoGiRo project 2020) The Five hundred meter Aperture Spherical Telescope (FAST) was originally described in (Nan 2006). The above-mentioned CDPM act in a crane configuration. Such robots, also called as Cable-suspended robots, are very well suited for suspended camera systems that are widely used in stadiums and arenas. Such systems consist of three major components: the reel—the motor drive and cables, the spar—the counterbalanced pan and tilt video camera, and central control, the computer software used by the operator to fly the camera (Cone 1985, Skycam 2020).

A limitation on the use of CDPMs are related to the mechanical feature of the cables, which can only work in tension. Therefore, the pose is feasible only for cables' configuration in which the static or dynamic equilibrium is assured under the constraint that the internal cable axial force must be positive. Although first research on the subject have treated cables as inextensible and massless, assuming them as perfect lines connecting the end-effector and pulleys (Roberts *et al*. 1998) it has been shown that axial and transversal flexibility should be considered for correct modelling. In particular, the axial flexibility can be taken into account as an equivalent stiffness model as it was proposed in Behzadipour (2006) for a single cable with pretension, using four springs. Lately, the current approach is to introduce mass of the cables taking into account transversal flexibility, either considering lumped masses (Ottaviano and Castelli 2010, Castelli *et al*. 2014) or continuum mass modeling (Merlet and dit Sandretto 2015, Ottaviano *et al*. 2019).

An interesting class of CDPMs is that in a crane configuration (also called suspended CDPM), in which gravity acts like an additional cable, and not all the end-effector DOFs can be controlled. Crane-type CDPM have attracted the interest of theoretical and applied research because they offer several advantages, such as the reduction of the number of cables, the overall costs and setup time, improved ease of assembly and a lower possibility of cable interference.

Referring to the kinematic study of suspended CDPMs, the challenging problem is that less than 6 DOFS may be controlled, so that when the cable lengths are assigned the end effector still has some freedom. Thus, its actual pose is determined by the wrenches acting upon it Abbasnejad and Carricato (2015) in which the problem has been defined as geometrico-static also expressing some connections between stability and energy.

The suspended CDPM presents limited workspace due to both tension limitations in real applications, i.e., upper bounds due to motor power and lower bounds due to low tensions at the lateral boundaries of the workspace yielding to worst end-effector positioning capabilities. Pulleys greatly influence the position capabilities of suspended CDPM, as it was shown in (Gonzalez-Rodriguez *et al*. 2017).

A passive carriage can be designed and added at the top of the frame, as it is proposed in this paper, achieving a larger workspace than the suspended CDPM one, i.e., with the same size as the desired inspection area. In the opposite, this new scheme presents non-desired vibration during the end-effector maneuvers. These vibrations can be removed by means of a more complex control strategy. The proposal is easily scalable and can be applied for inspection of large vertical surface of civil structures.

This paper is structured as follows: Section 2 describes the basics of suspended cable robots and the new proposal for increasing its workspace. Section 3 presents the kinematic and dynamics models for the proposed robot. Section 4 explains the control strategy developed for the proposed robot. Section 5 present the modelling and simulation results, showing that the workspace is increased without losing the end-effector controllability. Section 6 shows the experimental facility developed for the validation of the robot and the results obtained. Finally, section 7 states the main conclusions and further works.

(a) Commanded configuration (b) Suspended configuration

Fig. 1 Example of Commanded and Suspended configurations of CDPM

2. New proposal description

2.1 Basics

As aforementioned Cable-Driven Parallel Manipulators can be classified in Suspended or Commanded when all the vertical components of cable tension are against gravity direction or not, respectively (Pusey *et al*. 2004). For illustrative purpose, Fig. 1 represents a suspended and commanded configuration of a planar cable-driven robot in a vertical plane. In both schemes, the end-effector, which carries the inspection device that can be a camera (Adhikari *et al*. 2014) or laser (Wang *et al*. 2016), the frame and the cables are represented.

Commanded configuration requires a perfect synchronous control of cables' length but allows to move the end-effector with greater acceleration than 1G in the gravity direction by Gouttefarde (2008). On the contrary, suspended configuration is mechanically safer because a non-synchronous control of cables' length does not yield to destructive scenarios, but it only can move the end-effector at 1G in the gravity direction (Roberts *et al*. 1998). This work proposes a planar CDPM for large vertical surface inspection tasks.

Following sections describes the workspace limitation of conventional Cable-Driven Suspended Robot (CDPM) and the new proposal to obtain a feasible solution for a complete workspace inspection.

2.2 Workspace limitation

Workspace limitation of CDPM are related to the actuator system and the cables. End-effector pose is controlled by cable length variations. Cable lengths are typically controlled by means of the actuator system: a motor (usually coupled to a gearbox) and a winch. This winch angle is controlled by the motor and cable rolls in or out on it. As consequence, by controlling motor angles, cable length can be controlled, and the end-effector can be therefore positioned at the desired pose.

When the end-effector is placed at the upper part of the workspace, cables' tension is too high, due to the greater angle between cables and the vertical. This yields the need in motors to exert a very high torque to maintain the end-effector pose or to modify it (Rubio-Gómez *et al*. 2019). In this sense, the upper part of the workspace is inaccessible owing to the natural torque limitation of the motors (see Fig. 2, region A). On the other hand, when effector is located at the lateral areas of the workspace, some of the cable tensions are to low and cables suffer saggy effect Arsenault (2013) and the end-effector desired pose is lost (see Fig. 2, region B).

The size of the regions A and B with regards to the frame size depends of the frame width and height, the end-effector width and height, the mass of the end-effector and the cables. More details of this workspace limitation can be found in Fattah (Fattah and Agrawal 2002) or Castelli (Castelli *et al*. 2010).

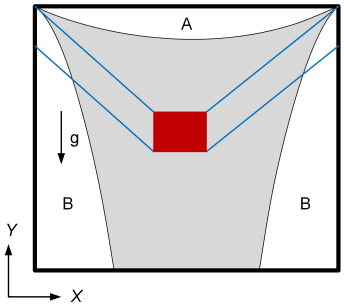

Fig. 2 Workspace limitation of conventional CDPM

2.3 New proposal

Our proposal is focused on enlarging the workspace of CDPMs without increasing the number of actuators. Adding a passive carriage (without active actuation) in the top of the frame and connecting the end-effector to the actuated winch though this passive carriage the workspace can be notoriously increased. Fig. 3 shows the new proposal together with the analogous conventional CDPMs for the planar case.

A simple analysis based on the static equilibrium of end-effector and carriage yields that, for the same active node, i.e., same motor-winch set, and the same cables, the workspace is notoriously increased. On the contrary, for the same end-effector position, our proposal presents an important drawback: the rigidity of the system decreases and the end-effector presents non-desirable vibrations (similar to a pendulum) which need to be controlled. Simulation Section details the workspace analysis together with the frequency characterization of the system.

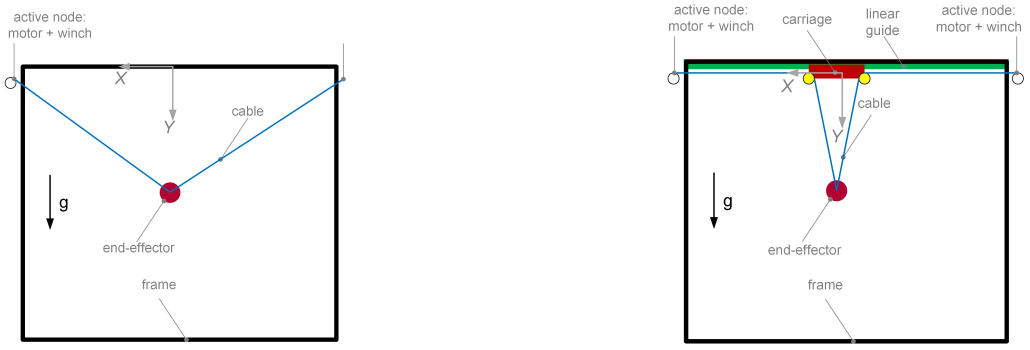

(a) Conventional configuration

(b) New proposal

Fig. 3 Planar CDPMs

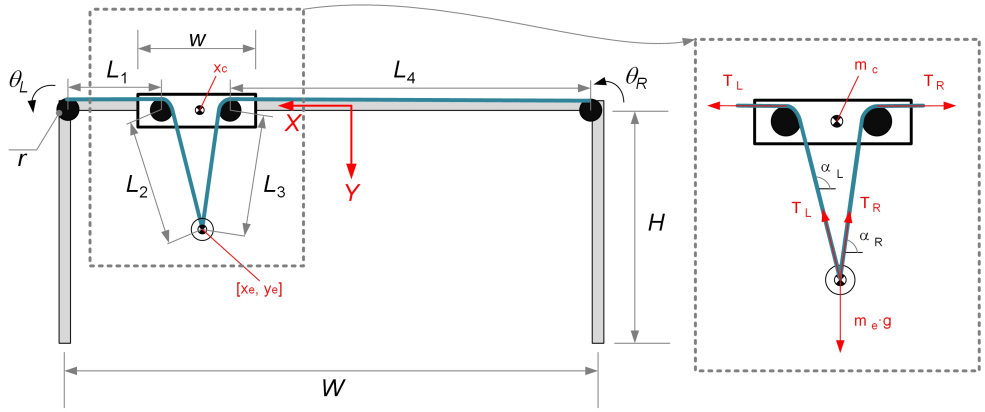

Fig. 4 Nomenclature for mathematical model

3. Mathematical model

3.1 Nomenclature

Fig. 4 represents the robot scheme including the nomenclature that is used for the mathematical formulation.

The dimensions of the frame are $W \times H$. The width of the carriage is w and its mass is m_c. The cable lengths are L_1, L_2, L_3 and L_4 according to the Scheme in Fig. 4 and the angles of segments L_2 and L_3 are α_L and α_R, respectively. The radius of the winches (active nodes) is r, since their angular position are θ_L and θ_R, respectively. The end-effector mass is m_e and its position is $[x_e, y_e]^T$. Finally, the tension of the cable of the left and the right segments are T_L and T_R, respectively.

3.2 Kinematic analysis

The system described in the proposal has three Degrees-Of-Freedom (DOF), x_e, y_e and x_c but only two controllable inputs, θ_L and θ_R. In this sense, for a given pair of value motor/winch angles, θ_L and θ_R, multiple combination of x_e, y_e and x_c can be found. Inverse kinematic problem consists on determining the required motor/winch angles, θ_L and θ_R, for positioning the end-effector in the desired position. On the contrary, the forward kinematic problem consists on determining where is the end-effector placed for a given pair of motor angle values, θ_L and θ_R. The inverse kinematic problem can be therefore expressed as $[\theta_L, \theta_R] = \Lambda^I(x_e, y_e, x_c)$ an has a unique solution. The forward kinematic problem has been denoted as $[x_e, y_e, x_c] = \Lambda^F(\theta_L, \theta_R)$ and has infinity solutions (Pott 2018a). The inverse kinematics will be applied to develop the dynamics model and in the control scheme for controlling the end-effector pose. The expression of Λ^I is detailed in Appendix A.

3.3 Dynamics model

This model describes the dynamic behavior of the system. The input variables are the torque exerted by the motors, τ_L and τ_R, and the output is the end-effector position, x_e and y_e (see Fig. 5).

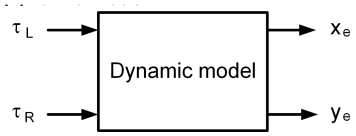

Fig. 5 Dynamic model of the system

Under the assumption of non-extensible cables (Pott 2018b) the dynamics of the motor/winch sets, end-effector and carriage must be considered to develop a simple but representative model

$$\begin{aligned} m_e\ddot{x}_e &= T_L\cos(\alpha_L) + T_R\cos(\alpha_R) \\ m_e\ddot{y}_e &= m_e g - T_L\sin(\alpha_L) - T_R\sin(\alpha_R) \\ m_c\ddot{x}_c + b_c\dot{x}_c &= T_L(1+\cos(\alpha_L)) \\ &\quad -T_R(1-\cos(\alpha_R)) \\ \tau_L &= J_L\ddot{\theta}_L + b_L\dot{\theta}_L + T_L r \\ \tau_R &= J_R\ddot{\theta}_R + b_R\dot{\theta}_R + T_R r \end{aligned} \tag{1}$$

being b_c the viscous friction coefficient of the carriage/linear guide, J_L and J_R the moments of inertia of the left and right motor/winch sets and b_L and b_R the viscous friction coefficient of the left and right motor/winch sets.

4. Control strategy

Let's denote $[x_e^*, y_e^*]$ the desired end-effector pose, and let's also assume that in steady state $x_e = x_c$. Under the point of view of the control two overall alternative are possible: (a) to directly control the end-effector position $[x_e, y_e]$ by measuring and feeding back it (control in *objective coordinates*); (b) to indirectly control the end-effector position by using inverse kinematics and measuring and feeding back the motor/winch coordinates (control in *joint coordinates*). Both strategies are shown in Fig. 6.

Control in *objective coordinates* requires an accurate and fast enough measurement of end-effector position (for example vision system). In addition, the controller dimension is 2×2 and 4 controllers block should be tuned. On the other hand, control in *joint coordinates* is more frequently applied because only require joint coordinates measurement (for example encoders) and only

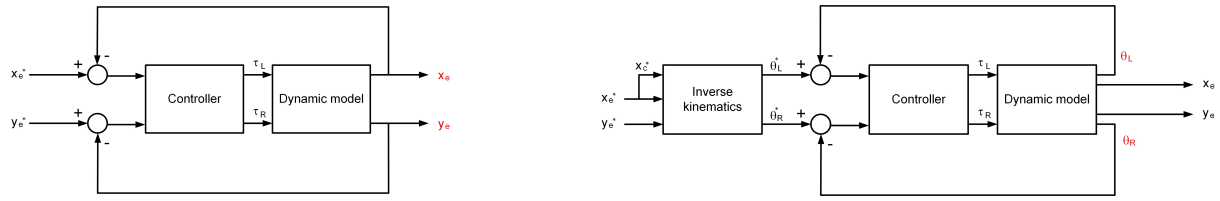

(a) Control in objective coordinates (b) Control in joint coordinates

Fig. 6 Feasible control strategies

$$\tau_R(s) = \theta_R(s)(J_R s^2 + b_R s) + z_R(s)$$

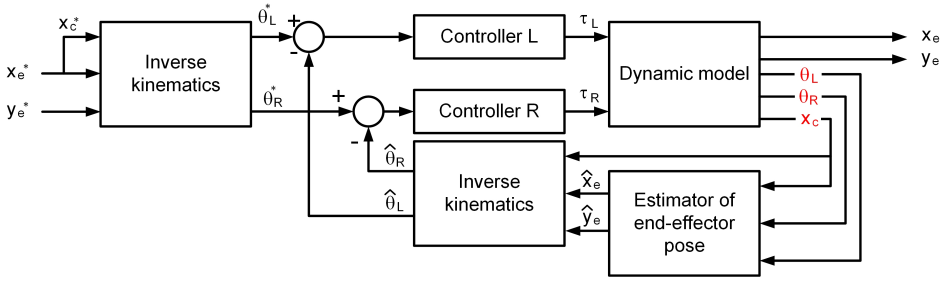

Fig. 7 Control scheme for positioning end-effector

two 1×1 uncoupled controllers must be tuned (Castillo-Garcia *et al*. 2017). Our control strategy is therefore based on control in joint coordinates but control scheme of Fig. 6(b) cannot be directly applied owing to the multiple solution of forward kinematics. In this sense, control scheme at Fig. 6(b) must be modified to obtain a unique solution of $[x_e, y_e]$ by measuring the joint coordinates, θ_L and θ_R together with the carriage position, x_c. The final control scheme is presented in Fig. 7. Note that an estimator block has been added in order to estimate the end-effector pose, $\hat{x}_e$ and $\hat{y}_e$, by means of the measurement of carriage position and motor/winch sets angular position, $[\hat{x}_e, \hat{y}_e] = \Xi(x_c,\ \theta_L, \theta_R)$. The expression of the estimator is detailed in Appendix A. In addition, a reference value of carriage position has been also added assuming steady state conditions ($x_e^* = x_c^*$).

Following sections show that both, simulations, and experimental results demonstrate the ability of this control scheme for controlling the end-effector pose. PID controllers have been tuned as controller block for demonstrating the feasibility of our robot proposal but other control techniques can be easily applied. Dynamics model (1) is nonlinear. In this way, controller blocks shown in Fig. 7 should be non-linear or linear but robust enough to compensate the non-linear behavior of the system. As control is defined in joint coordinates, dynamics of actuator can be rewritten as

$$\begin{aligned} \tau_L &= J_L\ddot{\theta}_L + b_L\dot{\theta}_L + z_L \\ \tau_R &= J_R\ddot{\theta}_R + b_R\dot{\theta}_R + z_R \end{aligned} \tag{2}$$

being z_L and z_R disturbances that the motors suffer which actually model the payload variation of the motors owing to the cables tension. Therefore, actuators dynamics result linear and Laplace Transform can be applied for obtaining the motor model

$$\tau_L(s) = \theta_L(s)(J_L s^2 + b_L s) + z_L(s) \tag{3}$$

Angular position of the motor/winch sets can be expressed as

$$\begin{aligned} \theta_L(s) &= \frac{1}{J_L s^2 + b_L s} \cdot \tau_L(s) + \frac{1}{J_L s^2 + b_L s} \cdot z_L(s) \\ \theta_R(s) &= \frac{1}{J_R s^2 + b_R s} \cdot \tau_R(s) + \frac{1}{J_R s^2 + b_R s} \cdot z_R(s) \end{aligned} \tag{4}$$

and the transfer function to be controlled can be written as

$$\begin{aligned} G_L(s) &= \frac{\theta_L(s)}{\tau_L(s)} = \frac{A_L}{s(s + B_L)} \\ G_R(s) &= \frac{\theta_R(s)}{\tau_R(s)} = \frac{A_R}{s(s + B_R)} \end{aligned} \tag{5}$$

Assuming a PID controller, $R(s) = K_p + K_d \cdot s + \frac{K_i}{s}$, where K_p, K_i and K_d are the proportional, integral and derivative constant (Ogata 2010), the controllers block shown are

$$\begin{aligned} Controller\ L = R_L(s) &= K_{pL} + K_{dL} \cdot s + \frac{K_{iL}}{s} \\ Controller\ R = R_R(s) &= K_{pR} + K_{dR} \cdot s + \frac{K_{iR}}{s} \end{aligned} \tag{6}$$

Conventional frequency domain tuning method has been applied to obtain the controllers parameters by fixing the desired values of gain crossover frequency and phase margin (Feliu-Batlle and Castillo-García 2014).

5. Simulations

5.1 Preliminaries

Simulations have been developed in Matlab® and Simulink®. A fixed sample time has been set to 1 ms using ode4 (Runge Kutta) as solver. The system has been simulated with the model parameters summarized in Table 1,

Table 1 Model parameters

Subsystem	Parameter	Value	Subsystem	Parameter	Value
Carriage	m_c	1.50 kg	Motor/ winch set	$J_R = J_L$	0.034 kgm^2
	b_c	1.00 Ns/m		$b_R = b_L$	0.039 Nms
	w	0.10 m		r	0.037 m
Frame	W	1.26 m	End-effector	m_e	2.00 kg
	H	2.00 m			

Table 2 Controllers summary

Controller	Gain crossover frequency (rad/s)	Phase margin (°)	K_p	K_i	K_d
L	121	90	4.718	1	4.072
R	121	90	4.718	1	4.072

according to the experimental platform (see Section 6). The controllers parameters, together with the frequency requirements to be obtained are summarized in Table 2.

5.2 Workspace analysis

Static workspace of CDPM can be easily obtained by computing the static equilibrium of force in the end-effector. Let us call τ_{max} the maximum torque that the motor/winch set can exert and T_{min} the minimum tension of cable to avoid saggy effect. The end-effector pose can be located at all the points of the workspace, compute the static equilibrium of force and check if the torque of the motor does not exceed the maximum one, τ_{max} and if the tension is greater than the minimum one, T_{min}. Fig. 8 compares the static workspace of the new proposal to the conventional architecture of CDSM shown in Fig. 3. A maximum allowed torque of 20 Nm and a minimum tension of 5 N have been assumed.

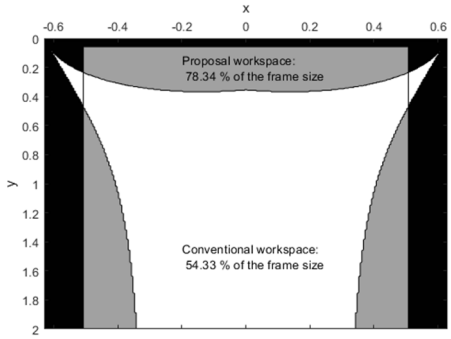

Fig. 8 Workspace comparison: Proposal vs. Conventional CDPM

Note that the workspace of the proposal is 16% greater than the conventional architecture of CDPM for the model parameters of Table 1. On the other hand, its boundary box is rectangular allowing to use our proposal for inspection of regular surfaces. For illustrative purpose, Fig. 9 compares both configurations when frame width increments (2 m, 4 m and 6 m). While conventional architecture loses feasible workspace when frame width increases, our proposal increase it and for a 6 m width frame conventional CDSM could only reach 19.80% of the frame since our proposal reaches up to 93.28% of the workspace surface.

5.3 End-effector position control

Dynamics model (1) is a second order system and 4th *Bezier* trajectories has been therefore implemented to ensure smooth trajectories of the end-effector and to avoid abrupt changes in the control signal values which could yield to non-desirable vibration of the end-effector. In order to illustrate the controlled system behavior, a horizontal (Fig. 10) and vertical (Fig. 11) simulations are summarized here.

Fig. 10 shows the result of a horizontal movement from $[x_e^*, y_e^*]_{ini} = [-0.200, 0.150]$ m to $[x_e^*, y_e^*]_{fin} = [0.200, 0.150]$ m. Note that the end-effector pose tracks the reference during all the trajectory. The average error obtained is 0.8 mm and the maximum following error is 1.2 mm.

Fig. 11 represents the result of a vertical movement from $[x_e^*, y_e^*]_{ini} = [0.000, 0.450]$ m to $[x_e^*, y_e^*]_{fin} = [0.000, 0.150]$ m. The end-effector pose tracks again the reference during all the trajectory. The average error obtained is

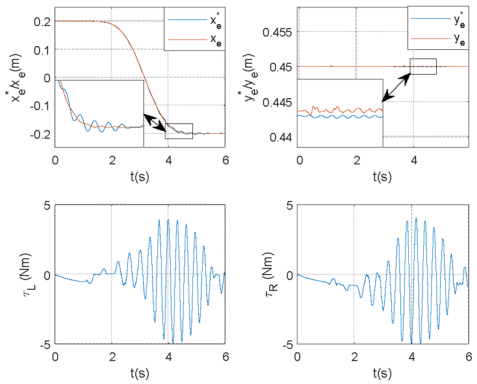

Fig. 10 Simulation: Horizontal movement

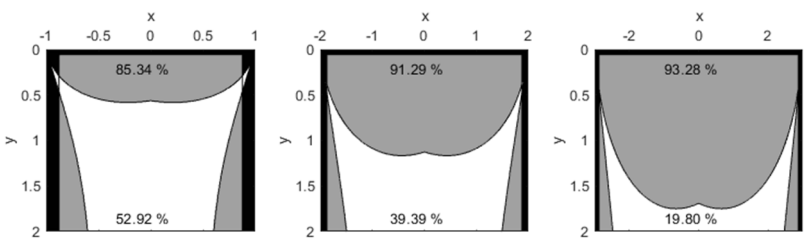

Fig. 9 Workspace comparison when frame width increases

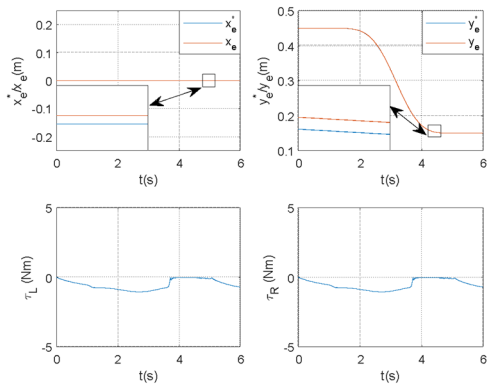

Fig. 11 Simulation: Vertical movement

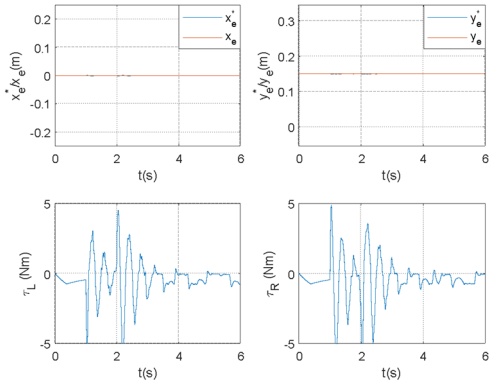

Fig. 12 Simulation: Disturbance rejection

0.4 mm and the maximum following error is 0.8 mm.

Table 3 summarizes the simulations results together to the experimental ones. The obtained error is lower than conventional errors obtained in CDSM which, for this workspace size, is around 10-20 mm (Maloletov *et al.* 2019). Finally, Fig. 12 represents the behavior of the system in presence of a disturbance in the carriage position, modeled as a force pulse of 10 N and a duration of 1 s. Note that the control system can reject the carriage disturbance maintaining the end-effector pose by increasing the control signal, motors torques during the disturbance effect.

6. Experiments

6.1 Platform description

The parameters values of the experimental platform are the same that the ones used in simulations section and summarized in Table 1. The frame is made of *bosch* aluminum profile and the winches and the carriage has been 3D printed in PLA. The motors are DC RE 40 model from *Maxon Motor* that have been couple to a worm gearbox and to the printed winches. Incremental encoders are couple to the motors to measure their angular positions. The carriage position is also measured by means of and incremental encoder by mean of a closed cable loop which rotates a pulley. Two *Maxon Motor* servoamplifier ESCON 70/10 are used for applying the control signal to the motors and a *National Instruments FPGA* based board (*MyRio*) has been used for implementing the real time control. Fig. 13 shows the final aspect of the prototype.

6.2 Results

In order to compute the tracking error of the experiments (in a similar way to simulations), a low-cost vision system has been developed. A 30 fps and 1920 × 1024 resolution camera has been used. Although the resolution of the camera only allows to track the end-effector with a resolution at real world of about 0.25 mm and a sample time of 33 ms.

Fig. 14 illustrates the results of the computer vision tracking algorithm developed in Matlab® for translating image coordinates to world coordinates and track the end-effector pose.

In a similar way to Simulation section, horizontal and vertical movements have been carried out in order to demonstrate the end-effector positioning. For both movements, the same 4th order Bezier trajectories of Simulation section have been implemented for ensuring a smooth evolution of the references and, as consequence, of the control signals.

Figs. 15 and 16 represents the end-effector reference position, x_e^* and y_e^*, the real time estimation of end-

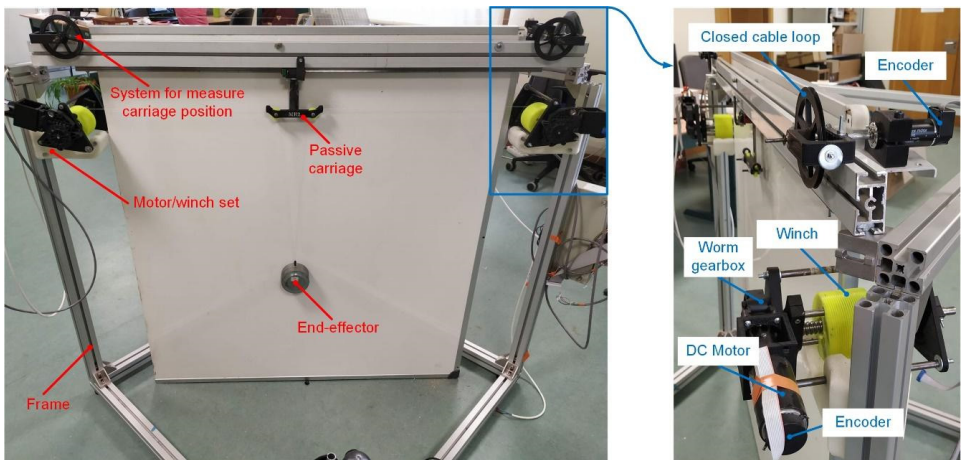

Fig. 13 Experimental platform

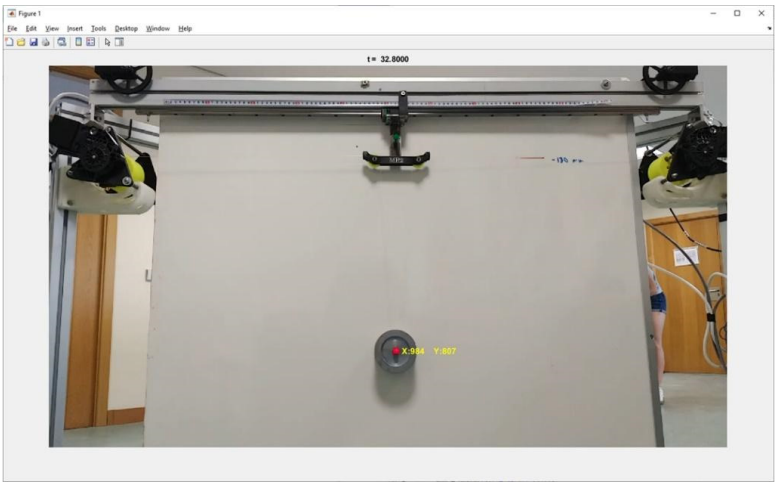

Fig. 14 Vision system for tracking end-effector pose

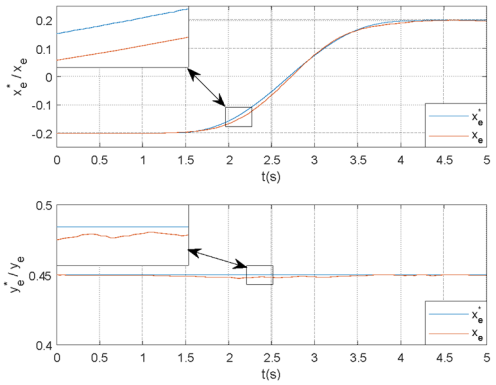

Fig. 15 Experiments: Horizontal movement

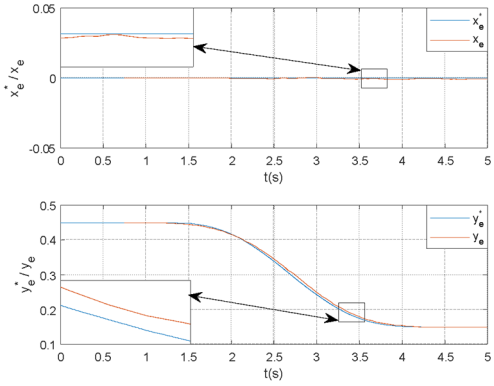

Fig. 16 Experiments: Vertical movement

effector pose, $\hat{x}_e$ and $\hat{y}_e$, and the offline measurement of end-effector pose by means of the vision system, x_e and y_e.

Fig. 15 shows the result of a horizontal movement from $[x_e^*, y_e^*]_{ini} = [-0.200,\ 0.150]$ m to $[x_e^*, y_e^*]_{fin} = [0.200,\ 0.150]$ m. Note that the end-effector pose tracks the reference during all the trajectory. The average error obtained is 3.2 mm and the maximum following error is 16 mm.

Fig. 16 represents the result of a vertical movement from $[x_e^*, y_e^*]_{ini} = [0.000, 0.450]$ m to $[x_e^*, y_e^*]_{fin} = [0.150, 0.000]$ m. The end-effector pose tracks again the reference during all the trajectory. The average error obtained is 1.7 mm and the maximum following error is 9.4 mm.

Finally, Fig. 17 represents an experiment at which a lateral external force is applied to the carriage. Table 3 summarizes the results obtained by simulations and experiments.

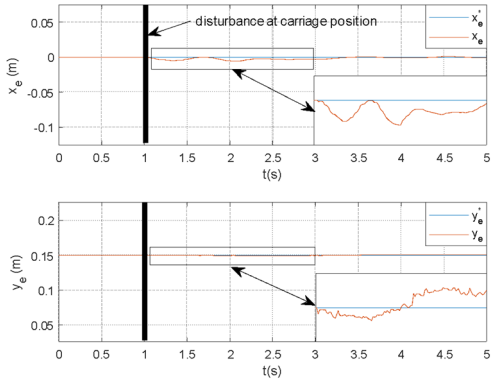

Fig. 17 Experiments: Disturbance rejection

Table 3 Summary of simulations and experiments

Movement	Initial pose (m)	Final pose (m)	Trajectory time (s)	Simulation /Experiments	Average following error (mm)	Maximum following error (mm)
Horizontal	[-0.20,0.15]	[0.20,0.15]	4	Simulation	0.8	1.2
				Experiment	3.2	16
Vertical	[0.45,0.00]	[0.15,0.00]	4	Simulation	0.4	0.8
				Experiment	1.7	9.4

During the application of the force (about 20 N) the controller is able to maintain the end-effector pose at the reference pose $[x_e^*, y_e^*] = [0, 0.15]$ m. The maximum divergence of the end-effector pose during the experiment is about 2 mm. These lateral external forces are intended to simulate real forces that the robot can suffer when operating in the presence of strong winds (Jeong *et al*. 2019).

7. Conclusions

In this work, a novel mechanical design based in the addition of a passive carriage to the upper part of the frame in a 2 degrees-of-freedom cable suspended robot has been proposed. The aim of this design is to significantly enlarge the robot workspace without increasing the torque requirements of the motors, allowing its application to the automatic inspection of large surfaces as the ones in civil infrastructures due to an efficient control system. A specific control approach has been designed for the elimination of vibrations that appeared inherent to the new design and also cancelling the effect of perturbations. For the validation of the mechanical and control proposals, both the robot dynamics and the control system have been mathematically modeled. Several tracking trajectories for the end-effector have been simulated, obtaining a tracking error not higher than 1mm and a good robustness to lateral force perturbations, similar to the ones that the robot can suffer in real operation conditions. To validate these results, a prototype with the same parameters has been built, the control system has been implemented in a real-time hardware and the simulations have been replicated experimentally, obtaining a very low tracking error and also observing a good capacity to reject force perturbations and maintaining the end-effector pose.

Further works in this research line must include the attaching of different inspection systems to the end-effector as cameras or laser to detect, reconstruct and analyze different kind of defects present in vertical surfaces of civil infrastructures as facades, dams or even in other fields as marine or aerospace engineering to inspect large ships or aircrafts, thanks to the modularity and quick deployment capacity of suspended cable robots.

Acknowledgments

The research described in this paper was financially supported by Research Fund for Coal and Steel grant agreement No. 800687 in the framework of DESDEMONA project. Authors wish to thank the financial Support provided by the university of Castilla-La Mancha and the European Social Fund through the pre-doctoral funding [2019/451].

References

Abbasnejad, G. and Carricato, M. (2012), "Real solutions of the direct geometrico-static problem of under-constrained cable-driven parallel robots with 3 cables: A numerical investigation", *Meccanica*, **47**(7), 1761-1773. https://doi.org/10.1007/s11012-012-9552-3

Adhikari, R.S., Bagchi, A. and Moselhi, O. (2014), "Automated condition assessment of concrete bridges with digital imaging", *Smart Struct. Syst., Int. J.*, **13**(6), 901-925. https://doi.org/10.12989/SSS.2014.13.6.901

Arsenault, M. (2013), "Stiffness analysis of a planar 2-dof cable-suspended mechanism while considering cable mass", In: *Cable-Driven Parallel Robots* (pp. 405-421), Springer, Berlin, Heidelberg.

Behzadipour, S. (2006), "Stiffness of cable-based parallel manipulators with application to stability analysis", *J. Mech. Des.*, **128**(1), 303-310.

BostelMan, R., Albus, J., Dagalakis, N. and Jacoff, A. (1996), "Robocrane project: an advanced concept for large scale manufacturing", In: *AUVSI-PROCEEDINGS-*, Citeseer, pp. 509-522.

CableRobot Simulator (2020), "Cable-driven parallel robots – motion simulation in a new dimension", Accessed: 2020-07-02. http://www.ipa.fraunhofer.de/en/cable-driven_parallel_robots.html

Castelli, G., Ottaviano, E. and González, A. (2010), "Analysis and simulation of a new Cartesian cable-suspended robot", *Proceedings of the Institution of Mechanical Engineers, Part C: Journal of Mechanical Engineering Science*, **224**(8), 1717-1726.

Castelli, G., Ottaviano, E. and Rea, P. (2014), "A Cartesian cable-suspended robot for improving end-users mobility in an urban environment", *Robot. Comput.-Integr. Manuf.*, **30**(3), 335-343.

Castillo-Garcia, F.J., Rea, P., Gonzalez-Rodriguez, A. and Ottaviano, E. (2017), "On the Design of a 4 Degrees-of-freedom Pick and Place Cable Suspended Parallel Manipulator", *Int. J. Robot. Automat. (IJRA)*, **6**(4), 286-302.

CoGiRo Project (2020), Accessed: 2020-07-10. http://www.lirmm.fr/cogiro/

Cone, L.L. (1985), "Skycam-an aerial robotic camera system", *Byte*, **10**(10), 122.

Fattah, A. and Agrawal, S.K. (2002), "Workspace and design analysis of cable-suspended planar parallel robots", *Proceedings of International Design Engineering Technical Conferences and Computers and Information in Engineering Conference*, Vol. 36533, pp. 1095-1103.

Feliu-Batlle, V. and Castillo-García, F.J. (2014), "On the robust control of stable minimum phase plants with large uncertainty in a time constant, A fractional-order control approach", *Automatica*, **50**(1), 218-224.

Gonzalez-Rodriguez, A., Castillo-Garcia, F.J., Ottaviano, E., Rea, P. and Gonzalez-Rodriguez, A.G. (2017), "On the effects of the design of cable-Driven robots on kinematics and dynamics models accuracy", *Mechatronics*, **43**, 18-27. http://dx.doi.org/10.1016/j.mechatronics.2017.02.002

Gouttefarde, M. (2008), "Characterizations of fully constrained poses of parallel cable-driven robots: a review", *Proceedings of International Design Engineering Technical Conferences and Computers and Information in Engineering Conference*, Vol. 43260, pp. 21-30.

Huang, T.L., Zhou, H., Chen, H.P. and Ren, W.X. (2016), "Stochastic modelling and optimum inspection and maintenance strategy for fatigue affected steel bridge members", *Smart Struct. Syst., Int. J.*, **18**(3), 569-584. https://doi.org/10.12989/SSS.2016.18.3.569

Jeong, S., Lee, J., Cho, S. and Sim, S.H. (2019), "Integrated cable vibration control system using Arduino", *Smart Struct. Syst., Int. J.*, **23**(6), 695-702. https://doi.org/10.12989/sss.2019.23.6.695

Jung, H.-J., Lee, J.-H., Yoon, S. and Kim, I.-H. (2019), "Bridge Inspection and condition assessment using Unmanned Aerial Vehicles (UAVs): Major challenges and solutions from a

practical perspective", *Smart Struct. Syst.*, *Int. J.*, **24**(5), 669-681. https://doi.org/10.12989/SSS.2019.24.5.669
Kawamura, S., Choe, W., Tanaka, S. and Pandian, S.R. (1995), "Development of an ultrahigh speed robot falcon using wire drive system", In: *Proceedings of IEEE International Conference on Robotics and Automation*, **1**, 215-220.
Kawamura, S., Kino, H. and Won, C. (2000), "High-speed manipulation by using parallel wiredriven robots", *Robotica*, **18**(1), 13-21.
Kim, C.W., Isemoto, R., McGetrick, P.J., Kawatani, M. and OBrien, E.J. (2014), "Drive-by bridge inspection from three different approaches", *Smart Struct. Syst.*, *Int. J.*, **13**(5), 775-796. https://doi.org/10.12989/SSS.2014.13.5.775
Lee, A.Y., Oh, J.K. and Choi, Y.J. (2010), "Bridge Inspection System using Robot", *J. Korea Robot. Soc.*, **5**(1), 77-84.
Maloletov, A.V., Fadeev, M.Y. and Klimchik, A.S. (2019), "Error Analysis in Solving the Inverse Problem of the Cable-driven Parallel Underactuated Robot Kinematics and Methods for their Elimination", *IFAC-PapersOnLine*, **52**(13), 1156-1161.
Merlet, J.-P. and dit Sandretto, J.A. (2015), "The forward kinematics of cable-driven parallel robots with sagging cables", In: Book; *Cable-Driven 190 Parallel Robots Editors*: *Andreas Pott*, *Tobias Bruckmann*. *Proceedings of the Second International Conference on Cable-Driven Parallel Robots*, *Book Series*: *Mechanisms and Machine Science*, **32**, 3-15.
Nan, R. (2006), "Five hundred meter aperture spherical radio telescope (fast)", *Sci. China Series G*, **49**(2), 129-148.
Ogata, K. (2010), *Modern Control Engineering*, Prentice hall
Ottaviano, E. and Castelli, G. (2010), "A Study on the Effects of Cable Mass and Elasticity in Cable-Based Parallel Manipulators", *Proceedings of the 18th CISM-IFToMM Symposium on Robot Design*, *Dynamics and Control*, Springer Ed. Udine, pp. 149-156.
Ottaviano, E., Arena, A., Gattulli, V. and Potenza, F. (2019), "Slackening effects in 2D exact positioning in cable-driven parallel manipulators", In: A. Pott, T. Bruckmann (Eds.), *Mechanisms and Machine Science*, *Vol. 74 of Cable-Driven Parallel Robots*. *CableCon 2019*, Springer, Cham, pp. 319-330.
Pott, A. (2018a), "Kinematic Codes", In: *Cable-Driven Parallel Robots*, Springer Tracts in Advanced Robotics, Vol. 120, Springer, Cham.
Pott, A. (2018b), "Kinematics with Nonstandard Cable Models", In: *Cable-Driven Parallel Robots*, Springer Tracts in Advanced Robotics, Vol. 120, Springer, Cham.
Pott, A., Mutherich, H., Kraus, W., Schmidt, V., Miermeister, P., Dietz, T. and Verl, A. (2013), "Cable-driven parallel robots for industrial applications: The ipanema system family", *Proceedings of the 44th International Symposium on Robotics* (*ISR*), pp. 1-6.
Pusey, J., Fattah, A., Agrawal, S. and Messina, E. (2004), "Design and workspace analysis of a 6–6 cable-suspended parallel robot", *Mech. Mach. Theory*, **39**(7), 761-778.
Roberts, R., Graham, T. and Lippitt, T. (1998), "On the inverse kinematics, statics, and fault tolerance of cable-suspended robots", *J. Robot. Syst.*, **15**(10), 581-597.
Rubio-Gómez, G., Rodríguez-Rosa, D., García-Vanegas, J.A., Gonzalez-Rodríguez, A., Castillo-García, F.J. and Ottaviano, E. (2019), "Chain Driven Robots: An Industrial Application Opportunity. A Planar Case Approach", In: *International Conference on Cable-Driven Parallel Robots*, Springer, Cham, pp. 13-22.
Skycam (2020), Accessed: 2020-07-10. https://en.wikipedia.org/wiki/Skycam
Wang, Q., Kim, M.K., Sohn, H. and Cheng, J.C. (2016), "Surface flatness and distortion inspection of precast concrete elements using laser scanning technology", *Smart Struct. Syst.*, *Int. J.*, **18**(3), 601-623. https://doi.org/10.12989/sss.2016.18.3.601
Yangwen, X., Qi, L., Yaqing, Z. and Bin, L. (2010), "Model aerodynamic tests with a wire-driven parallel suspension system in low-speed wind tunnel", *Chinese J. Aeronaut.*, **23**(4), 393-400. https://doi.org/10.1016/S1000-9361(09)60233-8

Appendix A. Kinematics problem expression

Assuming an initial position for the end effector (x_{e0}, y_{e0}), the initial cable length can be computed as

$$\begin{aligned} L_{10} &= \frac{D}{2} - x_{e0} - \frac{w}{2} \\ L_{20} &= \left(\left(\frac{d}{2}\right)^2 + y_{e0}^2 \right)^{\frac{1}{2}} \\ L_{30} &= L_{20} \\ L_{40} &= D - w - L_{10} \end{aligned} \tag{A1}$$

Assuming $x_c = x_e$, the cable lengths for any position of the end-effector can be calculated as

$$\begin{aligned} L_1 &= \frac{D}{2} - x_c - \frac{w}{2} \\ L_{40} &= D - w - L_1 \\ L_3 &= \left(y_e^2 + \left(x_e - L_4 + \frac{D}{2} \right)^2 \right)^{\frac{1}{2}} \\ L_2 &= \left(y_e^2 + \left(-x_e - L_1 + \frac{D}{2} \right)^2 \right)^{1/2} \end{aligned} \tag{A2}$$

And the inverse kinematics model yields

$$\begin{aligned} [\theta_L \ \theta_R \,] &= \Lambda^I(x_e, y_e, x_c) \\ &= \frac{1}{r} \cdot [L_1 + L_2 - L_{10} - L_{20} \ L_3 + L_4 - L_{30} - L_{40} \,] \end{aligned} \tag{A3}$$

On the other hand, considering that both the motor angles and the carriage position is known, the lengths of the cables can be computed as

$$\begin{aligned} L_1 &= \frac{D}{2} - x_c - \frac{w}{2} \\ L_4 &= \frac{D}{2} + x_c - \frac{w}{2} \\ L_2 &= r\theta_L + L_{10} + L_{20} - L_1 \\ L_3 &= r\theta_R + L_{30} + L_{40} - L_4 \end{aligned} \tag{A4}$$

Finally, the estimator block, $[\hat{x}_e, \hat{y}_e] = \Xi(x_c, \ \theta_L, \theta_R)$ yields as

$$\begin{aligned} [x_e \ y_e \,] &= \Xi(x_c, \theta_L, \theta_R) \\ &= \left[\frac{L_3^2 + 2wx_c - L_2^2}{2w} \ \frac{a \cdot b \cdot c \cdot e}{2w} \right] \end{aligned} \tag{A5}$$

being $a = L_2 + L_3 + w$, $b = (L_2 + L_3 - d)$, $c = L_2 - L_3 + d$ and $e = L_3 - L_2 + d$.

4.3 Contribution 2

Smart Structures and Systems, *Vol. 27, No. 2 (2021) 397-406*
DOI: https://doi.org/10.12989/sss.2021.27.2.397

Closed loop cable robot for large horizontal workspaces

Sergio Juárez-Pérez [1], Antonio González-Rodriguez [1], Guillermo Rubio-Gómez [1], David Rodríguez-Rosa [1], Erika Ottaviano [2] and Fernando J. Castillo-Garcia*[1]

[1] *Escuela de Ingeniería Industrial y Aeroespacial de Toledo* (*UCLM*), *Spain*
[2] *Facoltá di Ingegneria Industriale di Cassino* (*UNICAS*), *Italy*

(*Received July 16, 2020, Revised September 28, 2020, Accepted October 10, 2020*)

Abstract. Inspection and maintenance of civil structures are important issues for sustainability of existing and new infrastructures. Classical approach relies on large human activities eventually performed in unsafe conditions. This paper proposed a non-invasive solution for inspecting horizontal surface such as decks of bridges. The proposal presented here is based in cable-driven robots and allows to inspect large surfaces maintaining a very low vertical occupancy in comparison to the conventional architecture of this kind of robot. Using closed cables loop instead of a set of cables a device with low motorization power and very large workspace is designed and prototyped. As example of control an inverse dynamics technique is applied to control the end-effector where inspection tool is located, e.g., a vision system. Experimental results demonstrate that this novel device allows to inspect large horizontal surfaces, with low motorization and low vertical occupancy.

Keywords: cable robot; large workspace; flat large structures; automatic inspection

1. Introduction

In the recent past, a consistent research in the field of Robotics has been devoted to cable-based systems, reflecting the considerable interest according to the large and increasing number of applications. Cable-Driven Parallel Manipulators (CDPMs) use cables to control the end-effector pose, strengthening classic advantages characterizing closed-chain architectures, like large payloads, good dynamic performances, high efficiency, while providing peculiar advantages, such as light weight, large workspace, reduced manufacturing and maintenance costs, deployability and possibility to be moved and mounted on site, superior modularity and reconfigurability (Merlet, book). Moreover, one of the main advantages of CDPMs is that they can be easily adapted to fit certain application or performance requirements, demonstrating greater flexibility than classical robot designs composed by rigid links (Kozak *et al*. 2006, Roberts *et al*. 1998).

The above-mentioned main characteristics of CDPM, mainly related to the very large workspace for positioning, make them very attractive for a many task. One of the first applications dealt with NIST Robocrane (Albus *et al*. 1993) and the systems proposed in Havlik (2000), Nan and Peng (2000), Bosscher (2006). A prototype of a CDPM was developed to be used as suspension system for testing airplane models in wind tunnels, as described in (Yangwen *et al*. 2010). An ultrahigh speed robot design, FALCON-7 was proposed in Kawamura *et al*. (1995) where cables were modeled as non-linear springs taking into account axial flexibility, the model was further developed in Kawamura *et al*. (2000).

Engineering challenges also include material handling over large areas, positioning for heavy objects, rescue operations, service, assistance, rehabilitation, entertainment (Castelli *et al*. 2014) and even the Five hundred meter Aperture Spherical Telescope (FAST), as described in Nan (2006), which is the world's largest filled-aperture radio telescope and the second-largest single-dish aperture after the RATAN-600 in Russia. It consists of a fixed 500 m diameter dish built in a natural depression in the landscape having a novel design, using an active surface made of metal panels that can be tilted by a computer to help change the focus to different areas of the sky. The cabin containing the antenna is suspended by cable. FAST is considered operational nowadays after 3 years testing. The cable mass and sagging effects are not negligible, in this case.

As previously introduced, the most interesting application of CDPM deals with very large workspace, as for the virtual reality simulator (CableRobot Simulator 2020) in which eight supporting cables fully control the motion of a cabin. The design is scalable and can be reproduced in any scale. The IPAnema CDPM was designed for industrial processes (Pott *et al*. 2013).

Cable-suspended camera systems are commonly used in stadiums and arena, they are composed by actuation and transmission systems, most of the time motorized winches and pulleys, which are used to exert or retract cables connected to an end-effector. The end-effector is suspended and consist of a counterbalanced pan and tilt video camera, (Cone 1985, Skycam 2020).

Suspended CDPM is a crane type CDPM in which the end-effector is suspended by n supporting cables, they have attracted the interest of the research community since the

*Corresponding author, Professor,
E-mail: Fernando.Castillo@uclm.es

ISSN: 1738-1584 (Print), 1738-1991 (Online)

workspace is not cluttered by cables and there is less probability of cable interference make them more useful in practical application. Although several works in the literature, the study of these types of robots is still an open field. The major challenge in the position analysis of suspended CDPMs consists of the intrinsic coupling between kinematics and statics (or dynamics). For a fully-constrained CDPM in which the required set of output wrenches is guaranteed with purely tensile cable forces, the posture of the end-effector is determined in a purely geometric way by assigning cable lengths. Instead, for a suspended CDPM, even if the actuators are locked having assigned the cable lengths, the end-effector is still movable; indeed, the equilibrium configuration is determined by the applied forces. Therefore, the end-effector pose (position and orientation) depends on both the cable lengths and equilibrium equations. Moreover, as the end-effector pose depends on the applied external wrenches (forces and torques), it may change due to external disturbances. Therefore, it is necessary considering kinematics together with statics or dynamics equilibrium. The complexity of positioning capability of suspended CDPM is then increased and significantly more difficult than analogous tasks concerning rigid-link parallel manipulators. In the literature, some procedures have been presented, in (Abbasnejad and Carricato 2015) the problem has been defined as geometrico-static also expressing some connections between stability and energy (Carricato and Merlet 2013). The mass and elasticity of cables are taken into account in (Kozak *et al*. 2006, Pott 2010, Merlet 2016). An analytical model is presented for solving the DK and the IK problems of CDPMs with sag cables, based on a mixed formulation of a nonlinear elasto-static problem.

The problem of sagging is much more relevant for suspended CDPM, it has been shown in the literature that the effect in most of those cases cannot be neglected for correct modelling and use of CDPMs (Ottaviano and Castelli 2010, Irvine 1981). Another relevant issue for suspended CDPM is the pulleys that greatly influence the positioning capabilities, in Gonzalez-Rodriguez *et al*. 2017) a solution is proposed for a novel design solution.

In this work a novel design for suspending cable robot is proposed, focused on its optimization for large two-dimensional flat spaces perpendicular to gravity, strictly limiting the occupation in the gravity direction. The proposed cable robot scheme can be used for a great number of tasks carried out in workspaces of these characteristics. Considering the importance for an automatic inspection of large civil infrastructures (Jung *et al*. 2019, Kim *et al*. 2014), authors think that an interesting task for this type of robot would be to inspect the bottom of the large bridges decks (Huang *et al*. 2016) by adding different inspection devices to the end-effector as cameras (Adhikari *et al*. 2016) or laser (Wang *et al*. 2016). In this problem, the space occupied in the vertical direction must be reduced, while the workspace in the horizontal plane is large. Common cable driven suspended robots present serious technical problems when employed in this kind of workspaces, the proposed solution has been specifically designed to solve these problems.

The rest of the paper is organized as follows: Section 2 introduces the novel proposal; Section 3 presents the prototype for experimental validation. Section 4 details the experimental results in term of repeatability and, finally, Section 5 states the main conclusions and further works.

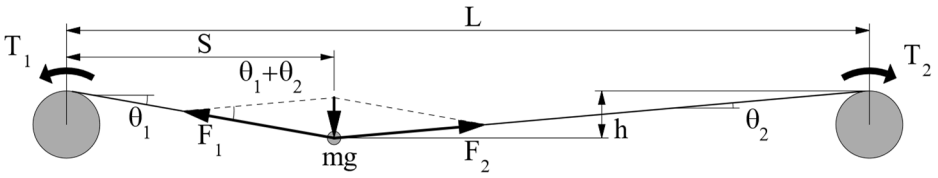

Fig. 1 Forces and torques in a 2D cable robot for a little h

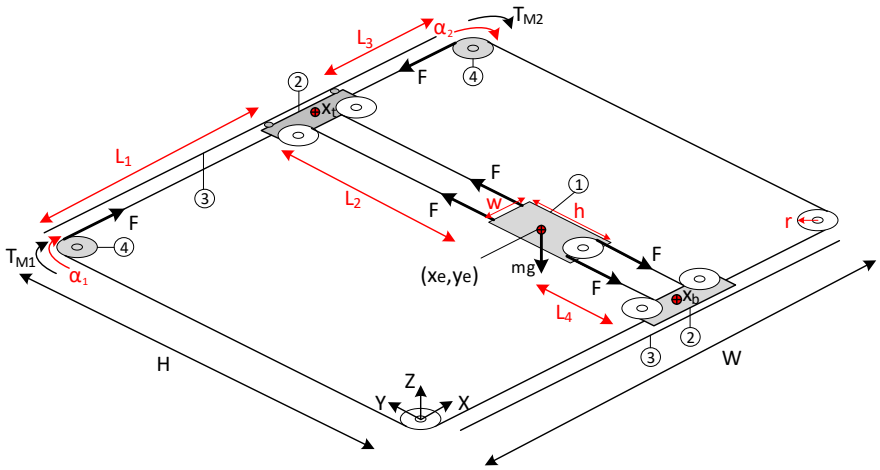

Fig. 2 Proposed 2D cable robot for high workspaces

2. Proposed solution

2.1 Description of the proposal

In cable-driven robots, the end-effector is connected to the frame by several cables. The more extended solution consists on using different cables that join the end-effector to different motors in the frame. Fig. 1 shows a conventional configuration for a suspended cable robot of 2 DOFs. The torque required in each motor is equal to the tension of the cable multiplied by the radius of the pulley or winch joined to the motor.

There are applications for cable robot, such as the inspection of the lower part of bridge decks, in which the workspace must be large in extension, but little space can be occupied in the vertical direction, due to the bridge characteristics. In this case the cable tensions will be very large, even for a light mass m, if L is much greater than h, as shown in Fig. 1.

As an example, if it is required to transport a light mass m = 10 kg with a speed of 1 m/s, for L = 100 m and a vertical occupancy h < 0.2 m, the tension of the cable will be greater than 10 KN for two cables, or greater than 5 kN for four cables. If the cable tension of this robot is high, the torque requirement of the motor is therefore very high, since the diameter of the pulleys has a minimum permissible due to the diameter of the cable. Great torque requirement implies a very high power if the velocity is not near to zero. In this case, the system of Fig. 1 needs 25 kW overall power for moving a 10 kg mass with 1 m/s speed. This represents a disproportionate amount of power.

In order to solve this problem, authors propose employing only one closed cable instead of different cable joined to different motors. The scheme of the proposed robot, along with the nomenclature used in the rest of the paper are shown in Fig. 2. Different elements of the robot shown in Fig. 2 are the end-effector (1), two driving pulleys ((4), grey pulleys) and free pulleys (white pulleys). The robot has also two carriages (2) and two linear guides (3). Cables can replace the guides so that the cars slide through them with new pulleys. (T_{M1}, T_{M2}) are the torques exerted by the left and right motors, respectively, (x_e, y_e) is the end-effector pose, (x_t, x_b) are the x-coordinates of the top and bottom carriages, respectively, (L_1, L_2, L_3, L_4) are the different cable lengths, (α_1, α_2) are the angles turned by the left and right motors, (W, H) are the frame width and height, (w, h) are the end-effector width and height and r is the pulley radius.

Fig. 2 shows the system in a static position. If the end effector is placed in the center of the workspace in the Y direction of movement, the forces will be exactly the same if the cable mass is neglected. If the Z coordinate of the end effector is much less than the distance to either carriages, the forces will be different but very similar. This implies a little reduction in the robot's workspace. Let's call S to the minimum horizontal distance between carriage and end effector, as it shown in Fig.1. The maximum difference between the forces F at both sides of the end effector is given when $L >> S$. In this case $\theta_2 = 0$, F_2 is almost horizontal and ratio F_1/F_2 is

$$\frac{F1}{F2} = \cos\left(\text{atan}\left(\frac{h}{S}\right)\right) \simeq 1 - \frac{1}{2}\left(\frac{h}{S}\right)^2 \quad (1)$$

In this way, for example, assuming that the end-effector cannot approach less than 10 times the maximum Z coordinate of the end effector, the ratio $1 > F_1/F_2 > 0.995$, and $F_1 - F_2 = 4.9$ N for a vertical force of 98 N.

Another consequence of the proposed approach will be that the tension forces F of the cables will be much greater than the vertical force generated by gravity on the end-effector. Unlike conventional cable robots, this force does not imply high torque in the motors, in fact, for the stationary situation the torque is near zero. The torque in the driven pulleys (4) is null when the end effector is not moving, since the cable does not end in the pulley and tensions in both sides of the pulley compensate each other.

Fig. 3 shows the robot when the end effector is moving with acceleration A in the Y direction. The tension of the four cables of the end-effector is different now, but its difference is only the inertial force required to accelerate the end-effector. For an acceleration of 1 m/s^2 that difference is an order of magnitude less than the gravity force, and several orders of magnitude less than the cable tension.

The torque on the driving pulleys is now $T_M = r\,(F + \Delta F - F) = r\Delta F$. For an acceleration of 1 m/s^2 and a

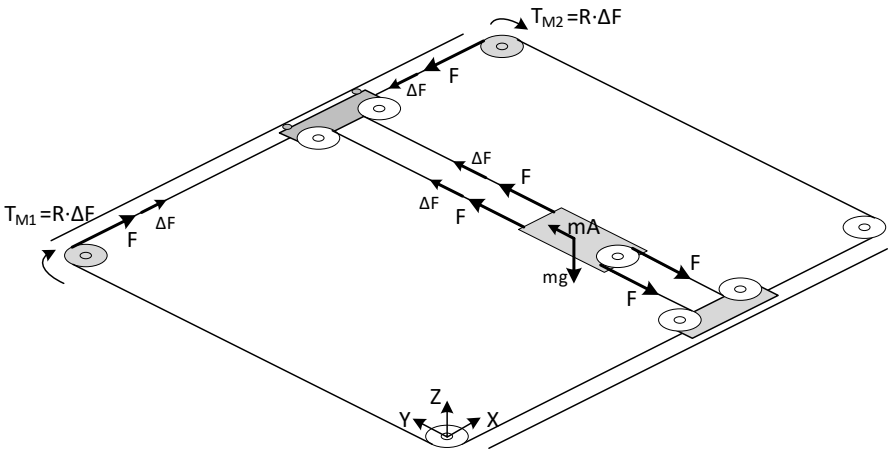

Fig. 3 Proposed 2D cable robot with Y acceleration

speed of 1 m/s it means an output power from the motor of only 10 W, if the friction on the pulley is neglected. This torque is so small that the practical equality between the branches of the cable can no longer be assumed due to a small Z coordinate. But, if this approximation is not neglected, this only adds 5 W more to the previous calculated power. In this way, by correctly choosing the components, the required power will be several orders of magnitude less than the power required for a conventional cable robot where the cable ends in motor pulleys.

The proposed cable robot scheme can be used for a great number of tasks carried out in large two-dimensional flat spaces perpendicular to gravity. The authors think that an interesting task for this type of robot would be to inspect the bottom of the large bridges deck (Huang *et al*. 2016) by adding different inspection devices to the end-effector as cameras (Adhikari *et al*. 2016) or laser (Wang *et al*. 2016). In this problem, the space occupied in the Z coordinate must be reduced, while the workspace in the X-Y axes is large.

Focusing on the workspace characteristics for which the robot has been designed, Fig. 4 shows two alternative schemes proposed for its optimization, as rigid guides are replaced by cables. Several parts of the robots are shown in Fig. 4 as the end-effector (1), the guidance cables (2), driving pulleys (3) and the bridge deck (4). The main dimension of the bridge is along the X-axis.

2.2 Drawbacks caused by friction in the proposed solution and possible solution

In Fig. 5 the proposed system is shown in a dynamic state. In this model the mass is concentrated in the end-effector, and the mass of the carriages is neglected. Dimensions of the end effector and carriage are also neglected compared to the width and the height of the robot frame. Fig. 5 shows a movement in the positive direction of x-axis. The system is represented in three phases of movement: acceleration (a), constant velocity (b) and deceleration (c).

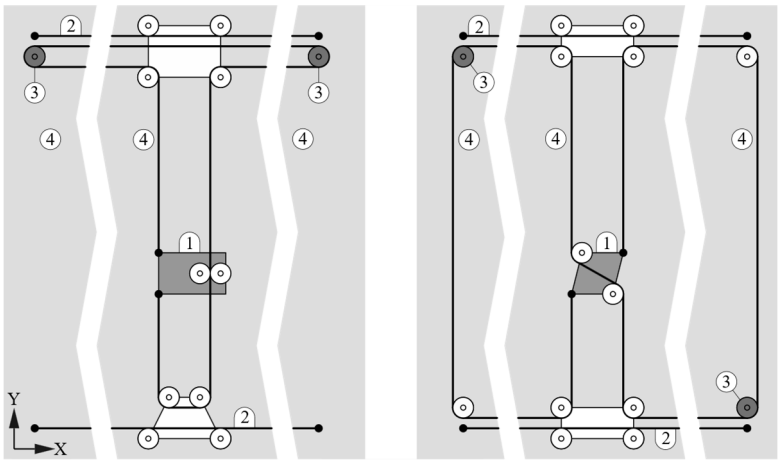

Fig. 4 Alternative schemes for a 2-DOF robot for large spaces

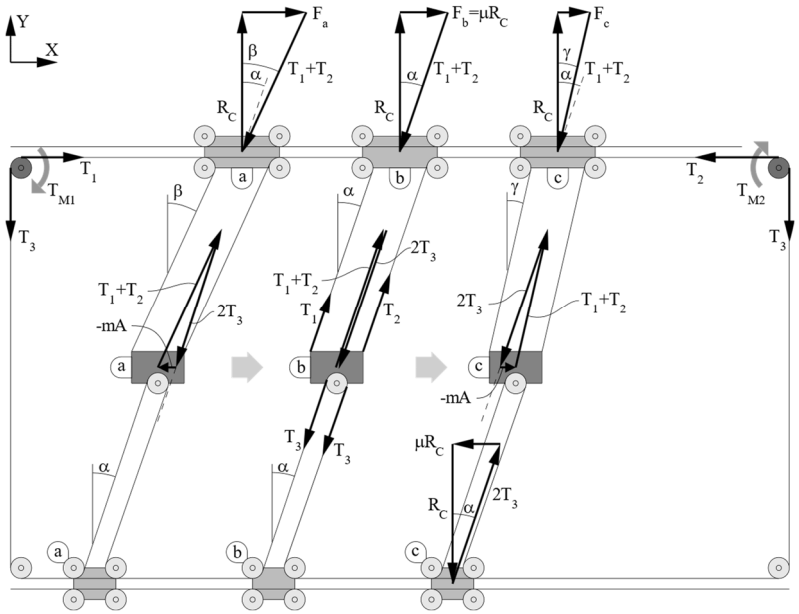

Fig. 5 Proposed 2D cable robot with X acceleration

In the constant velocity phase the end-effector has no inertial force, therefore the cables that connect them to both carriages must be parallel. This inclination in the carriage cables counteracts the friction force in the guides, with an angle α, as shown in the balance of forces of the carriage labeled as (b). Thus, the horizontal component of the cable tension force is $F_b = \mu R_c$, where μ is the friction coefficient and R_c is the normal reaction force in the carriages given by the guide. This horizontal force F_b is provided by the driving pulleys $F_b = r(T_{M2} - T_{M1})$, where r is the radius of the pulleys and T_{M2} and T_{M1} are the torque of the driving pulleys.

In the acceleration and deceleration, the cable forces in both sides of the end effector are not parallel in order to counteract the inertial force in the end-effector, as it is shown in Fig. 5. Anyway, in the passive branch of the robot (the connected to the free pulleys), the cables always have the same angle α, but in acceleration process the angle of the upper cables is β, while γ is this angle for the deceleration.

The lag in carriage movement is a major problem in maintaining robot positioning accuracy. This is because Coulomb's dry friction would maintain this lag when the carriages had stopped. If the precision is not important for the application of the cable robot, this scheme can be valid, although it would be recommended to maintain carriages friction as low as possible. To solve this problem, the modification of the general scheme shown in Fig. 6 is proposed. In it, two X-cables (a) have been added so that the parallel movement of both cables is forced. This solution presents the problem that with the two carriages located on the same vertical line, the inertial forces in the X direction of the end-effector can only be counteracted by elastic cable extensions.

2.3 Natural frequency of the system

The movement in the Y direction does not present much problem and would be similar than moving a mass on a guide, especially taking into account that the carriage movement is the same thanks to cables (a) in Fig. 6. This is due to the fact that the inertial forces are parallel to the end-effector cables.

Much more problematic is caused by movements in the X direction. Even if the robot application does not need

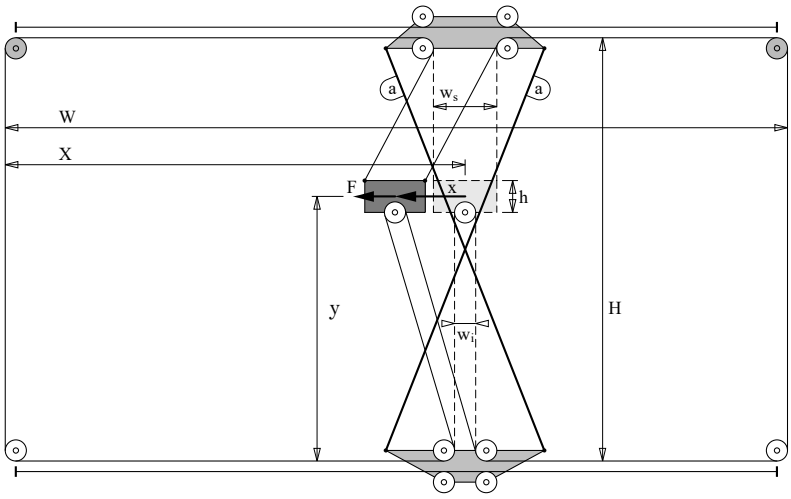

Fig. 6 Proposed solution of increase accuracy in 2D large cable robot

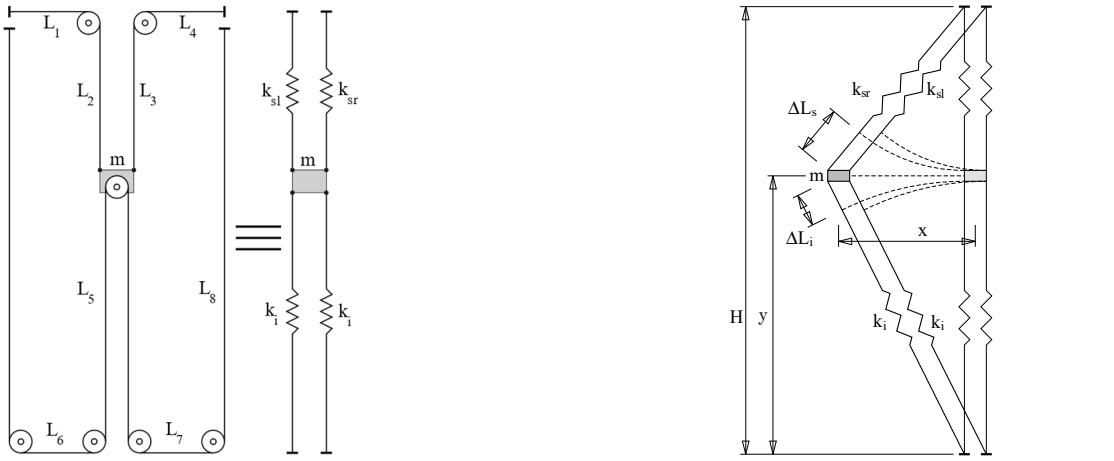

(a) Vibration model of the robot (b) Increment of cables length due to x displacement

Fig. 7 Models and nomenclature for natural frequency analysis

high precision, a dynamic model for vibration of the end-effector in the X direction is needed to control the robot. This vibration appears when the end-effector suffers inertial forces in the X direction, even with the motors stopped. The model shown in Fig. 7 will be used for obtaining the dynamic response.

The original scheme can be modeled with the four springs system shown in the right side of Fig. 7(a). The equivalent stiffness of the springs are

$$\begin{aligned} k_i &= 2\left(\frac{2}{k_5}+\frac{1}{k_6}+\frac{1}{k_7}\right)^{-1} \\ k_{sl} &= \frac{k_1+k_2}{k_1k_2} \\ k_{sr} &= \frac{k_3+k_4}{k_3k_4} \end{aligned} \tag{2}$$

where $k_n = (E \cdot A)/L_n$, being E the young modulus of the cable material, A the cross section of the cable and L_n the length of the n-th cable as numbered in Fig. 7(a).

Maintaining a low Z coordinate for the end effector implies the need to pre-stress the robot's cable system. Despite all the cables being connected in a single loop, different prestressing forces could be imposed on the three cable branches if the driven pulleys are actuated. Since the torque of the motor is not comparable to the torque generated by the systems' prestressing, this difference would be lost as soon as the motor of the driven pulleys loses its torque. For this reason, the prestressing will be considered to generate the same force for the three cable branches: the upper two and the lower one.

Dynamic equations will be obtained using Euler-Lagrange formulation and x as generalized coordinate. For obtaining the natural frequency of the system the motor will be considered stopped. The Lagrangian is

$$L = T - U_{sl} - U_{sr} - U_i \tag{3}$$

where

$$\begin{aligned} T &= \frac{1}{2}m\dot{x}^2 \\ U_{sl} &= \frac{1}{2}k_{sl}(\Delta L_s + \Delta L_{Psl})^2 \\ U_{sr} &= \frac{1}{2}k_{sr}(\Delta L_s + \Delta L_{Psr})^2 \\ U_i &= 2\left(\frac{1}{2}k_i(\Delta L_i + \Delta L_{Pi})^2\right) \end{aligned} \tag{4}$$

and where ΔL_i and ΔL_s are the length increment due to x displacement. ΔL_{Psl}, ΔL_{Psr} and ΔL_{Pi} are the length increase due to the prestressing of the cable. F_P is the prestressing of the cable, this force is unique and yields as

$$F_p/k_T = \Delta L_{PT} \tag{5}$$

where

$$\begin{aligned} \Delta L_{PT} &= \Delta L_{Psl} + \Delta L_{Psr} + 2\Delta L_{Pi} \\ k_T &= \left(\frac{1}{k_1}+\frac{1}{k_2}+\frac{1}{k_3}+\frac{1}{k_4}+\frac{2}{k_5}+\frac{1}{k_6}+\frac{1}{k_7}+\frac{2}{k_8}\right)^{-1} \end{aligned} \tag{6}$$

This fact allows calculating the increments of length due to the prestressing.

$$\begin{aligned} F_p/k_{sl} &= \Delta L_{Psl} \\ F_p/k_{sr} &= \Delta L_{Psr} \\ F_p/k_i &= \Delta L_{Pi} \end{aligned} \tag{7}$$

In the other hand, Fig. 6(b) shows the increment of the length of the cables due to the x movement of the mass

$$\begin{aligned} \Delta L_s &= \sqrt{(H-y)^2+x^2} - (H-y) \\ \Delta L_i &= \sqrt{y^2+x^2} - y \end{aligned} \tag{8}$$

where x, y are the end-effector displacement and H the frame height. In this way

$$\begin{aligned} \frac{\partial U_i}{\partial x} &= 2\frac{\partial}{\partial x}\left(\frac{1}{2}k_i\left(\sqrt{y^2+x^2}-y+\Delta L_{Pi}\right)^2\right) \\ &= \frac{xk_i\left(\sqrt{y^2+x^2}-y+\Delta L_{Pi}\right)}{\sqrt{y^2+x^2}} \end{aligned} \tag{9}$$

This derivate can be approximated by Taylor series.

$$\frac{\partial U_i}{\partial x} \cong 2\frac{xk_i\Delta L_{Pi}}{y} + 2\frac{x^3k_i}{2y^2}\left(1-\frac{\Delta L_{Pi}}{y}\right) + \cdots \tag{10}$$

Cubic terms of the previous expression can be neglected since $x << y$, $x << (H-y)$, $\Delta L_{Ps} << y$ and $\Delta L_{Ps} << (H-y)$. Thus, operating similarly for the upper branch

$$\begin{aligned} \frac{\partial U_i}{\partial x} &\cong 2\frac{xk_i\Delta L_{Pi}}{y} = 2\frac{xF_P}{y} \\ \frac{\partial U_{sl}}{\partial x} &\cong \frac{xk_{sl}\Delta L_{Psl}}{H-y} = \frac{xF_P}{H-y} \\ \frac{\partial U_{sr}}{\partial x} &\cong \frac{xk_{sr}\Delta L_{Ps}r}{H-y} = \frac{xF_P}{H-y} \end{aligned} \tag{11}$$

Now we have all the terms with which to build the Euler-Lagrange equation, with x being the generalized coordinate.

$$\frac{\partial L}{\partial x} - \frac{d}{dt}\frac{\partial L}{\partial \dot{x}} = 0 \Rightarrow m\ddot{x} + xF_P\left(\frac{2}{y}+\frac{2}{H-y}\right) = 0 \tag{12}$$

The natural frequency of the system obtained from equation (x) is

$$\omega_N = \sqrt{\frac{2HF_P}{mY(H-y)}} \tag{13}$$

Expression (13) represents the natural frequency of the system that depends on the y coordinate, the mass of the end-effector and the tension of the cable closed-loop. Fig. 9c, in Section 3, represents the mesh of ω_N values for the entire workspace of the robot compared with the experimental ones for model validation purpose.

2.3 Kinematics model

In this section the robot inverse kinematics model is explained, it allows to compute the angle to be turned by motors to reach an arbitrary end-effector pose. It is

employed for the control of the end-effector pose as explained in following sections. Following the nomenclature exposed in Fig. 2 and setting an initial point for the end-effector pose (x_0, y_0), the initial cable lengths can be computed as

$$\begin{aligned} L_{10} &= x_0 - \frac{w}{2}; & L_{20} &= H - y_0 - \frac{h}{2} \\ L_{30} &= W - x_0 - \frac{w}{2}; & L_{40} &= y_0 - \frac{h}{2} \end{aligned} \tag{14}$$

In a similar manner, cable length for an arbitrary end-effector pose can be computed as

$$\begin{aligned} L_1 &= x_e - \frac{w}{2}; & L_2 &= H - y_e - \frac{h}{2} \\ L_3 &= W - x_e - \frac{w}{2}; & L_4 &= y_e - \frac{h}{2} \end{aligned} \tag{15}$$

Assuming that the initial angle for the motors corresponds to (x_0, y_0), the inverse kinematics, $[\alpha_1, \alpha_2] = \Lambda^I(x_e, y_e)$, can be obtained

$$\begin{aligned} \alpha_1 &= \frac{1}{r}(L_1 + L_2 - L_{10} - L_{20}) \\ &= \frac{1}{r}(x_e - x_0 + y_0 - y_e) \\ \alpha_2 &= \frac{-1}{r}(L_3 + L_2 - L_{30} - L_{20}) \\ &= \frac{-1}{r}(x_0 - x_e + y_0 - y_e) \end{aligned} \tag{16}$$

3. Experimental platform

3.1 Description

Fig. 8 shows the experimental platform. The frame is made of steel profile and its dimensions are 2.5×2.0 m. The end-effector is 0.35×0.15 m and its weight is 1.2 kg. The upper and downer carriages are mounted on linear guides attached to the frame. The pulleys are made of nylon and their radius is 0.06 m.

The motors are stepper motor Nema 34 (3000 rpm, 27.8 Nm). The position reference is defined by means of

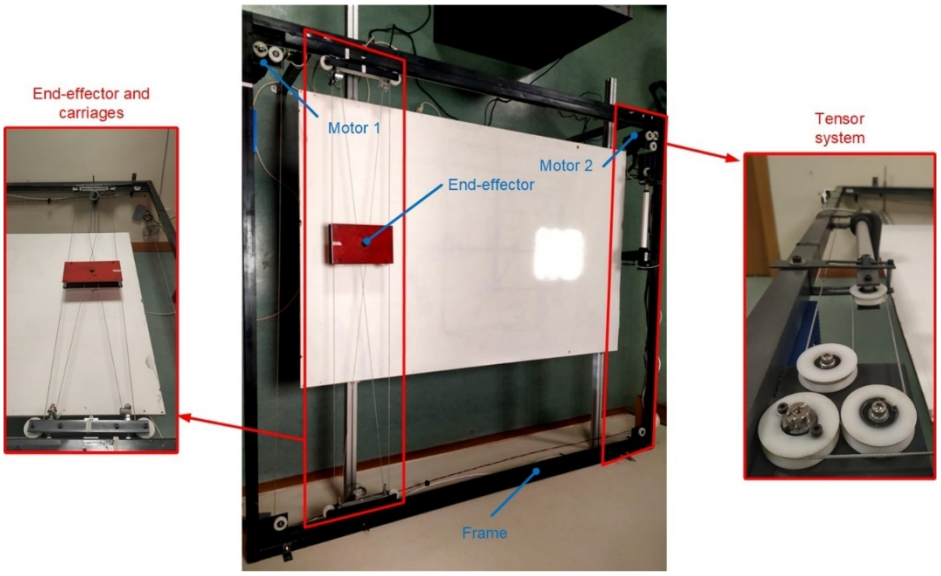

Fig. 8 Experimental platform.

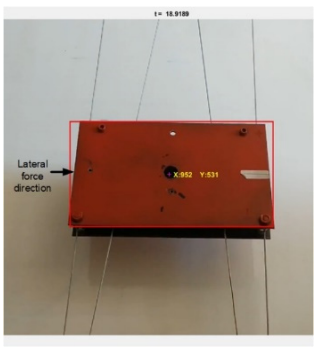

(a) Captured frame for vibration determination

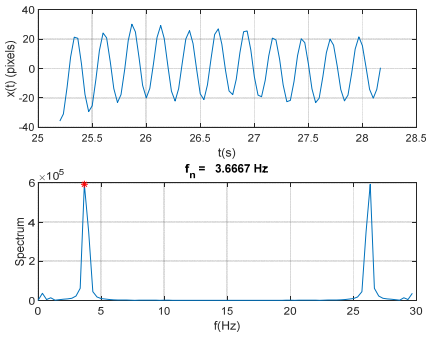

(b) Example of captured movement and natural frequency determination

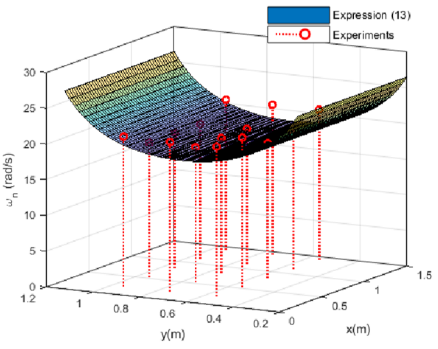

(c) Natural frequency: model vs. experiments

Fig. 9 Procedure for natural frequency determination

a Matlab® application which send the trajectory data to an Arduino Mega controller. This controller commands the movement of the motors by means of two position servocontrollers. The sample time used for the control scheme is 1 ms.

3.2 Frequency domain identification

Expression (13) is an approach to determine the natural frequency of the end-effector. This section details the experimental validation of (13). For a given pose, $[x_e,\ y_e]$ an instantaneous lateral force of 20N is applied to the end-effector on the direction of X axis. A vision system (1080 × 720 p and 60 fps) captures the dynamic image of the end-effector movement. An application developed in Matlab® determines the real word coordinates of the movement of the end-effector. By analysing the displacement of end-effector among X axis, the natural frequency, ω_n, can be determined. Fig. 9(a) shows and example of a captured frame since Fig. 9(b) shows an example of x movement of end-effector after applying the lateral force, the Fourier Transform of the displacement and the value of an example of the obtained natural frequency.

Following this procedure, the natural frequency of the end-effector can be experimentally determined for different end-effector pose and compared to expression (13) for validation purpose (see Fig. 9(c)). The maximum error committed between expression (13) and experiments is less than 10%. Section 4 demonstrates that expression (13) can be successfully applied to implement an easy closed loop for controlling the end effector pose.

4. Control approach and results

4.1 Control strategy

Fig. 10 represents the control strategy applied for controlling the proposed device. System dynamics represents the dynamics behaviour of the end-effector when is actuated by means of the stepper motors described in the previous section. In this sense, we are going to consider the dynamics behaviour of the controlled system (inner loop in Fig. 10), is of the form

$$\Psi(s)=\begin{bmatrix}\dfrac{\alpha_1(s)}{\alpha_1^*(s)} & 0\\ 0 & \dfrac{\alpha_2(s)}{\alpha_2^*(s)}\end{bmatrix}=\begin{bmatrix}\dfrac{K_1\omega_{n1}}{s^2+2\xi_1\omega_{n1}s+\omega_{n1}} & 0\\ 0 & \dfrac{K_2\omega_{n2}}{s^2+2\xi_2\omega_{n2}s+\omega_{n2}}\end{bmatrix} \tag{17}$$

being $K_1=K_2=1$ (zero steady state error provided by servocontrollers), $\omega_{n1}=\omega_{n2}$ and equal to the natural frequency identified in Section 3.2 and $\xi_1=\xi_2$ that has been set to 0.4.

The assumption that the inner loop presents a second order and linear dynamics is a strong assumption that is only used as an easy example to control the end-effector pose owing that the actuator system are stepper motors controlled by servocontrollers which dynamics is unknown.

If inner loop is of the form shown in (17), inverse dynamics can be expressed as

$$\Psi^{-1}(s)=\begin{bmatrix}\dfrac{s^2+2\xi_1\omega_{n1}s+\omega_{n1}}{K_1\omega_{n1}} & 0\\ 0 & \dfrac{s^2+2\xi_2\omega_{n2}s+\omega_{n2}}{K_2\omega_{n2}}\end{bmatrix} \tag{18}$$

Although $\Psi^{-1}(s)$ is a non-proper dynamics, it can be precomputed as shown in Fig. 10 in time domain as

$$\begin{aligned}\hat{\alpha}_1^*&=\frac{1}{K_1}\left(\alpha_1^*+2\xi_1\frac{d\alpha_1^*}{dt}+\frac{1}{\omega_{n1}}\frac{d^2\alpha_1^*}{dt^2}\right)\\ \hat{\alpha}_2^*&=\frac{1}{K_2}\left(\alpha_2^*+2\xi_2\frac{d\alpha_2^*}{dt}+\frac{1}{\omega_{n2}}\frac{d^2\alpha_2^*}{dt^2}\right)\end{aligned} \tag{19}$$

This control approach is a simple inverse dynamics technique which use the natural frequency identification of Section 3.2 to generate modified motor angle references, $\hat{\alpha}_1^*$ and $\hat{\alpha}_2^*$, to remove the non-desirable vibration of the end-effector when moves along X-axis.

For ensuring a smooth shape of $\hat{\alpha}_1^*$ and $\hat{\alpha}_2^*$, a third-order trajectory of the end-effector reference has been generated.

4.2 Results

4.2.1 Repeatability

The control approach has been experimentally tested and the end-effector pose, x_e and y_e has been checked by means of the vision system mentioned in Section 3.2.

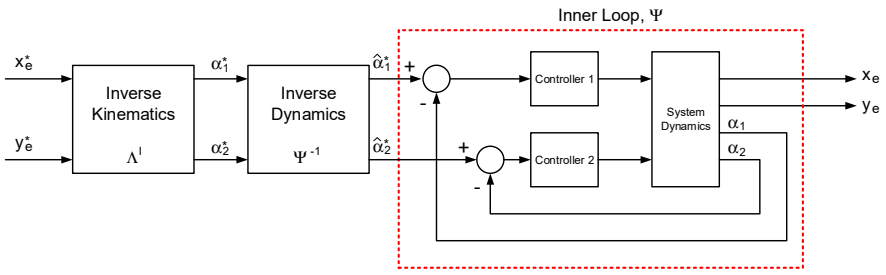

Fig. 10 Experimental platform

(a) Repeatability test: X-axis movement (b) Repeatability test: Y-axis movement

Fig. 11 Repeatability experiments

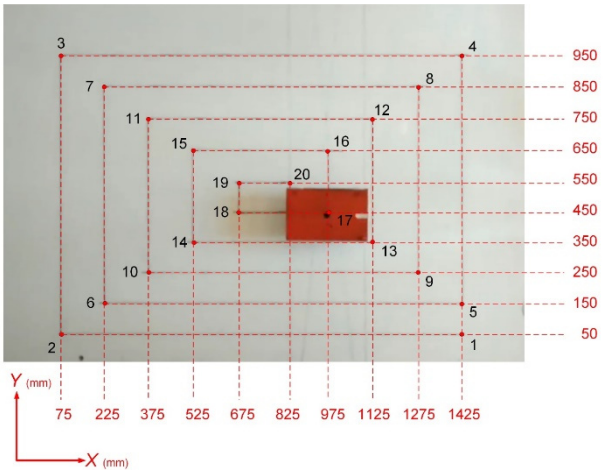

Fig. 12 Trajectory tracking experiment

First results are a related to the robot repeatability. A go and back X and Y-axis trajectories have been repeated 20 times, measuring the error after the 20 manoeuvres. Fig. 11 illustrates the experiments. The error committed for horizontal experiment is 1.6 mm and 0.5 mm for vertical one.

4.2.2 Trajectory tracking

Fig. 12 illustrate the 20-points trajectory executed to check the trajectory tracking of the end-effector.

Table 1 summarizes the steady state error and the maximum following error. Vertical movements naturally present less error than horizontal one. The maximum following error is 14.5 mm (trajectory 15-16) since the maximum steady state error is 2.6 mm (trajectory 18-19).

5. Conclusions

In this work, a novel mechanical design based in closed cable loop is presented for inspection of horizontal surface of civil structures. The proposal here is easily scalable for very large workspace maintaining the motorization of the robot. The device presents non-desirable vibration when moving along X-axis. A simple model for determining the natural frequency is developed and experimentally validated. This frequency characterization is applied for controlling the end-effector pose by using an inverse dynamics scheme, owing to the unknown dynamics of the stepper motors-controllers set. The results show that the robot presented here presents an accuracy about 15 mm for trajectory tracking and a maximum steady state error about 2-3mm.

This proposal is a novel solution to inspect horizontal surfaces if civil structures. This novel device has a low vertical occupancy so it can be considered a non-invasive solution.

Further works in this research line must include the attaching of different inspection systems to the end-effector

Table 1 Trajectory tracking results

Trajectory	Maximum following error (mm)	Steady state error (mm)	Trajectory	Maximum following error (mm)	Steady state error (mm)
1-2	8.9	1.2	11-12	7.5	2.2
2-3	2.1	1.8	12-13	6.2	1.2
3-4	7.2	1.8	13-14	2.5	2.5
4-5	1.8	1.4	14-15	6.0	1.4
5-6	12.4	2.4	15-16	14.5	2.5
f6-7	3.6	2.1	16-17	9.4	1.6
7-8	9.1	2.2	17-18	1.2	1.0
8-9	2.5	1.4	18-19	2.6	2.6
9-10	8.4	1.5	19-20	1.5	0.8
10-11	2.0	1.8			

as cameras or laser to detect, reconstruct and analyse different kind of defects present in horizontal surfaces of civil infrastructures as deck of bridges.

Acknowledgments

The research described in this paper was financially supported by Research Fund for Coal and Steel grant agreement No 800687 in the framework of DESDEMONA project. Authors wish to thank the financial Support provided by the university of Castilla-La Mancha and the European Social Fund through the pre-doctoral funding [2019/451].

References

Abbasnejad, G. and Carricato, M. (2015), "Direct geometrico-static problem of underconstrained cable-driven parallel robots with *n* cables", *IEEE Transact. Robot.*, **31**(2), 468-478. https://doi.org/10.1109/TRO.2015.2393173

Adhikari, R.S., Bagchi, A. and Moselhi, O. (2014), "Automated condition assessment of concrete bridges with digital imaging", *Smart Struct. Syst.*, *Int. J.*, **13**(6), 901-925. https://doi.org/10.12989/sss.2014.13.6.901

Albus, J., Bostelman, Dagalakis, N. (1993), "The nist robocrane", *J. Robot. Syst.*, **10**(5), 709-724.

Bosscher, P. (2006), "Cable-suspended robotic contour crafting system", *Automat. Constr.*, **17**, 45-55. https://doi.org/10.1016/j.autcon.2007.02.011

CableRobot Simulator (2020), "Cable-driven parallel robots – motion simulation in a new dimension", Accessed: 2020-07-10. http://www.ipa.fraunhofer.de/en/cable-driven_parallel_robots.html

Carricato, M. and Merlet, J.-P. (2013), "Stability analysis of underconstrained cable-driven parallel robots", *IEEE Transact. Robot.*, **29**(1), 288-296. https://doi.org/10.1109/TRO.2012.2217795

Castelli, G., Ottaviano, E. and Rea, P. (2014), "A Cartesian cable-suspended robot for improving end-users mobility in an urban environment", *Robot. Comput.-Integr. Manuf.*, **30**(3), 335-343. https://doi.org/10.1016/j.rcim.2013.11.001

Cone, L.L. (1985), "Skycam-an aerial robotic camera system", *Byte*, **10**(10), 122.

Gonzalez-Rodriguez, A., Castillo-Garcia, F.J., Ottaviano, E., Rea, P. and Gonzalez-Rodriguez A.G. (2017), "On the effects of the design of cable-Driven robots on kinematics and dynamics models accuracy", *Mechatronics*, **43**, 18-27. http://dx.doi.org/10.1016/j.mechatronics.2017.02.002

Havlik, S. (2000), "A cable-suspended robotic manipulator for large workspace operations", *Comput. Aided Civil Infrastruct. Eng.*, **15**(6), 56-68.

Huang, T.L., Zhou, H., Chen, H.P. and Ren, W.X. (2016), "Stochastic modelling and optimum inspection and maintenance strategy for fatigue affected steel bridge members", *Smart Struct. Syst.*, *Int. J.*, **18**(3), 569-584. https://doi.org/10.12989/SSS.2016.18.3.569

Irvine, H.M. (1981), "Cable Structures", The MIT Press.

Jung, H.J., Lee, J.H., Yoon, S. and Kim, I.H. (2019), "Bridge Inspection and condition assessment using Unmanned Aerial Vehicles (UAVs): Major challenges and solutions from a practical perspective", *Smart Struct. Syst.*, *Int. J.*, **24**(5), 669-681. https://doi.org/10.12989/sss.2019.24.5.669

Kawamura, S., Choe, W., Tanaka, S. and Pandian, S.R. (1995), "Development of an ultrahigh speed robot falcon using wire drive system", *Proceedings of IEEE International Conference on Robotics and Automattion*, **1**, pp. 215-220.

Kawamura, S., Kino, H. and Won, C. (2000), "High-speed manipulation by using parallel wiredriven robots", *Robotica*, **18**(1), 13-21. https://doi.org/10.1017/S0263574799002477

Kim, C.W., Isemoto, R., McGetrick, P., Kawatani, M. and O'Brien, E.J. (2014), "Drive-by bridge inspection from three different approaches", *Smart Struct. Syst.*, *Int. J.*, **13**(5), 775-796. https://doi.org/10.12989/sss.2014.13.5.775

Kozak, K., Zhou, Q. and Wang, J. (2006), "Static analysis of cable-driven manipulators with non-negligible cable mass", *IEEE Transact. Robot.*, **22**(3), 425-433. https://doi.org/10.1109/TRO.2006.870659

Merlet, J.-P. (2016), "A generic numerical continuation scheme for solving the direct kinematics of cable-driven parallel robot with deformable cables", *Proceedings of IEEE International Conference on Intelligent Robots and Systems*, pp. 4337-4343.

Nan, R. (2006), "Five hundred meter aperture spherical radio telescope (FAST)", In: *Science in China series G*, **49**(2), 129-148. https://doi.org/10.1007/s11433-006-0129-9

Nan, R. and Peng, B. (2000), "A chinese concept for 1km radio telescope", *Acta Astronautica*, **46**(10-12), 667-675. https://doi.org/10.1016/S0094-5765(00)00030-8

Ottaviano, E. and Castelli, G. (2010), "A study on the effects of cable mass and elasticity in cable-based parallel manipulators", *Proceedings of the 18th CISM-IFToMM Symposium*, *On Robot Design*, *Dynamics and Control*, Springer Ed. Udine, pp. 149-156.

Ottaviano, E., Arena, A., Gattulli, V. and Potenza, F. (2019), "Slackening effects in 2D exact positioning in cable-driven parallel manipulators", In: A. Pott, T. Bruckmann (Eds.), *Mechanisms and Machine Science*, **74**, Springer, Cham, pp. 319-330.

Pott, A. (2010), "An algorithm for real-time forward kinematics of cable-driven parallel robots", In: *Advances in Robot Kinematics*, Springer, pp. 529-538.

Pott, A., Mütherich, H., Kraus, W., Schmidt, V., Miermeister, P. and Verl, A. (2013), "IPAnema: a family of cable-driven parallel robots for industrial applications", In: *Cable-Driven Parallel Robots* (pp. 119-134), Springer, Berlin, Heidelberg.

Roberts, R., Graham, T. and Lippitt, T. (1998), "On the inverse kinematics, statics, and fault tolerance of cable-suspended robots", *J. Robot. Syst.*, **15**(10), 581-597.

Skycam (2020), Accessed: 2020-07-10. https://en.wikipedia.org/wiki/Skycam

Wang, Q., Kim, M.K., Sohn, H. and Cheng, J.C. (2016), "Surface flatness and distortion inspection of precast concrete elements using laser scanning technology", *Smart Struct. Syst.*, *Int. J.*, **18**(3), 601-623. https://doi.org/10.12989/sss.2016.18.3.601

Yangwen, X., Qi, L., Yaqing, Z. and Bin, L. (2010), "Model aerodynamic tests with a wire-driven parallel suspension system in low-speed wind tunnel", *Chinese J. Aeronaut.*, **23**(4), 393-400. https://doi.org/10.1016/S1000-9361(09)60233-8

4.4 Contribution 3

sensors

MDPI

Communication

New Sensor Device to Accurately Measure Cable Tension in Cable-Driven Parallel Robots

Guillermo Rubio-Gómez, Sergio Juárez-Pérez, Antonio Gonzalez-Rodríguez, David Rodríguez-Rosa, Lis Corral-Gómez, Alfonso I. López-Díaz, Ismael Payo and Fernando J. Castillo-García *

School of Industrial and Aerospace Engineering, University of Castilla-La Mancha, 45071 Toledo, Spain; guillermo.rubiogomez@uclm.es (G.R.-G.); sergio.juarez@uclm.es (S.J.-P.); antonio.gonzalez@uclm.es (A.G.-R.); david.rrosa@uclm.es (D.R.-R.); lis.corral@uclm.es (L.C.-G.); Alfonso.Lopez@uclm.es (A.I.L.-D.); Ismael.Payo@uclm.es (I.P.)

* Correspondence: fernando.castillo@uclm.es

Abstract: Cable-driven parallel robots are a special type of robot in which an end-effector is attached to a fixed frame by means of several cables. The position and orientation of the end-effector can be controlled by controlling the length of the cables. These robots present a wide range of advantages, and the control algorithms required have greater complexity than those in traditional serial robots. Measuring the cable tension is an important task in this type of robot as many control algorithms rely on this information. There are several well-known approaches to measure cable tension in cable robots, where a trade-off between complexity and accuracy is observed. This work presents a new device based on strain gauges to measure cable tension specially designed to be applied in cable-driven parallel robots. This device can be easily mounted on the cable near the fixed frame, allowing the cable length and orientation to change freely, while the measure is taken before the cable passes through the guiding pulleys for improved accuracy. The results obtained from the device show a strong repeatability and linearity of the measures

Keywords: tension measurement; cable-driven parallel robots; strain gauges

Citation: Rubio-Gómez, G.; Juárez-Pérez, S.; Gonzalez-Rodríguez, A.; Rodríguez-Rosa, D.; Corral-Gómez, L.; López-Díaz, A.I.; Payo, I.; Castillo-García, F.J. New Sensor Device to Accurately Measure Cable Tension in Cable-Driven Parallel Robots. *Sensors* **2021**, *21*, 3604. https://doi.org/10.3390/s21113604

Received: 14 April 2021
Accepted: 18 May 2021
Published: 21 May 2021

1. Introduction

Measuring stresses with strain gauges is very common in engineering. This technique has undoubted advantages but also has some disadvantages, specifically when applied to determine the tension in cables. The aim of this work is to propose a novel device to measure the tension in cables that are suitable for application in cable-driven parallel robots (CDPRs).

CDPRs are a special type of parallel manipulator where rigid links are replaced by cables; therefore, the end-effector is sustained by a set of n cables [1]. The length of each cable is controlled by means of a motor-winch set, usually located on a fixed frame. By controlling the cable lengths, the position (e.g., Khosravi and Taghirad [2]) and/or orientation (e.g., Tadokoro et al. [3]) of the end-effector can be controlled.

Some of the advantages that these manipulators provide compared to both serial manipulators and conventional parallel ones are the following:

- CDPRs present the most light-weight structure for a manipulator from the point of view of structural design [1].
- The motors only have to move the payload and the cables; therefore, CDPRs are able to move a much higher mass or to employ less energy.
- CDPRs can cover large workspaces, since very long cables are easy to wind [4].

Applications of cable force measurements on CDPRs are extensive. One of the most important drawbacks of CDPRs is the complexity of the robot dynamics and its strong nonlinear behavior [5]. This is due to the cable tension, which varies nonlinearly with the end-effector position and orientation. Due to this dynamic feature, the control effort

required to achieve a high level of precision in positioning/orientation of the robot is very high [6,7]. To achieve this, the most commonly employed control strategies are based on linearization of the nonlinear dynamic terms, usually by means of feedforward linearization [8–11] or by using inverse dynamics techniques [12].

In order to effectively employ the aforementioned approaches, the end-effector position must be precisely measured. Additionally, this measure must be carried out with a high enough time resolution to be used by the control loop, which should be within the order of milliseconds. To solve this, the most common procedure is to use the motor's encoder readings to estimate the end-effector position through kinematic models [13]. This allows for a high speed reading but, since the end-effector position is not directly measured but is just estimated, it yields position errors that cannot be neglected for most practical applications.

Another approach is to directly measure the end-effector position using computer vision techniques [14]. This method is accurate but has difficulty obtaining the required time resolution for the measures as a correct resolution requires processing a high amount of data.

In constrained CDPR, i.e., with the same number of cables as degrees of freedom of the end-effector [15], the cable tension distribution allows us to compute the end-effector position as long as tension measures are highly accurate. High speed measures can be obtained by using well-known force measurement principles.

Additionally, in overconstrained CDPR, i.e., with more cables than degrees of freedom of the end-effector [16], there are an infinite number of possible cable force distributions for a single end-effector pose; this means that force control algorithms, which rely on cable force measurements, are commonly used for adjusting tension levels to a feasible value [17,18]. Moreover, cable force measurements are required in CDPR for implementing contact control [19,20] or load identification [21] algorithms.

In summary, an accurately measure of cable tension in CDPR is required for estimating end-effector pose or/and for dynamics control purposes.

Some commercial off-the-shelf devices that could be located at the frame to measure cable tension can be found in the industry (see Figure 1) but their performance in range, resolution, or sensory latency make them unsuitable for application to CDPRs.

(**a**) ABQ Industrial

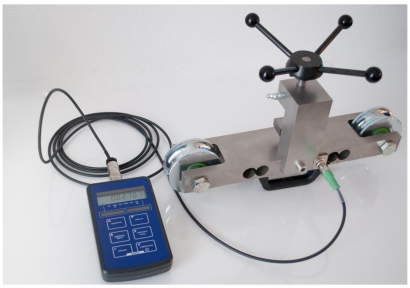

(**b**) Captronic

(**c**) Weite Technologies Co.

Figure 1. Examples of commercial off-the-shelf devices for measuring cable tension.

In that sense, most of the CDPR prototypes that include cable tension sensors present customized solutions. A relevant work is presented by Kraus et al. [22]. This paper compares the three main ways for estimating cable tension by means of force sensors (see Figure 2).

Some examples of estimating cable tension by means of a force sensor located at the pulley of the frame or end-effector, directly in the cable (see Figure 2a), are [22–24]. Winch-integrated sensors (see Figure 2b) can be found in [25–27]. Finally, we found that only in Scalera et al. [28] is the three-pulley concept (see Figure 2c) implemented for measuring the cable tension of CDPR.

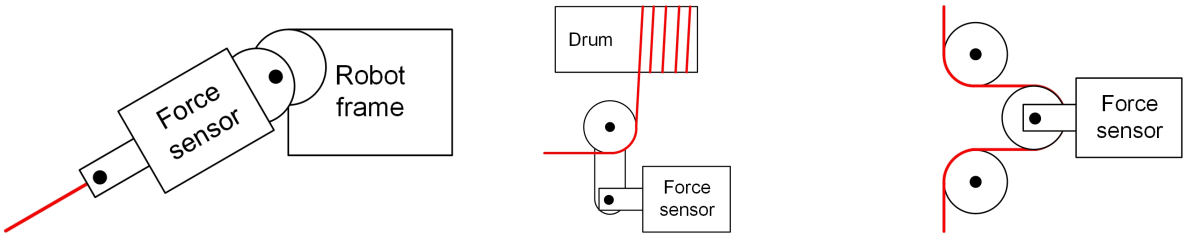

(**a**) Direct at the frame (**b**) Winch integrated (**c**) Using three pulleys

Figure 2. Examples of commercial off-the-shelf devices for measuring cable tension.

The first type of sensor can be placed directly on the end-effector (see Figure 2a), providing a more accurate measure as the force being applied to the end-effector is directly measured; however, it requires a wire cable supply or non-wire signal (with its correspondent large latency and lack of synchronism). This type of sensor can also be placed on the guiding pulleys of the actuators, as in [20,29,30]. As the sensor is attached to the robot frame, it must be placed in a position where the cable orientation does not change when the robots moves. Additionally, another drawback of this approach is that the sensor is placed after one or some guiding pulleys; therefore, the measured tension differs from the real tension due to the friction of the pulleys.

Winch-integrated sensors (see Figure 2b) simplify the integration into the mechanical design but provide some errors in the force such that the end-effector suffers owing to the friction losses of the winch and all pulleys.

Finally, the three-pulley concept (see Figure 2c) can also be placed at the point of interest but the inertia of the actuator is slightly increased by the inertia of each pulley that rotates during robot maneuvers. The friction of the pulleys can also be a disadvantage yielding non-accurate measurements.

All of the commercial-off-the-shelf sensors (Figure 1) or the ones based on the three-pulley concept (e.g., Scalera et al. [28]) are based on measuring the compression efforts of the link that supports the central pulley. Figure 3 illustrates the conceptual idea of both commercial and customized devices based on the three-pulley concept.

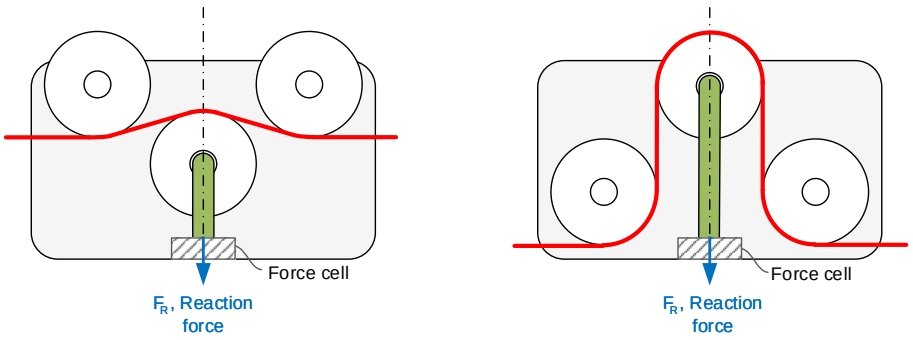

(**a**) Commercial of-the-shelf devices (**b**) Scalera et al. 2008 device

Figure 3. Three-pulley devices based on measuring compression efforts.

This work proposes a new sensor device that employs strain gauges to measure cable tension based on the three-pulley concept (see Figure 2c). Conceptualization of the proposal is based on estimating cable tension, not by measuring compression efforts but flexion ones by means of strain gauges (see Figure 4).

For the same cable tension, flexion efforts are significantly higher than compression ones, and therefore, for the same sensor system, the amplitude of the acquired signal is bigger, the resolution of the sensor is higher, and the typical noise of force cells or strain gauges has less influence on the acquired signal.

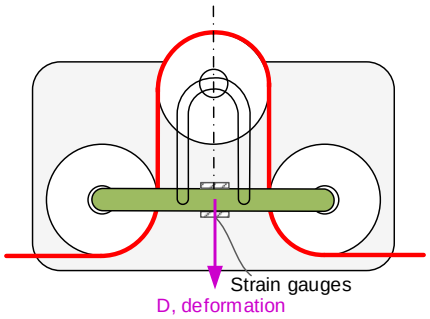

Figure 4. Conceptualization of our proposal.

This device is specifically designed to be easily employed in CDPR, as it allows the cable to run freely through the device while it can be fixed near the robot frame and before any guiding pulley, avoiding errors caused by pulley friction.

2. Materials and Methods

2.1. Mechanical Approach

To accurately measure the cable tension, we propose to measure the deformation caused by the cable in the bars that support a set of three pulleys. These three pulleys redirect the cable from its original rectilinear path. In this way, the higher the cable tension, the higher the deformation of these bars.

Figure 5 shows the schematic of the device. The cable is labeled 1, the bar where the strain gauges are located is labeled 2, the piece that supports the redirecting pulley is labeled 3, while the pulleys are labeled 4. Parts 2 and 3 are connected with a pair of bolts in points *P* and *Q*. Cable tensions are marked with arrows and the letter *T*. Three pulleys are used to guide the cable, all of them with radius *r*.

The forces produced in bar 2 by these cable tensions, along with its correspondent bending moment and axial force diagrams, are shown in Figure 6a).

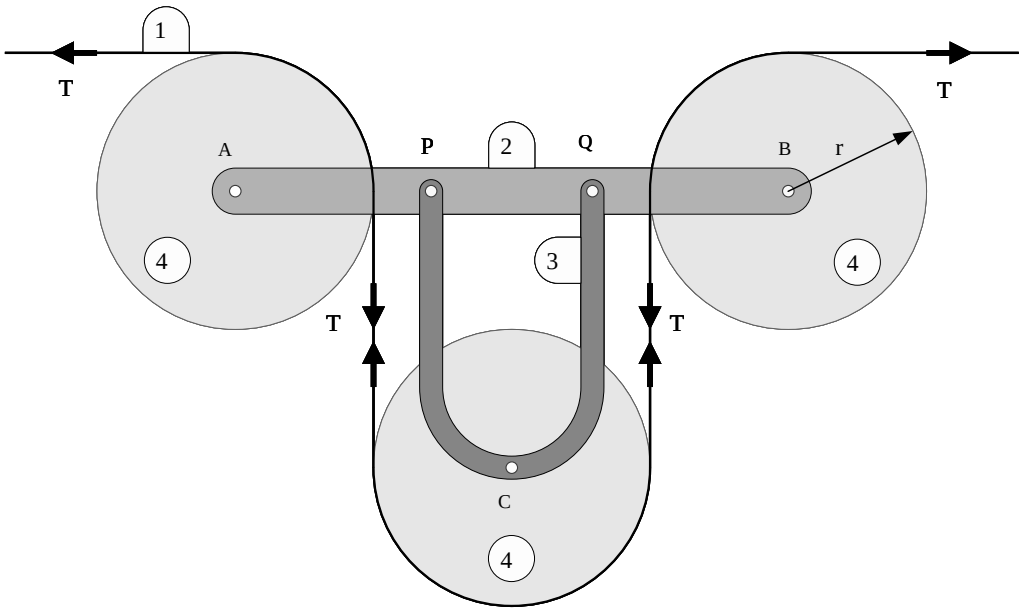

Figure 5. Scheme of the cable tension-measuring device. T = cable tension, r = pulley radius, A,B,C = pulley centers, P,Q = connection points between bars 2 and 3.

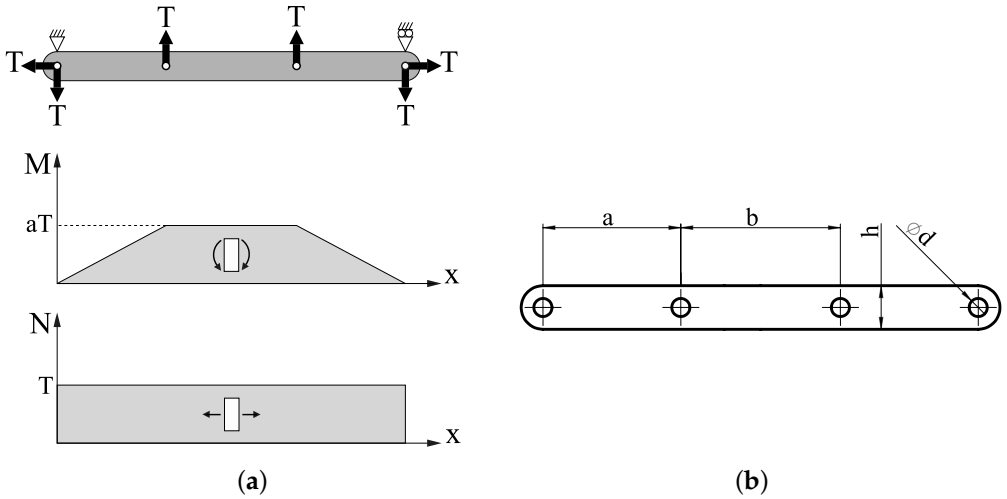

Figure 6. (**a**) Forces on the measuring bar. (**b**) Geometry of the measuring bar.

Note that the bending moment $M = aT$ and the axial force $N = T$ are constant in the area between points P and Q. In this area, the maximum normal stress occurs on the upper side of the section and the minimum occurs on the lower face. These values are as follows:

$$\begin{aligned} \sigma_{xx}^{max} &= \left(\frac{1}{he} + \frac{6a}{eh^2}\right)T \\ \sigma_{xx}^{min} &= \left(\frac{1}{he} - \frac{6a}{eh^2}\right)T \end{aligned} \tag{1}$$

where e is the thickness of bar 2 and where a and h are the geometrical characteristic of bar 2, shown in Figure 6b. Equation (1) shows that the stress is proportional to T. The stress $\sigma_{xx} = E\,\epsilon_{xx}$ is proportional to the deformation ϵ_{xx} through Young's modulus E since $\sigma_{yy}, \sigma_{zz} = 0$.

The dimensions of bar 2 must fulfill the hypotheses of the Euler Bernoulli beam in the Theory of Strength of Materials [31], which results in the stresses in (1) being only approximate. For this reason, an experimental calibration of the device is necessary. However, the tension between points P and Q is approximately constant, making this an optimal area to place the gauges.

The last important issue of the mechanics is the minimum allowed radius of the pulleys, which affects miniaturization of the device. The minimum radius, r_{min}, avoids the plasticity of the cable. Cable bending in the pulley gives the flexion stress in the cable. To obtain reasonable life from the device, a proper diameter for the pulley must be chosen. In general, the larger the size of the pulley with respect to the wire diameter, the longer the service life. Manufacturers provide tables with the minimum recommended pulley diameter. Let us denote d_c as the diameter of the cable. Without further information, a minimum ratio, $r_{min} \geq 30 \cdot d_c$ can be assumed to guarantee a reasonable cable life cycle.

2.2. Electronics and Instrumentation

As shown in (1), both σ_{xx}^{max} and σ_{xx}^{min} are proportional to the cable tension through a constant $k = \frac{1}{he} \pm \frac{6a}{eh^2}$ that has two terms: $k_1 = \frac{1}{he}$, which represents the stress due to axial tension N, and $k_2 = \frac{6a}{eh^2}$, which represent the stress caused by bending moment M.

The stress caused by bending moment M is considerably higher than that caused by axial tension as long as $a > h$, since $\frac{k_2}{k_1} = \frac{6a}{h}$. Therefore, the strain gauges are placed to measure M and to cancel N; this is achieved by positioning the strain gauges on the device as shown in Figure 7.

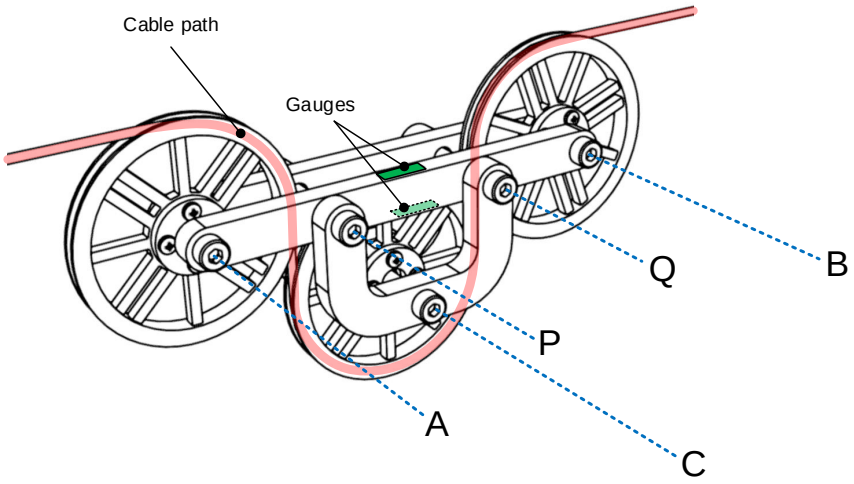

Figure 7. Strain gauges position for bending moment measurement. A,B,C = pulley centers, P,Q = connection points between bars 2 and 3.

Figure 8 shows the signal conditioning electronics, where V is the bridge voltage, R is a fixed value for resistances, e_0 is the bridge output, Rg_1 is the upper strain gauge, and Rg_2 is the lower strain gauge.

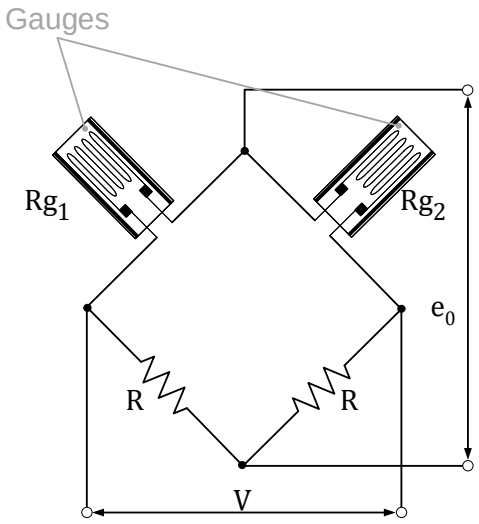

Figure 8. Signal conditioning electronics. R = fixed resistance, Rg_1 = upper strain gauge, Rg_2 = lower strain gauge, V = supply voltage, e_0 = output voltage.

The conditioning circuit yields the following expression for the bridge output:

$$e_0 = \frac{V}{2} K_s \cdot (\epsilon_1 - \epsilon_2) \tag{2}$$

where K_s is the gauge factor and ϵ_i is the deformation of the gauge Rg_i. Since $\epsilon_1 = \frac{\sigma_{xx}^{max}}{E}$ and $\epsilon_2 = \frac{\sigma_{xx}^{min}}{E}$, Equation (2) can be rewritten as follows:

$$e_0 = \frac{V}{2E} K_s \cdot \left(2 \frac{6a}{eh^2} T \right) \tag{3}$$

The signal conditioning electronics employed therefore allow us to cancel both of the axial strain effects and to multiply the bending moment effects by a factor of 2, reducing possible noise in the signal.

The bridge voltage, V, can be therefore acquired by a digital data acquisition device. If the resolution of the DAQ device is n bits, the measurement resolution, i.e., the minimum change that can be measured, is as follows:

$$\Delta V_m = \frac{V_{max} - V_{min}}{2^n} \tag{4}$$

with V_{max} and V_{min} being the maximum and minimum allowed measurements of the analog input of the DAQ device, respectively.

2.3. Prototype

A prototype of the device was built in order to analyze the repeatability, sensibility, and linearity of the measurement system as well as to obtain the calibration curve. The final device is shown in Figure 9. As can be seen, bars 2 and 3 in Figure 5 are duplicated on both sides in order to make a symmetrical system.

The prototype dimensions in Figure 6b) are $a = 38$ mm, $b = 44$ mm, $h = 12$ mm, $d = 5$ mm, and $e = 6$ mm. This yields a relation between K_2 and K_1 of $\frac{k_1}{k_2} = 19$, ensuring that stress generated by the bending moment is significantly higher than that generated by axial tension. The gauges employed have a gauge factor of $K_s = 2$. The signal provided by the electronic system is registered with a NI USB-6341 (National Instruments, Austin, TX, USA) data acquisition board in which the analog input channels have a resolution of 16 bits. Since e_0 lies in the range 0–5 V, the board range was set to ± 5 V, yielding a voltage reading resolution of 0.153×10^{-3} V.

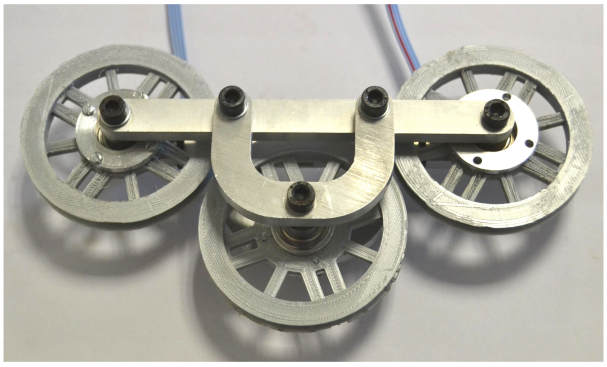

Figure 9. Prototype for validation.

3. Validation and Results

3.1. Experiments Protocol for Validation

The experimental setup shown in Figure 10 was employed for validation and calibration of the tension measurement prototype.

To apply a known load to the device, weight plates of 10, 15, and 20 kg were hanged from a 20 cm steel cable of 2.5 mm diameter. Every weight plate and the additional elements employed to attach them was weighted with a GRAM DSX-30 (GRAM DX, l'Hospitalet de Llobregat, Barcelona, Spain) precision weighing scale with a resolution of 2 g. Table 1 shows the masses employed for the validation experiments.

Figure 10. Experimental setup for validation.

Table 1. Weights employed for device validation and calibration.

Test Number	1	2	3	4	5	6	7	8	9	10	11	12
Mass (g)	10,103	15,105	20,074	25,118	30,088	35,089	40,087	45,102	50,095	55,096	60,094	65,110

To assess the repeatability of the measurement system, for each mass, five consecutive measures were taken, each one after releasing the mass, reloading, and waiting long enough for the device to reach a stationary state. Each measure was obtained by acquiring 1000 samples during 1 s and by calculating the mean voltage value. To ensure that the mean was a representative value of the sample data, the one-sample Kolmogorov–Smirnov test [32] was applied to one randomly selected measure out of each mass test. For every test, the null hypothesis suggesting that the data come from a standard normal distribution is not rejected at the 5% significance level. Figure 11 shows a comparison of the cumulative distribution function (CFD) of the sample data to that of a standard normal distribution.

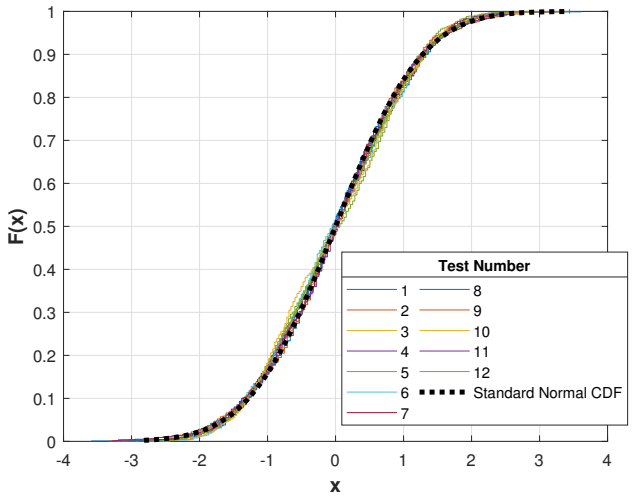

Figure 11. CDF for empirical data.

3.2. Repeatability

The repeatability of the measurement system is assessed by means of the box plot [33] of the measures made for each mass point. In order to compare the repeatability of measures

from different tests, the box plot is obtained from the values normalized to the mean value. The results are shown in Figure 12.

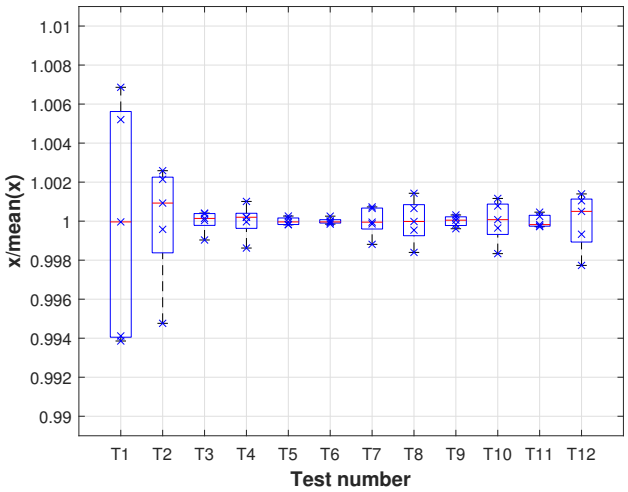

Figure 12. Repeatability results.

As can be observed, for every test, the maximum difference with the mean value of the values between percentiles 25th and 75th is less than 0.5%. Additionally, it can be observed that there are no outliers in the values of any test and that the median value of each test has a difference with a mean value of less than 0.1%.

3.3. Linearity and Calibration

In Figure 13, the measurements are represented versus the corresponding weights along with the first-order polynomial fitted to the experimental data. As can be observed, the linearity is very strong since $R^2 = 0.9984$ and the relation between voltage and mass is as follows:

$$M = 20778.1 \times V + 5234.4 \quad (5)$$

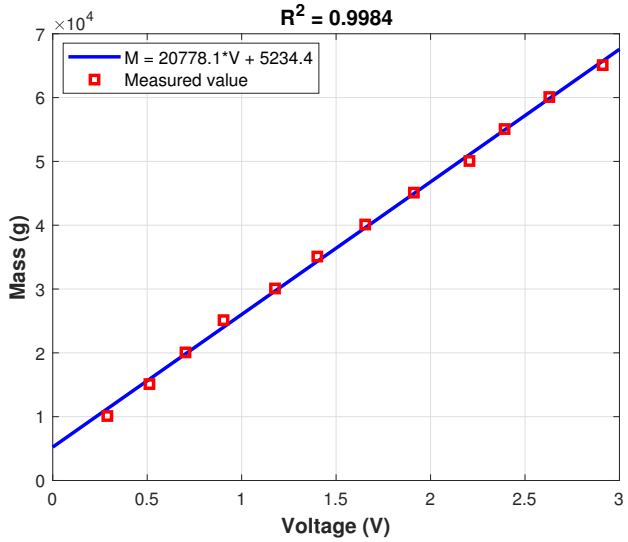

Figure 13. Calibration results.

3.4. Dynamics Analysis

The previous sections demonstrated that the device yields accurate measurements of cable tension under static conditions.

This section preliminarily analyses the influence of natural movement of the robot during its maneuvers on the cable tension measurement. In order to demonstrate that

tension remains constant during the cable travel and that the friction loses can be considered negligible, the following experiment was carried out. A mass of 10 kg was attached to a blocked winch, which was suddenly released, allowing the mass to freely fall under the effect of gravity. A sketch of the experiment setup is shown in Figure 14.

The mass was released from a height of 2.5 m, and measurements were taken until the mass collided with the floor; however, for the sake of readability, only the measurements up to 200 ms before the collision are shown. A set of 10 consecutive experiments was carried out.

To assess the coherence of the obtained experimental results, a simple dynamic model was employed, which considers the winch inertia and viscous friction, the mass, and its friction with air but neglects the friction in the sensor pulleys. The model parameters are shown in Table 2; these parameters were obtained experimentally by means of a GRAM DSX-30 (GRAM DX, l'Hospitalet de Llobregat, Barcelona, Spain) precision weighing scale and an incremental quadrature encoder OMROM E6B2-CWZ6C (OMROM, Osaka, Japan) with a resolution of 1000 ppr.

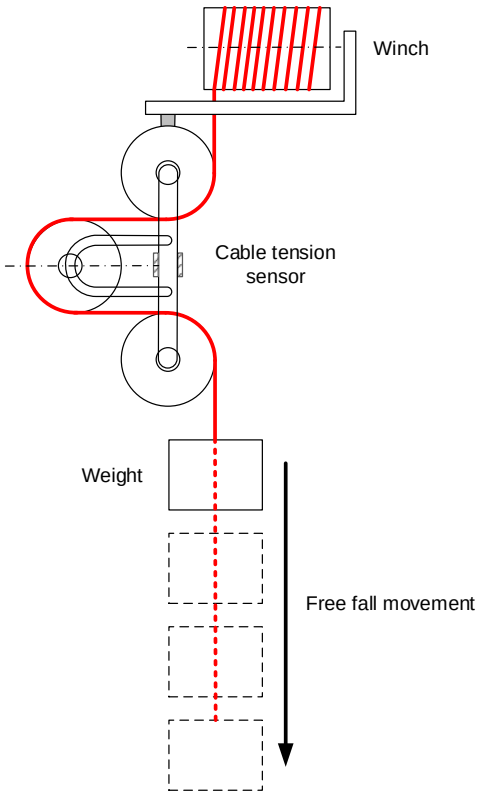

Figure 14. Sketch of the dynamic test approach.

Table 2. Weights employed for device validation and calibration.

Parameter	Units	Value
Weight mass	Kg	10.103
Weight air friction coefficient	Ns/m	0.0102
Winch mass	Kg	0.0465
Winch radius	m	0.06
Winch Inertia	Kg $\times$ m^2	0.000837
Winch viscous friction	Nm $\times$ s	0.000837

Figure 15 shows the experimental results together with the simulation results. The x-axis was adjusted so that the moment when tension starts changing matches for each test and the simulation. As can be observed, experimental results mainly match the results

obtained from the simulation, validating the assumption that sensor pulley friction can be neglected for dynamic measures. The differences observed at the beginning of the tests can be explained by the differences in the way that the winch was released, since this was done manually. Additionally, a very good concordance between the steady state values and the original static value of the tension can be observed, which suggests that the rotation of the sensor pulleys has little influence on the measurement. The oscillations that can be observed from 0.2 s can be explained as the weight inevitably oscillates during the fall. This effect does not occur in a real cable robot.

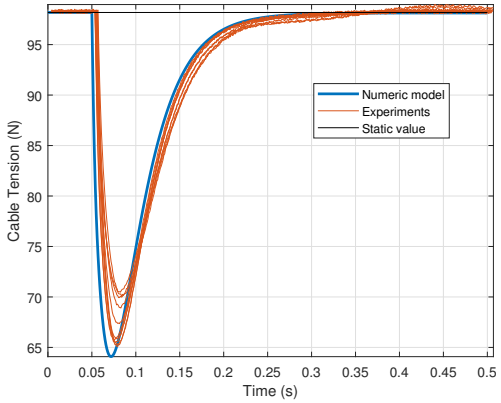

Figure 15. Results of the dynamic test.

4. Conclusions

In this work, a novel device to measure tension in cables, specially designed for application in cable-driven parallel robots was proposed.

The mechanical principle and the device design were detailed along with the required electronics and instrumentation. In this paper, a prototype with a range from 100 N to 650 N was built, but the design presented here can be easily scaled for other tension ranges.

Finally, the results of repeatability, calibration, and linearity of the device were exposed. Regarding the repeatability of the device, the maximum deviation along all measures with respect to the mean is 0.6%. The measures show high linearity as the R^2 value of the fitting to a first-order polynomial is 0.9984.

Author Contributions: Conceptualization, F.J.C.-G., A.G.-R. and I.P.; methodology, S.J.-P. and D.R.-R.; software, G.R.-G. and L.C.-G.; validation, G.R.-G. and L.C.-G.; formal analysis, A.I.L.-D. and D.R.-R.; investigation, S.J.-P. and A.G.-R.; resources, A.G.-R. and I.P.; data curation, G.R.-G. and F.J.C.-G.; writing—original draft preparation, L.C.-G., G.R.-G. and F.J.C.-G.; writing—review and editing, L.C.-G., G.R.-G. and F.J.C.-G.; visualization, A.I.L.-D., S.J.-P. and D.R.-R.; supervision, A.I.L.-D., S.J.-P. and D.R.-R.; project administration, A.G.-R. and I.P.; funding acquisition, I.P. All authors have read and agreed to the published version of the manuscript.

Funding: This work was supported by the Universidad de Castilla-La Mancha through the pre-doctoral grant number 2019/451 and by the Research Fund for Coal and Steel grant agreement No. 800687 in the framework of the DESDEMONA project.

Institutional Review Board Statement: Not applicable.

Informed Consent Statement: Not applicable.

Data Availability Statement: Data available on request due to restrictions eg privacy or ethical. The data presented in this study are available on request from the corresponding author. The data are not publicly available due to research group policy.

Conflicts of Interest: The authors declare no conflict of interest.

References

1. Pott, A. Introduction. In *Cable-Driven Parallel Robots: Theory and Application*; Springer International Publishing: Cham, Switzerland, 2018; pp. 1–13.
2. Khosravi, M.A.; Taghirad, H.D. Robust PID control of cable-driven robots with elastic cables. In Proceedings of the 2013 First RSI/ISM International Conference on Robotics and Mechatronics (ICRoM), Tehran, Iran, 13–15 February 2013; pp. 331–336.
3. Tadokoro, S.; Murao, Y.; Hiller, M.; Murata, R.; Kohkawa, H.; Matsushima, T. A motion base with 6-DOF by parallel cable drive architecture. *IEEE/ASME Trans. Mechatron.* **2002**, *7*, 115–123. [CrossRef]
4. Zi, B.; Duan, B.; Du, J.; Bao, H. Dynamic modeling and active control of a cable-suspended parallel robot. *Mechatronics* **2008**, *18*, 1–12. [CrossRef]
5. Wang, T.; Tong, S.; Yi, J.; Li, H. Adaptive inverse control of cable-driven parallel system based on type-2 fuzzy logic systems. *IEEE Trans. Fuzzy Syst.* **2014**, *23*, 1803–1816. [CrossRef]
6. Schenk, C. Modelling and Control of a Cable-Driven Parallel Robot: Methods for Vibration Reduction and Motion Quality Improvement. Master's Thesis, Universitat Stuttgart, Stuttgart, Germany, 2019.
7. Zake, Z.; Chaumette, F.; Pedemonte, N.; Caro, S. Vision-based control and stability analysis of a cable-driven parallel robot. *IEEE Robot. Autom. Lett.* **2019**, *4*, 1029–1036. [CrossRef]
8. Alp, A.B.; Agrawal, S.K. Cable suspended robots: Design, planning and control. In Proceedings of the 2002 IEEE International Conference on Robotics and Automation (ICRA'02), Washington, DC, USA, 11–15 May 2002; Volume 4, pp. 4275–4280.
9. Alp, A.; Agrawal, S.K. Cable suspended robots: Feedback controllers with positive inputs. In Proceedings of the 2002 American Control Conference, Anchorage, AK, USA, 8–10 May 2002; Volume 1, pp. 815–820.
10. Oh, S.R.; Agrawal, S.K. Cable-suspended planar parallel robots with redundant cables: Controllers with positive cable tensions. In Proceedings of the 2003 IEEE International Conference on Robotics and Automation, Taipei, Taiwan, 14–19 September 2003; Volume 3, pp. 3023–3028.
11. Zheng, Y.Q. Feedback Linearization Control of a Wire-Driven Parallel Support System in Wind Tunnels. In Proceedings of the Sixth International Conference on Intelligent Systems Design and Applications, Jian, China, 16–18 October 2006.
12. Zarebidoki, M.; Lotfavar, A.; Fahham, H. Effectiveness of adaptive passivity-based trajectory tracking control of a cable-suspended robot. In Proceedings of the International Conference on Trends in Mechanical and Industrial Engineering, Bangkok, Thailand, 23–24 December 2011.
13. Gonzalez-Rodriguez, A.; Castillo-Garcia, F.; Ottaviano, E.; Rea, P.; Gonzalez-Rodriguez, A. On the effects of the design of cable-Driven robots on kinematics and dynamics models accuracy. *Mechatronics* **2017**, *43*, 18–27. [CrossRef]
14. Dallej, T.; Gouttefarde, M.; Andreff, N.; Dahmouche, R.; Martinet, P. Vision-based modeling and control of large-dimension cable-driven parallel robots. In Proceedings of the 2012 IEEE/RSJ International Conference on Intelligent Robots and Systems, Vilamoura-Algarve, Portugal, 7–12 October 2012; pp. 1581–1586.
15. Castillo-Garcia, F.; Rea, P.; Gonzalez-Rodriguez, A.; Ottaviano, E. On the Design of a 4 Degrees-of-Freedom Pick and Place Cable Suspended Parallel Manipulator. *Int. J. Robot. Autom. (IJRA)* **2017**, *6*, 286–302. [CrossRef]
16. Pott, A.; Mütherich, H.; Kraus, W.; Schmidt, V.; Miermeister, P.; Verl, A. IPAnema: A family of cable-driven parallel robots for industrial applications. In *Cable-Driven Parallel Robots*; Springer: Cham, Switzerland, 2013; pp. 119–134.
17. Kraus, W.; Schmidt, V.; Rajendra, P.; Pott, A. System identification and cable force control for a cable-driven parallel robot with industrial servo drives. In Proceedings of the 2014 IEEE International Conference on Robotics and Automation (ICRA), Hong Kong, China, 31 May–7 June 2014; pp. 5921–5926.
18. Kraus, W.; Miermeister, P.; Schmidt, V.; Pott, A. Hybrid position-force control of a cable-driven parallel robot with experimental evaluation. *Mech. Sci.* **2015**, *6*, 119–125. [CrossRef]
19. Reichert, C.; Bruckmann, T. Unified contact force control approach for cable-driven parallel robots using an impedance/admittance control strategy. In Proceedings of the 14th IFToMM World Congress, Taipei, Taiwan, 25–30 October 2015; pp. 645–654.
20. Ho, W.Y.; Kraus, W.; Mangold, A.; Pott, A. Haptic interaction with a cable-driven parallel robot using admittance control. In *Cable-Driven Parallel Robots*; Springer: Cham, Switzerland, 2015; pp. 201–212.
21. Kraus, W.; Schmidt, V.; Rajendra, P.; Pott, A. Load identification and compensation for a cable-driven parallel robot. In Proceedings of the 2013 IEEE International Conference on Robotics and Automation, Karlsruhe, Germany, 6–10 May 2013; pp. 2485–2490.
22. Kraus, W.; Kessler, M.; Pott, A. Pulley friction compensation for winch-integrated cable force measurement and verification on a cable-driven parallel robot. In Proceedings of the 2015 IEEE International Conference on Robotics and Automation (ICRA), Seattle, WA, USA, 26–30 May 2015; pp. 1627–1632.
23. Piao, J.; Kim, E.S.; Choi, H.; Moon, C.B.; Choi, E.; Park, J.O.; Kim, C.S. Indirect force control of a cable-driven parallel robot: Tension estimation using artificial neural network trained by force sensor measurements. *Sensors* **2019**, *19*, 2520. [CrossRef] [PubMed]
24. Picard, E.; Caro, S.; Claveau, F.; Plestan, F. Pulleys and force sensors influence on payload estimation of cable-driven parallel robots. In Proceedings of the 2018 IEEE/RSJ International Conference on Intelligent Robots and Systems (IROS), Madrid, Spain, 1–5 October 2018; pp. 1429–1436.
25. Otis, M.J.D.; Nguyen-Dang, T.L.; Laliberte, T.; Ouellet, D.; Laurendeau, D.; Gosselin, C. Cable tension control and analysis of reel transparency for 6-dof haptic foot platform on a cable-driven locomotion interface. *Int. J. Electr. Electron. Eng.* **2009**, *3*, 16–29.

26. Song, D.; Zhang, L.; Xue, F. Configuration optimization and a tension distribution algorithm for cable-driven parallel robots. *IEEE Access* **2018**, *6*, 33928–33940. [CrossRef]
27. Aflakian, A.; Safaryazdi, A.; Masouleh, M.T.; Kalhor, A. Experimental study on the kinematic control of a cable suspended parallel robot for object tracking purpose. *Mechatronics* **2018**, *50*, 160–176. [CrossRef]
28. Scalera, L.; Gallina, P.; Seriani, S.; Gasparetto, A. Cable-based robotic crane (CBRC): Design and implementation of overhead traveling cranes based on variable radius drums. *IEEE Trans. Robot.* **2018**, *34*, 474–485. [CrossRef]
29. Ottaviano, E.; Ceccarelli, M.; De Ciantis, M. A 4–4 cable-based parallel manipulator for an application in hospital environment. In Proceedings of the 2007 Mediterranean Conference on Control & Automation (MED'07), Athens, Greece, 27–29 June 2007; pp. 1–6.
30. Richter, T.; Lorenc, S.J.; Bernold, L.E. Cable based robotic work platform for construction. In Proceedings of the 15th International Symposium on Automation and Robotics in Construction, Munchen, Germany, 31 March–1 April 1998; pp. 137–144.
31. Timoshenko, S.; Young, D.H. *Elements of Strength of Materials*; Van Nostrand: Princeton, NJ, USA, 1962.
32. Massey, F.J., Jr. The Kolmogorov-Smirnov test for goodness of fit. *J. Am. Stat. Assoc.* **1951**, *46*, 68–78. [CrossRef]
33. McGill, R.; Tukey, J.W.; Larsen, W.A. Variations of box plots. *Am. Stat.* **1978**, *32*, 12–16.

4.5 Additional results

In this section, other contributions made by the author into the field of cable driven parallel robots during the realization of this thesis are presented. Table 4.2 lists the contributions made as book chapters in the proceedings of the fourth and fifth International Conference on Cable-Driven Parallel Robots.

Table 4.2: Book chapters published during this thesis

Title	**Type of contribution**	**Publication**	**Author order**
A Practical Force Correction Method for Over-Constrained Cable-Driven Parallel Robots[1] [64]	Book chapter	Cable-Driven Parallel Robots. CableCon 2021. Mechanisms and Machine Science, vol 104. Springer, Cham	Third
Chain Driven Robots: An Industrial Application Opportunity. A Planar Case Approach [94]	Book chapter	Cable-Driven Parallel Robots. CableCon 2019. Mechanisms and Machine Science, vol 74. Springer, Cham.	First

[1] This contribution was awarded with the Best Student Paper recognition in the Fifth International Conference on Cable-Driven Parallel Robots

Table 4.3 shows the list of end of degree projects in the field of CDPR supervised by the author during the realization of the thesis.

Table 4.3: End-of-degree works supervised during this thesis

Title	**Student**	**Entity**	**Date**
Diseño y puesta en marcha de un nuevo robot paralelo comandado mediante cables en bucle cerrado	Marta Criado Neumeister	Universidad de Castilla-La Mancha	01/07/2021
Nueva propuesta de robot comandado mediante cables planar para el aumento de su espacio de trabajo	Fernando Romero-Salazar Gómez	Universidad de Castilla-La Mancha	01/07/2021
Fractional order controllers for increasing the feasible workspace of cable driven robots	Alejandro Santos Aranda	Universidad de Castilla-La Mancha	07/09/2020
A new proposal for increasing the feasible workspace of cable driven robots	Enrique Bravo Pleite	Universidad de Castilla-La Mancha	24/06/2020
Diseño, fabricación y puesta en marcha de un robot comandado mediante cables para labores de inspección	Daniel Duran Dovalle	Universidad de Castilla-La Mancha	26/06/2019

Chapter 5

Conclusions and future works

In this chapter, the conclusions of this thesis are summarized. Subsequently, the research lines that should be continued after this work are detailed.

5.1 Conclusions

In this thesis, the practical application of cable driven parallel robots to tasks that are performed in very large, planar and either vertical or horizontal areas is first addressed. Due to the nature of the workspace of interest, the use of cable driven parallel robots of the suspended kind, i.e. with all cables acting against gravity direction, results more convenient. However, when the workspace is either large and/or perpendicular to gravity, conventional suspended cable driven robots present drawbacks that make its employment unsuitable from the practical point of view. The main drawback is the extremely high required motorization power to reach the full desired workspace.

In this sense, two novel mechanical designs are proposed for each of the workspace shapes under consideration. Besides the advantages provided by the new mechanical designs, several challenges arise for the proper control of the new robots. Specific control strategies are proposed and experimentally validated in prototypes of each robot.

For the feasible employment of suspended cable driven parallel robots to large, planar, vertical workspaces, the modification of the conventional suspended cable robot with 2 cables and 2 translational degrees of freedom is proposed. This modification consist on the addition of a passive carriage to the upper part of the robot frame, which moves along a linear guide attached to the frame. This modification allows to maintain a much more convenient angle between cables and the gravity direction, allowing to reach a larger workspace without the requirement for an increased the motor power.

A drawback of this new design is a reduced stiffness in the horizontal axis. To solve this problem, a specific control approach has been proposed to eliminate undesirable vibrations in this axis as well as rejecting external perturbations. To preliminary validate this control approach, the robot and the control system have been mathematically modeled and simulated for several trajectories and the presence of perturbations that model the real ones that the robot can suffer in real operation.

Finally, a prototype of the robot has been built to experimentally validate the design and the control approach. The maximum horizontal trajectory tracking error obtained is 1.2mm and 16mm for simulation and experiments, respectively while the corresponding average error is 0.8mm and 3.2mm. For a vertical movement, the maximum error is 0.8mm and 9.4mm for simulation and experiments, while the average error is 0.4mm and 1.7mm for this movement. During the experimental disturbance rejection experiment, the control system is able to keep a maximum deviation of the end-effector pose of 2mm.

The second case of study is the application of suspended cable driven parallel robots in large planar working areas, where gravity acts perpendicular to the working plane and the occupancy of the space in the gravity direction has to be strictly reduced. To this end, a modification of the conventional robot based on the employment of a closed cable loop is proposed.

The geometry of the robot required for this workspace shape makes it unfeasible to use the typical configuration where cables end in the drum, as very high cable tensions yield a very high motor power requirement. Consequently, a new mechanical configuration with the particularity that cables do not end in the motors but instead they pass through driven

pulleys and passive carriages are introduced is proposed.

It allows to keep the high cable tension required for a low occupancy of the vertical space, while maintaining power requirements within feasible limits. With this new design, the torque that has to be exerted by motors in static situation is near to zero, while for accelerating the end-effector, only the inertial force and the the force required for overcome the friction of carriages has to be generated.

This new geometry causes undesired vibrations on the main axis of the working plane, i.e. the axis perpendicular to the virtual line formed by the end-effector and the carriages in the static situation. To overcome this problem, in first place, a model of the natural frequency of the system in that axis on the whole robot workspace has been developed, modeling cables as linear springs. This model, has been experimentally validated in a prototype of the robot, by exciting the system with a force in the direction under consideration, on different points of the workspace and measuring the frequency by means of computer vision techniques.

Subsequently, this model is employed to cancel undesired vibrations by the dynamic inversion approach, which allows to obtain modified reference angles for the motors from those obtained from the inverse kinematic model. To prove the performance of the proposed control strategy, it has been implemented in the robot prototype. As the prototype uses stepper motors with position servocontrollers with unknown dynamics, a linear, second-order system with the natural frequency obtained from the model is supposed for the motors dynamics.

The trajectory tracking performance of the robot is tested on the prototype by performing 19 linear trajectories both in the x and y axes and measuring the position by computer vision techniques. A maximum following error of 14.5mm is obtained while the average maximum following error along the performed trajectories is 5.76mm. The maximum steady-state error is 2.6mm and the average steady-state error along the trajectories is 1.77mm.

The final contribution of this thesis is related to the problem of measuring cable tension in CDPR. In this sense a novel device to measure cable tension is designed specifically for its application in CDPR. This device is a three pulley mechanism that allows the cable to run freely through it.

The cable generates a bending force in the device structure that is proportional to its tension. This deformation is then measured by means of strain gauges. The device, that can be easily placed near the end-effector frame, but before any additional guiding pulley, provides a linear and low noise measure of the tension.

A prototype with a measuring range of 100N to 650N has been built to validate the proposed concept. Static measures from the prototype show a good repeatability with a maximum deviation from the mean along all measures of 0.6%. The R^2 vale of the results fitting to a first order polynomial is 0.9984 which shows the high linearity of the measures.

Additionally, a preliminary study on the quality of the dynamic measures has been performed. Experimental results of the dynamic test were compared with those obtained from a simple dynamic model which considers winch inertia and viscous friction, but neglects the inertia of the pulleys in the measurement device. The good agreement between experimental and numerical results suggest that the error in the dynamic measurements caused by the device pulleys inertia can be neglected.

5.2 Future works

In this section, the continuation of the research lines that this work has focused on is detailed. The future research is organized according to the three main contributions of this work.

Considering the prototype that has been proposed and tested for working in large planar vertical areas, immediate further research on this line will include testing the robot performance with different equipment attached to the end-effector and in real-environment situations with wind, etc.

In a more general way, including passive carriages in planar CDPR opens an interesting field. This concept can be extended to over-constrained cable driven parallel robots by adding passive carriages in both the upper and lower parts of the frame. This allows to have the advantage of increased stiffness in the plane directions of planar OC CDPR while significantly extending its feasible workspace thanks to the redesigned geometry.

On the other hand, this novel design will bring the need of developing the mathematical foundations of the robot, i.e. kinematic, static and dynamic models. The problem of the force distribution inherent to OC CDPR will then be coupled with the new kinematic model which will represent a challenge itself. Moreover, the dynamic control of the robot will have to be studied in detail, as hybrid position-force control will be required for the feasible operation of the robot.

In relation the proposed prototype for large, horizontal working areas, further research will include assessing the robot performance with real tools attached to the end-effector, and improve the trajectory tracking capabilities by using a more comprehensive dynamic model of the robot.

With a more general point of view, using closed cable loop in CDPR also opens an interesting research line within CDPR. Different variations of the proposed geometry have been already outlined to compensate undesired vibrations of the end-effector. These new geometries still have to be investigated, numerically modeled and experimentally validated. Moreover, the concept of closed cable loops can be applied to spatial CDPRs, which will mainly represent a challenge from the design point of view, however, potential advantages can be obtained as the cable does not end in the drum and the cable tension can be significantly increased.

Considering any kind of planar CDPR, another aspect which has not been considered in this thesis is the stiffness of the robot in the direction perpendicular to the working plane. This will be of special relevance in the vertical case of study. Therefore, further research must study possibilities to increase it as duplicating the cables in the a parallel plane and coordinating cables movement in both circuits. Another option is to rely on the contact of the end-effector with some surface if the application allows it.

Regarding cable tension measurements, further research on this line must include testing the device in a real CDPR ans use the provided measures for control purposes. Additionally, a more detailed study must be carried out on the performance of the dynamic measurements in a real environment, i.e. during the operation of a CDPR with high dynamic capabilities.

Acknowledgment

Author wish to thank the university of Castilla-La Mancha and the European Social Fund for their financial support through the pre-doctoral funding [2019/451] and mobility grant for doctoral students 2020. This work was partially supported by EU Call RFCS-2017 through the research project DESDEMONA (grant agreement number 800687).

References

[1] R. Verhoeven, "Analysis of the workspace of tendon-based stewart platforms," Ph.D. dissertation, Universität Duisburg-Essen, Fakultät für Ingenieurwissenschaften ..., 2004.

[2] A. Pott, H. Mütherich, W. Kraus, V. Schmidt, P. Miermeister, and A. Verl, "Ipanema: a family of cable-driven parallel robots for industrial applications," in *Cable-Driven Parallel Robots*. Springer, 2013, pp. 119–134.

[3] R. Bostelman, J. Albus, N. Dagalakis, A. Jacoff, and J. Gross, "Applications of the nist robocrane," in *Proceedings of the 5th International Symposium on Robotics and Manufacturing*, vol. 5, 1994.

[4] M. Hiller, S. Fang, S. Mielczarek, R. Verhoeven, and D. Franitza, "Design, analysis and realization of tendon-based parallel manipulators," *Mechanism and Machine Theory*, vol. 40, no. 4, pp. 429–445, 2005.

[5] S. Kawamura and K. Ito, "A new type of master robot for teleoperation using a radial wire drive system," in *Proceedings of 1993 IEEE/RSJ International Conference on Intelligent Robots and Systems (IROS'93)*, vol. 1. IEEE, 1993, pp. 55–60.

[6] J.-P. Merlet, "Kinematics of the wire-driven parallel robot marionet using linear actuators," in *2008 IEEE International Conference on Robotics and Automation*. IEEE, 2008, pp. 3857–3862.

[7] J.-P. Merlet and D. Daney, "A new design for wire-driven parallel robot," in *Proceedings 2nd International Congress, Design and Modelling of Mechanical Systems*, 2007.

[8] D. Surdilovic and R. Bernhardt, "String-man: a new wire robot for gait rehabilitation," in *IEEE International Conference on Robotics and Automation, 2004. Proceedings. ICRA'04. 2004*, vol. 2. IEEE, 2004, pp. 2031–2036.

[9] M. A. Khosravi and H. D. Taghirad, "Robust pid control of cable-driven robots with elastic cables," in *Robotics and Mechatronics (ICRoM), 2013 First RSI/ISM International Conference on*. IEEE, 2013, pp. 331–336.

[10] S. Tadokoro, Y. Murao, M. Hiller, R. Murata, H. Kohkawa, and T. Matsushima, "A motion base with 6-dof by parallel cable drive architecture," *IEEE/ASME transactions on mechatronics*, vol. 7, no. 2, pp. 115–123, 2002.

[11] A. Pott, "Introduction," in *Cable-Driven Parallel Robots. Springer Tracts in Advanced Robotics*. Cham: Springer International Publishing, 2018, pp. 1–13. [Online]. Available: $https://doi.org/10.1007/978-3-319-76138-1_1$

[12] M. Zarebidoki, A. Lotfavar, and H. Fahham, "Effectiveness of adaptive passivity-based trajectory tracking control of a cable-suspended robot," in *International Conference on Trends in Mechanical and Industrial Engineering*, 2011.

[13] L. Gagliardini, S. Caro, M. Gouttefarde, and A. Girin, "Discrete reconfiguration planning for cable-driven parallel robots," *Mechanism and Machine Theory*, vol. 100, pp. 313–337, 2016.

[14] B. Zi, B. Duan, J. Du, and H. Bao, "Dynamic modeling and active control of a cable-suspended parallel robot," *Mechatronics*, vol. 18, no. 1, pp. 1–12, 2008.

[15] G. Rosati, P. Gallina, A. Rossi, and S. Masiero, "Wire-based robots for upper-limb rehabilitation," *International Journal of Assistive Robotics and Mechatronics*, vol. 7, pp. 3–10, 2006.

[16] J. v. Zitzewitz, G. Rauter, R. Steiner, A. Brunschweiler, and R. Riener, "A versatile wire robot concept as a haptic interface for sport simulation," in *Robotics and Automation, 2009. ICRA'09. IEEE International Conference on.* IEEE, 2009, pp. 313–318.

[17] Y. Mao and S. K. Agrawal, "Design of a cable-driven arm exoskeleton (carex) for neural rehabilitation," *IEEE Transactions on Robotics*, vol. 28, no. 4, pp. 922–931, 2012.

[18] H. Vallery, P. Lutz, J. von Zitzewitz, G. Rauter, M. Fritschi, C. Everarts, R. Ronsse, A. Curt, and M. Bolliger, "Multidirectional transparent support for overground gait training," in *2013 IEEE 13th International Conference on Rehabilitation Robotics (ICORR)*. IEEE, 2013, pp. 1–7.

[19] G. Castelli and E. Ottaviano, "Modelling and simulation of a cable-based parallel manipulator as an assisting device," in *Computational Kinematics*. Springer, 2009, pp. 17–24.

[20] G. Castelli, E. Ottaviano, and P. Rea, "A cartesian cable-suspended robot for improving end-users' mobility in an urban environment," *Robotics and Computer-Integrated Manufacturing*, vol. 30, no. 3, pp. 335–343, 2014.

[21] M. M. Wu, G. L. Brown, K.-Y. A. Kim, J. Kim, and K. E. Gordon, "Gait variability following abrupt removal of external stabilization decreases with practice in incomplete spinal cord injury but increases in non-impaired individuals," *Journal of neuroengineering and rehabilitation*, vol. 16, no. 1, p. 4, 2019.

[22] Y. Zou, N. Wang, X. Wang, H. Ma, and K. Liu, "Design and experimental research of movable cable-driven lower limb rehabilitation robot," *IEEE Access*, vol. 7, pp. 2315–2326, 2019.

[23] P. Bosscher, R. L. Williams II, L. S. Bryson, and D. Castro-Lacouture, "Cable-suspended robotic contour crafting system," *Automation in construction*, vol. 17, no. 1, pp. 45–55, 2007.

[24] A. Pott, C. Meyer, and A. Verl, "Large-scale assembly of solar power plants with parallel cable robots," in *ISR 2010 (41st International Symposium on Robotics) and ROBOTIK 2010 (6th German Conference on Robotics)*. VDE, 2010, pp. 1–6.

[25] A. Lytle, F. Proctor, and K. Saidi, "Control of cable robots for construction applications," in *Parallel manipulators, towards new applications*. InTech, 2008.

[26] J.-B. Izard, M. Gouttefarde, C. Baradat, D. Culla, and D. Sallé, "Integration of a parallel cable-driven robot on an existing building façade," in *Cable-driven parallel robots*. Springer, 2013, pp. 149–164.

[27] T. Heyden and C. Woernle, "Dynamics and flatness-based control of a kinematically undetermined cable suspension manipulator," *Multibody System Dynamics*, vol. 16, no. 2, pp. 155–177, 2006.

[28] T. Bruckmann, W. Lalo, K. Nguyen, and B. Salah, "Development of a storage retrieval machine for high racks using a wire robot," in *International Design Engineering Technical Conferences and Computers and Information in Engineering Conference*, vol. 45035. American Society of Mechanical Engineers, 2012, pp. 771–780.

[29] Y.-Q. Zheng, "Feedback linearization control of a wire-driven parallel support system in wind tunnels," in *Sixth International Conference on Intelligent Systems Design and Applications*, 2006.

[30] Z. Yaqing, L. Qi, and L. Xiongwei, "Initial test of a wire-driven parallel suspension system for low speed wind tunnels," in *12th IFToMM World Congress on the Theory of Machines and Mechanisms, Besancon*, 2007.

[31] C. Sturm, L. Wildan, and T. Bruckmann, "Wire robot suspension systems for wind tunnels," in *Wind tunnels and experimental fluid dynamics research*. InTech, 2011.

[32] C. Bauer, "Device and method for detecting the inventory of a selling and/or storing device, and a storage-managing system equipped with said device," Jan. 28 2011, wO 2012 101248.

[33] K. H. Voss, V. van der Wijk, and J. L. Herder, "Investigation of a cable-driven parallel mechanism for interaction with a variety of surfaces, applied to the cleaning of free-form buildings," in *Latest Advances in Robot Kinematics*. Springer, 2012, pp. 261–268.

[34] K. Voss, V. van der Wijk, and J. L. Herder, "A cable-driven parallel mechanism for the interaction with hemispherical surfaces," in *New Trends in Mechanism and Machine Science*. Springer, 2013, pp. 409–417.

[35] P. D. Campbell, P. L. Swaim, and C. J. Thompson, "Charlotte™ robot technology for space and terrestrial applications," *SAE transactions*, pp. 641–648, 1995.

[36] B. Duan, Y. Qiu, F. Zhang, and B. Zi, "On design and experiment of the feed cable-suspended structure for super antenna," *Mechatronics*, vol. 19, no. 4, pp. 503–509, 2009.

[37] J.-P. Merlet, *Parallel robots*. Springer Science & Business Media, 2005, vol. 128.

[38] M. Fabritius and A. Pott, "An inverse kinematic code for cable-driven parallel robots considering cable sagging and pulleys," in *European Conference on Mechanism Science*. Springer, 2020, pp. 423–431.

[39] A. Pott, "On the limitations on the lower and upper tensions for cable-driven parallel robots," in *Advances in Robot Kinematics*. Springer, 2014, pp. 243–251.

[40] T. Wang, S. Tong, J. Yi, and H. Li, "Adaptive inverse control of cable-driven parallel system based on type-2 fuzzy logic systems," *IEEE Transactions on Fuzzy Systems*, vol. 23, no. 5, pp. 1803–1816, 2014.

[41] C. Schenk, "Modelling and control of a cable-driven parallel robot: methods for vibration reduction and motion quality improvement," Ph.D. dissertation, University of Stuttgart, 2019.

[42] Z. Zake, F. Chaumette, N. Pedemonte, and S. Caro, "Vision-based control and stability analysis of a cable-driven parallel robot," *IEEE Robotics and Automation Letters*, vol. 4, no. 2, pp. 1029–1036, 2019.

[43] W.-J. Shiang, D. Cannon, and J. Gorman, "Optimal force distribution applied to a robotic crane with flexible cables," in *Proceedings 2000 ICRA. Millennium Conference. IEEE International Conference on Robotics and Automation. Symposia Proceedings (Cat. No. 00CH37065)*, vol. 2. IEEE, 2000, pp. 1948–1954.

[44] M. Hassan and A. Khajepour, "Analysis of bounded cable tensions in cable-actuated parallel manipulators," *IEEE Transactions on Robotics*, vol. 27, no. 5, pp. 891–900, 2011.

[45] S. Bouchard, C. Gosselin, and B. Moore, "On the ability of a cable-driven robot to generate a prescribed set of wrenches," *Journal of Mechanisms and Robotics*, vol. 2, no. 1, 2010.

[46] Z. Cui, X. Tang, S. Hou, and H. Sun, "Non-iterative geometric method for cable-tension optimization of cable-driven parallel robots with 2 redundant cables," *Mechatronics*, vol. 59, pp. 49–60, 2019.

[47] A. Pott, "An improved force distribution algorithm for over-constrained cable-driven parallel robots," in *Computational Kinematics*. Springer, 2014, pp. 139–146.

[48] J. Lamaury and M. Gouttefarde, "A tension distribution method with improved computational efficiency," in *Cable-driven parallel robots*. Springer, 2013, pp. 71–85.

[49] M. Gouttefarde, J. Lamaury, C. Reichert, and T. Bruckmann, "A versatile tension distribution algorithm for n-dof parallel robots driven by $n+2$ cables," *IEEE Transactions on Robotics*, vol. 31, no. 6, pp. 1444–1457, 2015.

[50] W. Kraus, "Force control of cable-driven parallel robots," Ph.D. dissertation, University of Stuttgart, 2016.

[51] M. A. Khosravi and H. D. Taghirad, "Robust pid control of fully-constrained cable driven parallel robots," *Mechatronics*, vol. 24, no. 2, pp. 87–97, 2014.

[52] A. Pott, "Classification and architecture," in *Cable-Driven Parallel Robots. Springer Tracts in Advanced Robotics*. Cham: Springer International Publishing, 2018, pp. 45–117. [Online]. Available: https://doi.org/10.1007/978-3-319-76138-1_3

[53] A. Ming and T. Higuchi, "Study on multiple degree-of-freedom positioning mechanism using wires. i: Concept, design and control," *International Journal of the Japan Society for Precision Engineering*, vol. 28, no. 2, pp. 131–138, 1994.

[54] A. Pott, "Kinematic codes," in *Cable-Driven Parallel Robots. Springer Tracts in Advanced Robotics*. Cham: Springer International Publishing, 2018, pp. 119–155. [Online]. Available: https://doi.org/10.1007/978-3-319-76138-1_4

[55] ——, "Geometric and static foundations," in *Cable-Driven Parallel Robots. Springer Tracts in Advanced Robotics*. Cham: Springer International Publishing, 2018, pp. 15–44. [Online]. Available: https://doi.org/10.1007/978-3-319-76138-1_2

[56] G. Rubio-Gómez, S. Juárez, D. Rodríguez-Rosa, E. Bravo, E. Ottaviano, A. Gonzalez-Rodriguez, and F. J. Castillo-Garcia, "Addition of passive-carriage for increasing workspace of cable robots: automated inspection of surfaces of civil infrastructures," *Smart Structures and Systems*, vol. 27, no. 2, p. 387, 2021.

[57] S. Juárez-Pérez, A. González-Rodriguez, G. Rubio-Gómez, D. Rodríguez-Rosa, E. Ottaviano, and F. J. Castillo-Garcia, "Closed loop cable robot for large horizontal workspaces," *Smart Structures and Systems*, vol. 27, no. 2, p. 397, 2021.

[58] J.-P. Merlet, "Efficient kinematics of a 2-1 and 3-1 cdpr with non-elastic sagging cables," in *International Conference on Cable-Driven Parallel Robots*. Springer, 2021, pp. 3–12.

[59] A. Pott, "Workspace," in *Cable-Driven Parallel Robots. Springer Tracts in Advanced Robotics*. Cham: Springer International Publishing, 2018, pp. 157–227. [Online]. Available: https://doi.org/10.1007/978-3-319-76138-1_5

[60] D. Surdilovic, J. Radojicic, and J. Krüger, "Geometric stiffness analysis of wire robots: A mechanical approach," in *Cable-driven parallel robots*. Springer, 2013, pp. 389–404.

[61] V. Schmidt, W. Kraus, and A. Pott, "Presentation of experimental results on stability of a 3 dof 4-cable-driven parallel robot without constraints," in *Cable-Driven Parallel Robots*. Springer, 2015, pp. 87–99.

[62] A. Pott, "Dynamics," in *Cable-Driven Parallel Robots. Springer Tracts in Advanced Robotics*. Cham: Springer International Publishing, 2018, pp. 229–254. [Online]. Available: $https://doi.org/10.1007/978-3-319-76138-1_6$

[63] E. Ottaviano and G. Castelli, "A study on the effects of cable mass and elasticity in cable-based parallel manipulators," in *ROMANSY 18 Robot Design, Dynamics and Control*. Springer, 2010, pp. 149–156.

[64] M. Fabritius, C. Martin, G. R. Gomez, W. Kraus, and A. Pott, "A practical force correction method for over-constrained cable-driven parallel robots," in *International Conference on Cable-Driven Parallel Robots*. Springer, 2021, pp. 117–128.

[65] W. Shang, B. Zhang, B. Zhang, F. Zhang, and S. Cong, "Synchronization control in the cable space for cable-driven parallel robots," *IEEE Transactions on Industrial Electronics*, vol. 66, no. 6, pp. 4544–4554, 2018.

[66] A. R. Emmens, S. A. Spanjer, and J. L. Herder, "Modeling and control of a large-span redundant surface constrained cable robot with a vision sensor on the platform," in *Cable-Driven Parallel Robots*. Springer, 2015, pp. 249–260.

[67] C. Reichert, K. Müller, and T. Bruckmann, "Robust internal force-based impedance control for cable-driven parallel robots," in *Cable-Driven Parallel Robots*. Springer, 2015, pp. 131–143.

[68] S. Khalilpour, R. Khorrambakht, H. Taghirad, and P. Cardou, "Robust cascade control of a deployable cable-driven robot," *Mechanical Systems and Signal Processing*, vol. 127, pp. 513–530, 2019.

[69] T. Dallej, M. Gouttefarde, N. Andreff, M. Michelin, and P. Martinet, "Towards vision-based control of cable-driven parallel robots," in *2011 IEEE/RSJ International Conference on Intelligent Robots and Systems*. IEEE, 2011, pp. 2855–2860.

[70] T. Dallej, M. Gouttefarde, N. Andreff, R. Dahmouche, and P. Martinet, "Vision-based modeling and control of large-dimension cable-driven parallel robots," in *2012 IEEE/RSJ International Conference on Intelligent Robots and Systems*. IEEE, 2012, pp. 1581–1586.

[71] R. Chellal, L. Cuvillon, and E. Laroche, "Model identification and vision-based h_∞ position control of 6-dof cable-driven parallel robots," *International Journal of Control*, vol. 90, no. 4, pp. 684–701, 2017.

[72] H. Kino, T. Yahiro, F. Takemura, and T. Morizono, "Robust pd control using adaptive compensation for completely restrained parallel-wire driven robots: Translational systems using the minimum number of wires under zero-gravity condition," *IEEE Transactions on Robotics*, vol. 23, no. 4, pp. 803–812, 2007.

[73] Z. Zake, F. Chaumette, N. Pedemonte, and S. Caro, "Control stability workspace for a cable-driven parallel robot controlled by visual servoing," in *International Conference on Cable-Driven Parallel Robots*. Springer, 2021, pp. 284–296.

[74] R. Chellal, L. Cuvillon, and E. Laroche, "A kinematic vision-based position control of a 6-dof cable-driven parallel robot," in *Cable-Driven Parallel Robots*. Springer, 2015, pp. 213–225.

[75] M. Hamann and C. Ament, "Model-based control of a planar 3-dof cable robot using exact linearization," in *Cable-Driven Parallel Robots*, M. Gouttefarde, T. Bruckmann, and A. Pott, Eds. Cham: Springer International Publishing, 2021, pp. 260–270.

[76] J. Lamaury and M. Gouttefarde, "Control of a large redundantly actuated cable-suspended parallel robot," in *2013 IEEE International Conference on Robotics and Automation*. IEEE, 2013, pp. 4659–4664.

[77] S. Abdelaziz, L. Barbé, P. Renaud, M. de Mathelin, and B. Bayle, "Control of cable-driven manipulators in the presence of friction," *Mechanism and Machine Theory*, vol. 107, pp. 139–147, 2017.

[78] G. Pittiglio, A. Kogkas, J. O. Vrielink, and G. Mylonas, "Dynamic control of cable driven parallel robots with unknown cable stiffness: a joint space approach," in *2018 IEEE International Conference on Robotics and Automation (ICRA)*. IEEE, 2018, pp. 948–955.

[79] R. Babaghasabha, M. A. Khosravi, and H. D. Taghirad, "Adaptive robust control of fully-constrained cable driven parallel robots," *Mechatronics*, vol. 25, pp. 27–36, 2015.

[80] X. Aguas, M. Herrera, O. Camacho, and P. Leica, "A sliding mode control for a planar 4-cable direct driven robot," in *2018 International Conference on Information Systems and Computer Science (INCISCOS)*. IEEE, 2018, pp. 23–28.

[81] P. Ren and Y. Sun, "Sliding mode set point control of a six-dof cable-suspended parallel robot with tension constraints and uncertain disturbances," in *ASME 2018 International Design Engineering Technical Conferences and Computers and Information in Engineering Conference*. American Society of Mechanical Engineers, 2018, pp. V05BT07A018–V05BT07A018.

[82] Y. Wang, K. Zhu, F. Yan, and B. Chen, "Adaptive super-twisting nonsingular fast terminal sliding mode control for cable-driven manipulators using time-delay estimation," *Advances in Engineering Software*, vol. 128, pp. 113–124, 2019.

[83] J. Yang, H. Su, Z. Li, D. Ao, and R. Song, "Adaptive control with a fuzzy tuner for cable-based rehabilitation robot," *International Journal of Control, Automation and Systems*, vol. 14, no. 3, pp. 865–875, 2016.

[84] S. Kawamura, H. Kino, and C. Won, "High-speed manipulation by using parallel wire-driven robots," *Robotica*, vol. 18, no. 1, pp. 13–21, 2000.

[85] S. Fang, D. Franitza, M. Torlo, F. Bekes, and M. Hiller, "Motion control of a tendon-based parallel manipulator using optimal tension distribution," *IEEE/ASME Transactions On Mechatronics*, vol. 9, no. 3, pp. 561–568, 2004.

[86] I. Chawla, P. M. Pathak, L. Notash, A. K. Samantaray, Q. Li, and U. K. Sharma, "Neural network-based inverse kineto-static analysis of cable-driven parallel robot considering cable mass and elasticity," in *International Conference on Cable-Driven Parallel Robots*. Springer, 2021, pp. 50–62.

[87] A. B. Alp and S. K. Agrawal, "Cable suspended robots: design, planning and control," in *Robotics and Automation, 2002. Proceedings. ICRA'02. IEEE International Conference on*, vol. 4. IEEE, 2002, pp. 4275–4280.

[88] A. Alp and S. K. Agrawal, "Cable suspended robots: Feedback controllers with positive inputs," in *American Control Conference, 2002. Proceedings of the 2002*, vol. 1. IEEE, 2002, pp. 815–820.

[89] S.-R. Oh and S. K. Agrawal, "Cable-suspended planar parallel robots with redundant cables: Controllers with positive cable tensions," in *IEEE International Conference on Robotics and Automation*, vol. 3. IEEE; 1999, 2003, pp. 3023–3028.

[90] Y. Wang, L. Liu, J. Chen, F. Ju, B. Chen, and H. Wu, "Practical robust control of cable-driven robots with feedforward compensation," *Advances in Engineering Software*, vol. 145, p. 102801, 2020.

[91] J. Lamaury, M. Gouttefarde, A. Chemori, and P.-E. Hervé, "Dual-space adaptive control of redundantly actuated cable-driven parallel robots," in *2013 IEEE/RSJ International Conference on Intelligent Robots and Systems*. IEEE, 2013, pp. 4879–4886.

[92] S. Khalilpour, R. Khorrambakht, M. Harandi, H. Taghirad, and P. Cardou, "Robust dynamic sliding mode control of a deployable cable driven robot," in *Electrical Engineering (ICEE), Iranian Conference on*. IEEE, 2018, pp. 863–868.

[93] M. Gouttefarde, T. Bruckmann, and A. Pott, *Cable-Driven Parallel Robots: Proceedings of the 5th International Conference on Cable-Driven Parallel Robots*. Springer, 2021, vol. 74.

[94] G. Rubio-Gómez, D. Rodríguez-Rosa, J. A. García-Vanegas, A. Gonzalez-Rodríguez, F. J. Castillo-García, and E. Ottaviano, "Chain driven robots: An industrial application opportunity. a planar case approach," in *International Conference on Cable-Driven Parallel Robots*. Springer, 2019, pp. 13–22.

[95] T.-L. Huang, H. Zhou, H.-P. Chen, and W.-X. Ren, "Stochastic modelling and optimum inspection and maintenance strategy for fatigue affected steel bridge members," *Smart Struct. Syst*, vol. 18, no. 3, pp. 569–584, 2016.

[96] J.-K. Oh, G. Jang, S. Oh, J. H. Lee, B.-J. Yi, Y. S. Moon, J. S. Lee, and Y. Choi, "Bridge inspection robot system with machine vision," *Automation in Construction*, vol. 18, no. 7, pp. 929–941, 2009.

[97] B. J. Lee, D. H. Shin, J. W. Seo, J. D. Jung, and J. Y. Lee, "Intelligent bridge inspection using remote controlled robot and image processing technique," in *International Symposium on Automation and Robotics in Construction (ISARC), Seoul, Korea*, 2011, pp. 1426–1431.

[98] R. R. Murphy, E. Steimle, M. Hall, M. Lindemuth, D. Trejo, S. Hurlebaus, Z. Medina-Cetina, and D. Slocum, "Robot-assisted bridge inspection," *Journal of Intelligent & Robotic Systems*, vol. 64, no. 1, pp. 77–95, 2011.

[99] S. Jung, S. Song, S. Kim, J. Park, J. Her, K. Roh, and H. Myung, "Toward autonomous bridge inspection: A framework and experimental results," in *2019 16th International Conference on Ubiquitous Robots (UR)*. IEEE, 2019, pp. 208–211.

[100] S. Schröder, "Under constrained cable-driven parallel robot for vertical green maintenance," in *International Conference on Cable-Driven Parallel Robots*. Springer, 2021, pp. 389–400.

[101] G. Abbasnejad and M. Carricato, "Real solutions of the direct geometrico-static problem of under-constrained cable-driven parallel robots with 3 cables: A numerical investigation," *Meccanica*, vol. 47, no. 7, pp. 1761–1773, 2012.

[102] G. Mottola, C. Gosselin, and M. Carricato, "Dynamically feasible motions of a class of purely-translational cable-suspended parallel robots," *Mechanism and Machine Theory*, vol. 132, pp. 193–206, 2019.

[103] W. Kraus, M. Kessler, and A. Pott, "Pulley friction compensation for winch-integrated cable force measurement and verification on a cable-driven parallel robot," in *IEEE International Conference on Robotics and Automation (ICRA)*. IEEE, 2015, pp. 1627–1632.

[104] G. Rubio-Gómez, S. Juárez-Pérez, A. Gonzalez-Rodríguez, D. Rodríguez-Rosa, L. Corral-Gómez, A. I. López-Díaz, I. Payo, and F. J. Castillo-García, "New sensor device to accurately measure cable tension in cable-driven parallel robots," *Sensors*, vol. 21, no. 11, p. 3604, 2021.